(2)

MEMORANDUM REPORT BRL-MR-3960

BRL

TERMINAL BALLISTICS TEST AND ANALYSIS GUIDELINES FOR THE PENETRATION MECHANICS BRANCH

JOHN A. ZOOK
KONRAD FRANK
GRAHAM F. SILSBY

JANUARY 1992

U.S. ARMY LABORATORY COMMAND

BALLISTIC RESEARCH LABORATORY
ABERDEEN PROVING GROUND, MARYLAND

NOTICES

Destroy this report when it is no longer needed. DO NOT return it to the originator.

Additional copies of this report may be obtained from the National Technical Information Service, U.S. Department of Commerce, 5285 Port Royal Road, Springfield, VA 22161.

The findings of this report are not to be construed as an official Department of the Army position, unless so designated by other authorized documents.

The use of trade names or manufacturers' names in this report does not constitute indorsement of any commercial product.

REPORT DOCUMENTATION PAGE

Form Approved
OMB No. 0704-0188

1. AGENCY USE ONLY (Leave blank)	2. REPORT DATE	3. REPORT TYPE AND DATES COVERED
	January 1992	Final, January 1989–January 1991

4. TITLE AND SUBTITLE

Terminal Ballistics Test and Analysis Guidelines for the Penetration Mechanics Branch

5. FUNDING NUMBERS

PR: 1L162618AH80

6. AUTHOR(S)

John A. Zook, Konrad Frank, and Graham F. Silsby

7. PERFORMING ORGANIZATION NAME(S) AND ADDRESS(ES)

U.S. Army Ballistic Research Laboratory
ATTN: SLCBR-TB-P
Aberdeen Proving Ground, MD 21005-5066

8. PERFORMING ORGANIZATION REPORT NUMBER

9. SPONSORING/MONITORING AGENCY NAME(S) AND ADDRESS(ES)

U.S. Army Ballistic Research Laboratory
ATTN: SLCBR-DD-T
Aberdeen Proving Ground, MD 21005-5066

10. SPONSORING/MONITORING AGENCY REPORT NUMBER

BRL-MR-3960

11. SUPPLEMENTARY NOTES

12a. DISTRIBUTION/AVAILABILITY STATEMENT

Approved for public release; distribution is unlimited.

12b. DISTRIBUTION CODE

13. ABSTRACT (Maximum 200 words)

An introductory handbook describing kinetic energy terminal ballistics methods (experimental and analytic) as performed at the BRL.

14. SUBJECT TERMS

handbook; terminal ballistics; penetration; perforation; ballistic limit; kinetic energy

15. NUMBER OF PAGES

127

16. PRICE CODE

17. SECURITY CLASSIFICATION OF REPORT	18. SECURITY CLASSIFICATION OF THIS PAGE	19. SECURITY CLASSIFICATION OF ABSTRACT	20. LIMITATION OF ABSTRACT
UNCLASSIFIED	UNCLASSIFIED	UNCLASSIFIED	UL

INTENTIONALLY LEFT BLANK.

TABLE OF CONTENTS

LIST OF FIGURES

!NTENTIONALLY LEFT BLANK.

LIST OF TABLES

INTENTIONALLY LEFT BLANK.

1. INTRODUCTION

The principal mission of the Penetration Mechanics Branch (PMB) of the Terminal Ballistics Division (TBD) of the Ballistic Research Laboratory (BRL), Aberdeen Proving Ground, MD, is research and development leading to improvements in the terminal ballistic performance of kinetic energy (KE) long rod penetrators. This is done by using computer modeling and by experimental tests. In terms of the number of shots fired, the experimental testing is predominantly done at reduced scale using laboratory guns with bore diameters of 20 to 30 mm. The reduced scale penetrators are of simplified geometry compared with their full-scale counterparts. The penetrator is usually a monolithic right-circular-cylinder metal rod with a hemispheric nose made from either tungsten alloy (WA) or depleted uranium (DU).

Terminal ballistics is that part of the science of ballistics that relates to the interaction between a projectile (penetrator) and a target. In general, the projectile is the "package" which flies through the air. The penetrator is the part of the projectile which "digs" into the target, inflicting damage to the target.

The primary measure of the effectiveness of a penetrator attacking a specific target is its ballistic limit velocity. The ballistic limit velocity is the impact speed required to just get through the target placed at the specified angle of obliquity. It is described more fully in Section 8.

The goal in writing this handbook is to provide sufficient background information for a novice in terminal ballistics to conduct useful experiments and to serve as a reference source for those who are experienced. It describes the methodology for determining the effectiveness of a penetrator and attempts to standardize on definitions, symbols, and procedures. The pages are identified according to section to expedite finding a particular topic.

The bibliography following the reference list includes some references which have not been used explicitly in this report. They are listed as a source of further information for the interested reader.

2. THE FIRING RANGE

2.1 The Gun System. The guns which are used for terminal ballistics testing of small-caliber penetrators (Range 110) consist of a 37-mm gun breech assembly with a custom-made, replaceable 26-mm smoothbore barrel. The hot propellant gases progressively erode the gun bore at the breech end of the barrel. The erosion is exacerbated by the high flame temperatures of the burning propellant. Therefore, the propellant with the lowest flame temperature which produces acceptable velocities is used. When the erosion has increased to the point where the muzzle velocity falls below expectation or the projectile experiences excessive yaw, the barrel is rebored to clean it up. The following are the current standard bore sizes.

BORE DIAMETER

Initial	1.042 in
First rebore	1.090 in
Second rebore	1.105 in
Third rebore	1.125 in

A barrel is discarded when excessive wear occurs after the second or third (depending on the barrel history) rebore.

An oversized obturator (described in a later section) is used in order to minimize gas leakage past the projectile while it travels down the tube. The launch package is inserted using a special fixture and rammed in to place with a hydraulic jack.

2.2 The Flash X-ray System. High-speed (flash) radiography is used to record and study dynamic events where interposed material, smoke, flame, debris, or pressure variations exclude the use of high-speed optical cameras. In ballistics testing, pulse duration is in the range of 3 to 70 ns (3×10^{-9} to 70×10^{-9} s). Associated with each x-ray tube is a pulse generator and a bank of capacitors which are charged up (in a parallel mode) with a 20 kV (20,000 V) high voltage power supply. The bank of capacitors, referred to as the pulser, are discharged in series (resulting in a summation of the voltages across the

capacitors) through the associated x-ray tube. The x-ray tubes used at the BRL are rated at 150 kV, 300 kV or, occasionally, 450 kV. The voltage rating is the maximum voltage which the pulser should supply upon discharge. Higher voltage rated systems are available but are expensive and are needed only in special situations.

A schematic of a typical firing range setup (using flash radiography) is shown in Figure 1 and is described in Grabarek and Herr (1966). A pair of x-ray tubes (also called x-ray heads) are located in a horizontal plane orthogonal (at a 90° angle) to the line of fire in front of the target (stations 1 and 2) and another pair in the same plane behind the target (stations 3 and 4). There usually is only one x-ray tube located vertically (station 1). A tube could be placed at station 2 if the target is at zero obliquity, but for oblique targets, the target is likely to block the field of view of that tube. This is also the reason why a tube is not located vertically at station 3. A tube could be placed at station 4 in order to determine the angular spread of the debris cloud (mostly target particles, but including some penetrator material, especially if the penetrator breaks up). In this case, a film cassette would have to be located in a horizontal plane back of and below the target—in about the same relative position as the one in front of the target. In most cases, only the residual velocity of the penetrator is of interest. A penetrator impacting a target with near zero total yaw (see Section 5) can be expected to remain in the same vertical plane which passes through the line of fire. Therefore, no additional useful information can be obtained from a film exposed by a tube in the vertical plane above and behind the target.

A multiflash record of the projectile before impact and just after impact (for "finite" thickness targets) is obtained from this system. The first set of x-ray tubes (station 1) are flashed after a short time delay in response to the projectile passing through a trigger screen (normally a break screen, although, a make screen could be used). After a preset time delay, the tube(s) at station 2 flash. The same sequence is repeated for the x-ray tubes behind the target plate (at stations 3 and 4).

The x-radiation is attenuated by any high density object in the field of view. Any x-radiation which reaches the film cassette containing x-ray sensitive film is enhanced by impinging on an image intensifier screen in contact with the film. The resulting radiation fully exposes the film in all areas except those where the radiation was attenuated, thereby

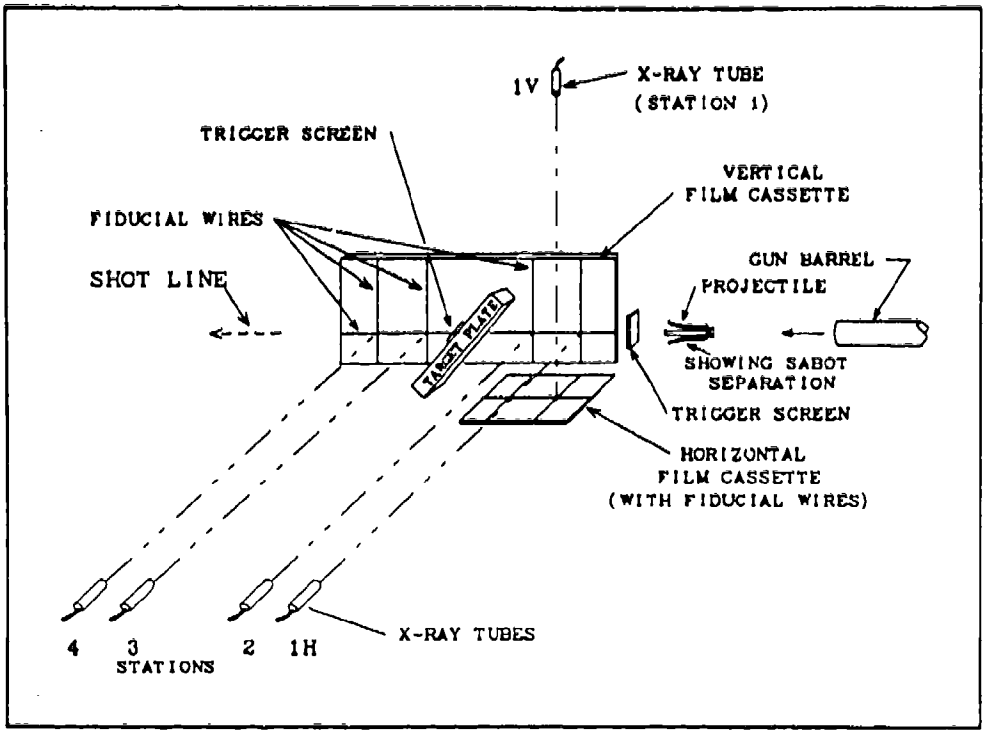

Figure 1. Typical Firing Range X-ray System.

producing an image of the projectile on the film. The images of the projectile on the film may overlay each other to some extent, making it difficult to determine the end points of the images in the overlapping region.

Figure 2 depicts the chronological sequence needed to obtain the radiographic images which are required for calculating striking and residual velocities. The projectile perforates a trigger screen (see Figure 3 for the makeup of the trigger screen), thereby breaking the conductive path on the screen (break screen) or completing the circuit (make screen). This triggers a time delay unit. At the end of the preset time delay, the delay unit sends a signal that triggers the appropriate pulser unit connected to each x-ray tube at station 1. A high-voltage, high-current electrical pulse is transmitted via a high-voltage cable to the corresponding x-ray tube, which then emits a sharp x-ray pulse (less than 0.1 μs duration). The first time delay unit also triggers another time delay unit. At the end of the second time delay, the x-ray tubes located at station 2 are triggered, producing the second image of the projectile on the film.

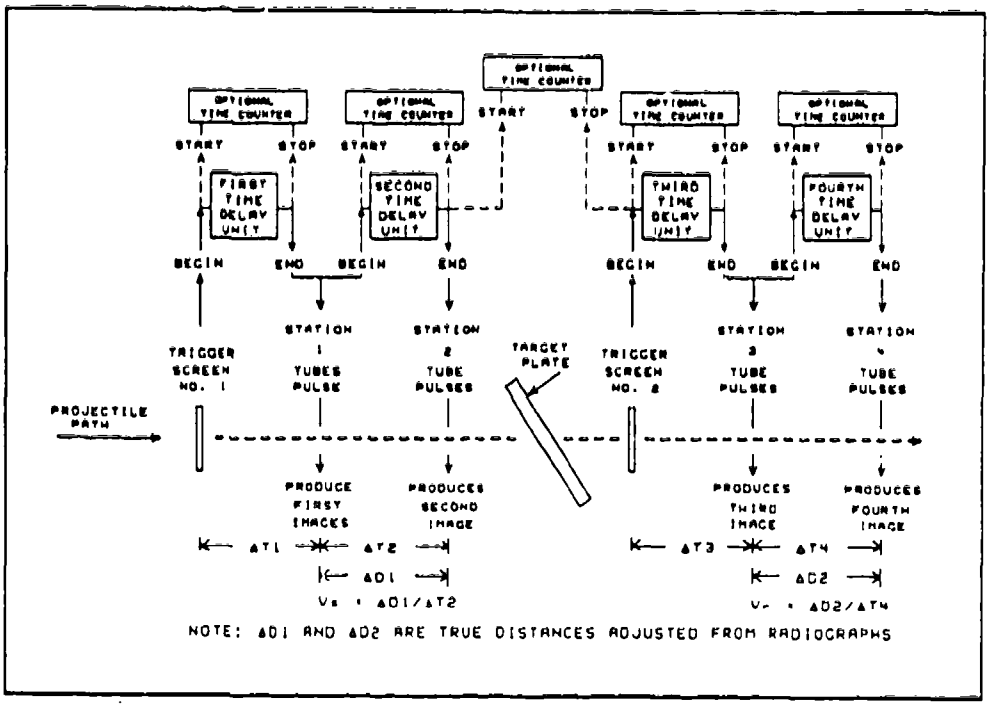

Figure 2. Chronological Sequence of X-ray System Events.

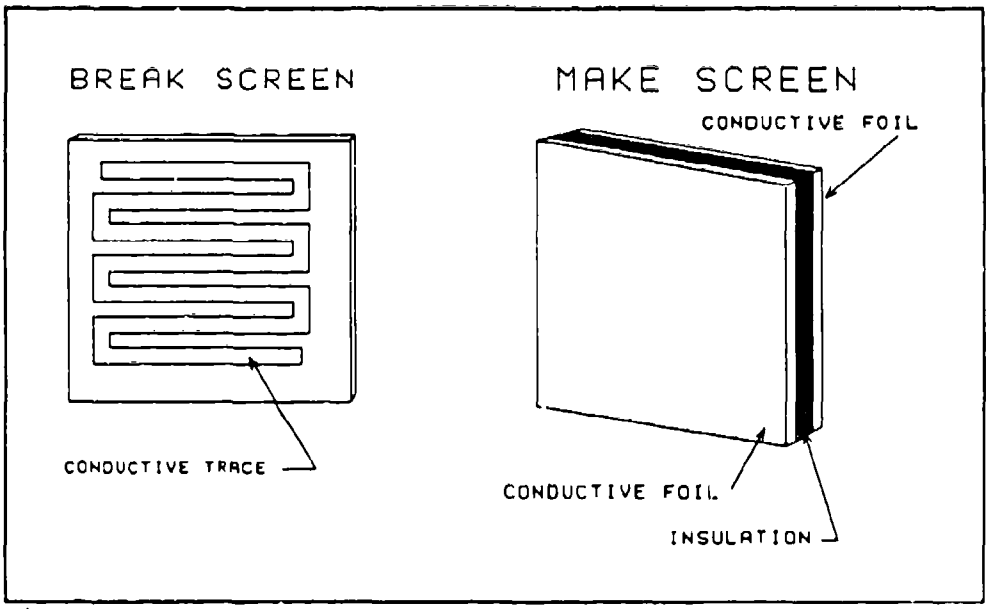

Figure 3. Trigger Screen Construction Schematic.

The same process is repeated behind the target to obtain the images needed for calculating residual velocity. The trigger screen, in this case, is usually taped to the back of the target plate with a 1-in thick piece of foam rubber separating the screen from the target.

Optional time counters may be used to verify the time delay produced by each time delay unit, although the time delay units in current use have proven accurate to within 1 μs of the preset value. The optional time counter indicated in Figure 2 between stations 2 and 3 is desirable since it can be used to calculate the length of time the penetrator spends in the target.

In order to relate the coordinates that are measured on the film to actual spatial coordinates of the projectile at the moment the x-ray tube flashed, there must be some reference lines (fiducial lines) on the film. These fiducial lines are produced by metal wires which are strung directly in front of the x-ray film cassette so that there is an orthogonal cross directly opposite the center axis of each x-ray tube. The image of these fiducial wires appears on the film.

As the tube-to-film distance increases by moving the x-ray head further away from the film, the multiplier factor (needed to adjust the film coordinates to actual space coordinates) becomes closer to 1 (always between 0 and 1) because the image of the projectile on the film becomes less magnified. The magnification factor will be covered in more detail in Section 5. The tube-to-film distance is restricted, however, because the strength of the x-radiation is attenuated with distance since the radiation is spread out over a larger surface area (the radiation is contained within a cone which has its apex at the tip of the x-ray tube). The quality of the image on the film is largely determined by the strength of the radiation impinging on the film. The greater the contrast between the image and the rest of the film, the easier it is to "read" the film accurately.

Table 1 is a chronological record of the distances between the x-ray tubes, the shot line (line of fire), and the film planes at a x-ray station for Range 110G. The same values are used from one station to another during any particular time period. Table 2 shows the distances for Range 110E.

Table 1. Chronological Record of Distances: Range 110G (Nonhazardous Material Range)

Description	Symbol	Distance (in)	Distance (mm)
Horizontal tube to vertical film plane	X_{hf}	48	1,219.2
(Beginning April 1976)		60	1,524.0
(Beginning 25 March 1985)		62.5	1,587.5
(Beginning March 1986)		70	1,778.0
Vertical tube to horizontal film plane	Y_{hf}	48	1,219.2
(Beginning April 1976)		60	1,524.0
(Beginning March 1986)		69	1,752.6
Shot line to vertical film plane	X_{sf}	8	203.2
(Beginning 25 March 1985)		11	279.4
(Beginning March 1986		16.5	419.1
Shot line to horizontal film plane	Y_{sf}	8	203.2
(Beginning March 1986)		15.25	393.7

Table 2. Chronological Record of Distances: Range 110E (Hazardous Material Range)

Description	Symbol	Distance (in)	Distance (mm)
Horizontal tube to vertical film plane	X_{hf}	72	1,828.8
(Beginning January 1985)		80	2,032.0
Vertical tube to horizontal film plane	Y_{hf}	72	1,828.8
(Beginning January 1985)		80.25	2,038.4
Shot line to vertical film plane	X_{sf}	8	203.2
(Beginning January 1985)		18.75	476.2
Shot line to horizontal film plane	Y_{sf}	8	203.2
(Beginning January 1985)		18.75	476.2

3. PROCEDURE BEFORE FIRING

3.1 Scaling Methodology. One method of scaling consists of determining a reduced mass and computing a scale length that is the full-scale length multiplied by the cube root of the ratio of the reduced-scale to full-scale masses. For example, if the full-scale mass is 4,160 g and the reduced scale is 65 g, then the reduced-scale length is $\sqrt[3]{65/4160} = \frac{1}{4}$ of the full-scale length. Another method is to specify the scale factor (e.g., 1/4 scale) of the mass and use that to compute a scaled length from the full-scale length.

Given a scale factor 1/N (e.g., N = 4), scaling affects the various parameters in the following way (a scale factor of 1 means that parameter does not change with scale).

	Parameter	Scale Factor
Penetrator:	Length	1/N
	Diameter	1/N
	Density	1
	Mass	$1/N^3$
	Energy	$1/N^3$
	Strength	1
	Velocity	1
	Time	1/N
Target:	Thickness (depth)	1/N
	Obliquity	1
	Hardness (strength)	1*

* The hardness of plates which are rolled during the manufacturing process usually change with thickness (heat treatment might be needed to adjust the hardness to scale to 1).

Experimentally, it has been found that there are slight differences between scaling theory and reality. Recent experiments suggest that the penetrator diameter causes a deviation from

scaling theory. For example, the velocity ballistic limit seems to be a function of penetrator diameter when the values of all other parameters have been adjusted.

3.2 Target Plate. The target is usually rolled homogeneous armor (RHA) or high hardness armor (HHA). Some tests might require 5083, 7039, or 2024ST aluminum targets. Tests are usually done with single-plate targets, but some programs require testing with multiple-plate spaced targets (two plates, usually of different thickness, parallel to each other and separated by an air space or three plates of different thicknesses parallel to each other and separated by equally spaced air gaps). Some tests require laminated plate targets or target plates of nonferrous material.

The military specifications for the manufacturing process and the material properties of RHA are described in the document MIL-A-12560G(MR) (1984) dated 15 August 1984. The document MIL-S-13812B(MR) (1971) has the same composition and hardness specifications but is not as detailed as MIL-A-12560G(MR). The military specifications for HHA are found in MIL-A-46100C (1983).

The following information is recorded regarding the target plate:

(1) the type of material (usually rolled homogeneous armor - RHA),

(2) the thickness of the target in millimeters or inches - metric units are preferred since metric units are to be used in reports,

(3) the Brinell hardness number (BHN), which is measured with a standard Brinell hardness tester (see Section 3.2.2); the units are not specified because of the way the BHN is defined,

(4) the mass of the target in grams, and

(5) the length and width of the target plate (not usually recorded); a typical size used in Range 110 is 6 × 18 in for oblique angle shots and 6 × 12 in for perpendicular impact shots.

3.2.1 Target Material Hardness. Hardness is a material property that correlates well with the ballistic resistance of materials. It is related to the strength and work hardening properties of the material. There are various methods for measuring hardness, but all rely on using a fixed force (generally a hydraulic press) to advance a penetrator or indenter into the material until balanced by the material's strength. The deformation or strain caused by the penetration varies within the volume of the material, as does the characteristic work hardening, so that the single number obtained from the hardness test represents an average value of the compressive and shear strengths of the material that are typical of penetrator-target interactions. The equipment needed to perform a Brinell hardness test is simple and portable. The test can be performed in a matter of a few minutes and has become the customary test for hardness.

3.2.2 Brinell Hardness Number. The Brinell hardness test involves forcing (using a hydraulic press) a hardened sphere (usually 10 mm in diameter) under a known load (usually 3,000 kg) into the surface of the material under test. The Brinell hardness can then be determined by measuring the diameter of the impression by means of a microscope supplied with the tester unit and referring to a chart which relates the diameter to the hardness. It is best to use an average of two diameter measurements which are orthogonal to each other in order to eliminate effects of anisotropy. If the chart is not available, the BHN is calculated by the following equation:

$$BHN = \frac{2F}{\pi D \left[D - \sqrt{(D^2 - d^2)} \right]},$$

where F is the load in kilograms force (which represents the force exerted by that value of kilograms mass accelerated by gravity under standard conditions at the surface of the earth), π can be approximated by 3.14, D is the diameter of the indentor sphere in millimeters, and d is the maximum diameter of the indentation made in the surface of the test plate measured in millimeters. The effect of this equation is to divide the load which was applied (measured in kilograms) by the actual surface area of the indentation measured in square millimeters. The units are kilograms-force/mm^2, but are rarely stated. To convert to units of pressure, multiply

by the acceleration of gravity (9.8×10^7 g-cm/sec^2) to obtain dyn/cm^2 (dynes are units of force; pressure = force/area). To convert from dyn/cm^2 to pascals (N/m^2), divide by 10.

In making the test, the surface should be prepared by cleaning (may require lightly grinding) the area where the test will be made. The rear surface of the plate should rest on an anvil which is flat. The load should be applied steadily and should remain for at least 15 s in the case of ferrous materials (steel, RHA, etc.) and 30 s in the case of nonferrous materials (aluminum, etc.). Longer periods may be necessary for certain soft materials that exhibit creep at room temperature. The depth of the impression should not be greater than 1/10 of the thickness of the material tested; if it is, a different size ball should be used or a lighter load applied using the same ball (Baumeister and Marks 1967). Ideally, the test should be performed at several different locations on both the front and rear surfaces of the target plate. Then an average value could be reported or all the test values if they differ significantly (see Table 3 for BHN for RHA as specified in MIL-S-13812B(MR) [1971]).

3.2.3 Rockwell Hardness. The Rockwell hardness test is similar to the Brinell. There are two major differences. First, the indentor may be either a steel ball or a spherical-tipped conical diamond of 120° angle and 0.2-mm tip radius, called a "brale." Secondly, the load is applied in two stages. A minor load of 10 kg is first applied, the dial is set to 0, and the major load of 60, 100, or 150 kg is applied. The reading of depth of penetration is taken after the major load is removed but while the minor load is still applied. The hardness is then determined from the scale. Deep penetrations yield low hardness numbers, while shallow penetrations represent high hardness numbers.

The Rockwell B test uses a 1/16-in ball and a major load of 100 kg. It is used for relatively soft targets. The Rockwell C test uses the brale for the indentor rather than the ball and a major load of 150 kg. It may be used for measuring "hard" targets beyond the range of Brinell (Baumeister and Marks 1967).

Rockwell C values are approximately related to the Brinell hardness (BHN) by the following equations:

Table 3. Brinell Hardness Specifications for RHA

Thickness Range				3,000 kg load BHN range	Brinell indentation diameter
in		equiv. mm		kg-f/mm^2	mm
0.250	0.499	6.35	12.67	341-388	3.30-3.10
0.500	0.749	12.70	19.02	331-375	3.35-3.15
0.750	1.249	19.05	31.72	321-375	3.40-3.15
1.25	1.99	31.75	50.55	293-331	3.55-3.35
2.00	3.99	50.80	101.35	269-311	3.70-3.45
4.00	6.99	101.60	177.55	241-277	3.90-3.65
7.00	8.99	177.80	228.35	223-262	4.05-3.75
9.00	12.00	228.60	304.80	212-248	4.15-3.85

$$BHN = 164.9 + 0.8563R_c + 0.1071R_c^2 ,$$

and

$$R_c = -124.3 + 26.01\,BHN^{\frac{1}{3}} - 0.06062\,BHN ,$$

over the range of R_c 20.5–51.6 (BHN 229–495). The value for the BHN calculated with the first equation is within 2 of the tabulated value (Bethlehem Steel Company) for any R_c within the range stated previously. The equation is less accurate for R_c values below 20.5 and deviates by large amounts for values above 51.6. The value of R_c using the second equation is within 0.5 of the tabulated value over the range $229 < BHN < 495$.

3.2.4 Other Material Tests. Other hardness tests are the Vickers test, the Scleroscope test, the Monotron test, and the Herbert pendulum test. These tests, including the Rockwell and Brinell, measure surface hardness. Tests which measure resistance to fracture are the Charpy impact test and the Izod test (Baumeister and Marks 1967).

3.3 The Projectile (Kinetic Energy). The projectile is the package which travels from the muzzle of the gun to the target. For a launch package which includes a discarding sabot, the projectile loses the sabot near but downrange from the muzzle. What is called the projectile is the part which reaches the target. On impact, more parts of the projectile might be lost which do not contribute to penetration (e.g., the nose of the projectile [its purpose is to reduce drag while aerodynamic, i.e., flying through air]). The part which actually penetrates the target is, logically, called the penetrator.

PMB designs and tests only KE projectiles. The Warhead Mechanics Branch (WMB) of TBD designs and tests chemical energy (explosive) projectiles such as shaped charges, explosively formed fragments, and fragmentation projectiles. The terminal ballistics of each can be modeled the same way as for a kinetic energy penetrator. They differ in the delivery system. For example, a shaped charge consists of a cone (made of copper, aluminum or titanium, but usually copper) which is backed by explosive. The conical liner and the explosive are usually encased in a metal cylinder. A proximity or impact fuse on the nose activated by the target as the shaped charge warhead approaches causes the explosive to detonate. The result of the interaction of the explosive with the cone is to produce a very high speed jet of conic liner material as the explosive gasses crush the cone into a metallic glob, called the slug, which travels at a moderate speed. The jet, however, travels at speeds exceeding 4,000 m/s. If the target is at the proper distance when the jet is formed, the jet can penetrate a large thickness of RHA (on the order of 500 mm for a 42° apex angle copper cone with an 80-mm base diameter and 830 g of comp B explosive encased in an aluminum cylinder 3.6-mm thick). For more information on shaped charges, see Walters and Zukas (1989) and Zukas (1991). In addition, there are numerous BRL reports written or coauthored by R. Allison, A. Arbuckle, C. Aseltine, G. Birkoff, H. Breidenbach, F. Brundick, J. Clark, R. DiPersio, J. Harrison, R. Karpp, S. Kronman, V. Kucher, J. Longbardi, J. Majerus, A. Merendino, J. Panzarella, J. Regan, W. Rodas, B. Scott, S. Segletes, R. Shear, J. Simon, R. Vitali, W. Walters, and L. Zernow.

3.3.1 The Penetrator. Most of the penetrators which are tested in Range 110 are long rods with hemispheric noses. Other possible shapes for the nose are ogival and conic. A conic nose section which does not include the apex (pointed end) is know as the frustum of the cone.

PMB also tests full-scale projectiles in outdoor firing ranges (e.g., the Transonic Range). These usually involve high L/D penetrators (L/D > 15) which require tail fins to achieve aerodynamic stability.

The following should be recorded with regard to the penetrator:

(1) the type of material (e.g., tungsten or DU),

(2) the density of the material (grams per cubic centimeter),

(3) the mass in grams,

(4) the diameter in inches or millimeters (specify),

(5) the length (measured from base to tip) in the same units as the diameter,

(6) and the shape of the nose (flat, if it has no nose).

(7) If the nose is neither flat or hemispheric, the length of the nose and any other distinguishing dimensions should also be recorded. For a conic frustum, the diameter of the flat part of the front end should be recorded as well as the height (length of the nose) of the frustum. For all conic and conic section nose shapes, the cone apex angle should be recorded (a note should be made as to whether the angle is the full angle or the half angle).

3.3.2 The Sabot Assembly. The standard laboratory (indoor range - quarter scale) sabot assembly consists of the carrier (which is frequently called the sabot), the pusher plate, and the obturator. The carrier currently used in Range 110 is made of polypropulux #944 and consists of four symmetric sections which fit together along the length of the carrier. The pusher plate is a disk currently made from 17-4-PH steel, heat treated to a Rockwell hardness R_c 45 (the Rockwell hardness C test is similar to the Brinell hardness test but uses a small conic indentor and a lighter loading condition). R_c 45 corresponds to a BHN of about 420. The obturator is made from the same material as the carrier.

The purpose of the carrier is to prevent the rod from balloting (hitting the sides) while passing through the barrel of the gun. The carrier splits apart after exiting the muzzle of the gun as the result of aerodynamic forces acting on beveled front-end sections. This reduces the drag on the projectile and allows the projectile (penetrator) to stabilize in free flight.

The pusher plate absorbs the setback forces of the gun upon launching the projectile. It also keeps a uniform pressure applied across the rear surface of the carrier and penetrator.

The obturator provides a gas seal to prevent the gases produced by the burning propellant from escaping in the forward direction while the sabot assembly is within the gun barrel. It also serves to push the sabot assembly through the gun tube.

The principal reason for using the sabot assembly is that it simplifies launching penetrators which vary widely in size without having to change the gun system. Figure 4 shows a drawing of a typical sabot assembly. An exploded view is shown in Figure 5.

The mass of the entire launch package (penetrator plus sabot assembly) is needed to determine the proper powder curve to consult when determining the amount of propellant required to achieve a particular striking velocity. This value will also act as a check on the other mass values recorded since the sum of the mass of the individual parts should be close to the value of the total mass. Figure 6 is a schematic of the launch package.

The data to be recorded with respect to the sabot assembly involve the following:

(1) the mass of the carrier,
(2) the mass of the pusher plate,
(3) the mass of the obturator, and
(4) the mass of the launch package.

It is also advisable to measure the diameter of the carrier and the diameter of the obturator.

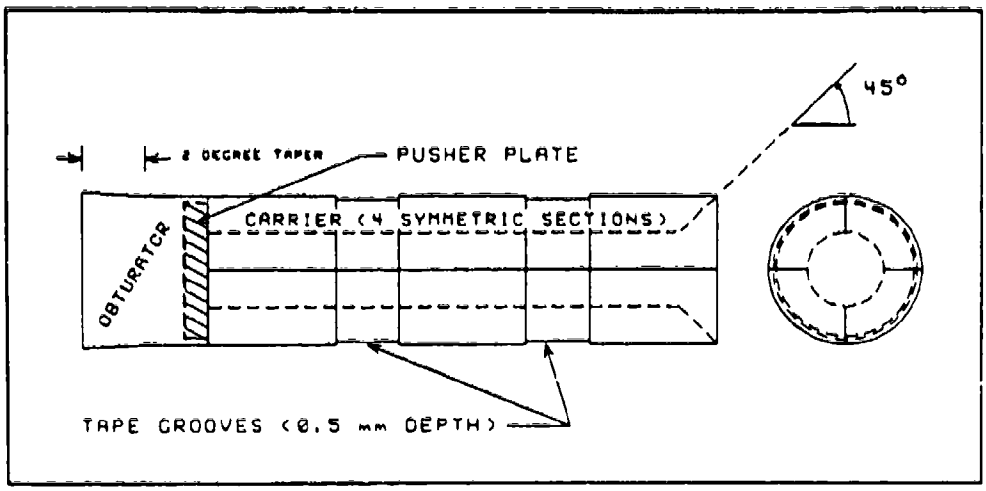

Figure 4. Diagram of a Typical Sabot Assembly.

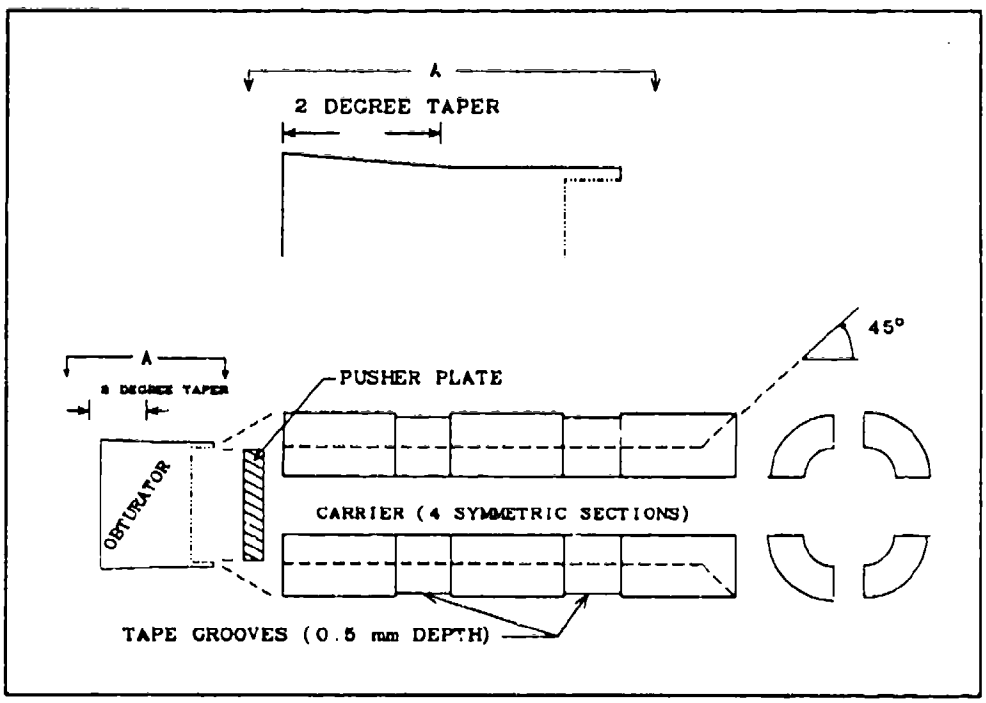

Figure 5. Exploded View of Sabot Assembly.

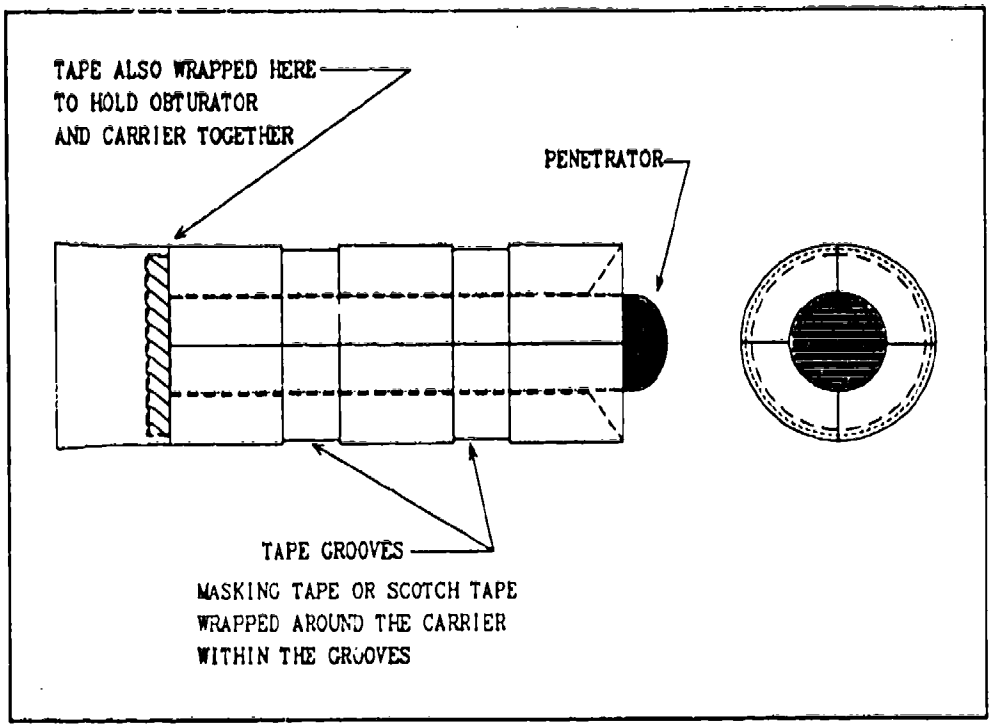

Figure 6. The Launch Package.

3.4 Selecting a Striking Velocity. The first step in determining an initial striking velocity for a particular penetrator and target configuration is to estimate the ballistic limit (the highest striking velocity which will result in a zero residual velocity) (see the last part of this section for a method for estimating the ballistic limit velocity). The first striking velocity should be about 250 m/s above the estimated ballistic limit (or the highest velocity obtainable).

If the result is a penetration (sometimes referred to as a partial penetration), then increase by another 250 m/s (or as high as possible). If the result was a perforation, then select the midpoint between that striking velocity and the estimated ballistic limit or the highest partial (if it is greater than the estimated ballistic limit). Continue this procedure until several perforations with small impact yaw and with measured striking and residual velocities have been achieved. It is desirable that at least one shot result in a low residual velocity (below 400 m/s).

The accuracy in determining the actual ballistic limit increases as the difference between the highest penetration and the lowest perforation (sometimes referred to as a complete

penetration) decreases. Because of differences between impact conditions (e.g., penetrator yaw relative to target orientation on impact), it is possible to have a penetration occur at a velocity higher than that of a perforation. Refer to Sections 8.2 and 8.3 for an explanation of how to handle this situation.

A method for estimating the ballistic limit a priori is given in Lambert (1978). This method is the following. Set $z = \frac{T\,[\sec(\theta)]^{0.75}}{D}$, where T is the target thickness, D is the penetrator diameter, θ is the target obliquity, and sec is the secant function (= 1/cos(θ)). The ballistic limit velocity for RHA targets can be estimated from the following:

$$V_L = 4{,}000 \left(\frac{L}{D}\right)^{0.15} \sqrt{\frac{\left(z + e^{-z} - 1\right) D^3}{M}} \ ,$$

where M is the penetrator mass, and the units for L, D, and T are centimeters, M in grams, and V_L in m/s. The value 4,000 is related to RHA as the target material. For other target materials, a different value should be used. For aluminum targets (density of 2.77 g/cc), a suggested value is 1,750.

A discussion of the rationale behind these equations is given in Zukas et al. (1982).

3.5 Determining Time Delays. After a striking velocity has been selected, it is necessary to calculate the proper time delays between the trigger screen being activated and the x-ray tubes being pulsed. It is desirable to have the x-ray tubes flash when some part of the penetrator is directly in front of the x-ray tube as it flashes. For station 1, it is necessary to determine the distance along the shot line from the trigger screen to a point in front of the x-ray tubes at station 1. At station 2, the required distance is the distance between the x-ray tubes of station 1 and those of station 2. The time delays may then be calculated from one of the following equations:

$$\text{Time Delay } (\mu s) = 25{,}400 \text{ Distance (in) / Velocity (m/s)},$$
$$= 1{,}000 \text{ Distance (mm) / Velocity (m/s)}.$$

Calculating time delays for the stations behind the target is more difficult because the residual velocity must be estimated. A quick estimate may be made from solving the following equation:

$$V_r = \sqrt{V_s^2 - V_L^2} ,$$

where V_r is the residual velocity, V_s is the striking velocity, and V_L is the estimated ballistic limit (see Section 3.5 for a method to estimate the ballistic limit). Then the time delays may be calculated in the same manner as in front of the target but using V_r rather than V_s.

Generally, it is better to use a larger value for the distance than the distance between adjacent x-ray tubes at stations 3 and 4 to calculate that time delay, unless those tubes are well separated—the limitation is determined by the size of the x-ray film. However, care must be taken when the target is at an oblique angle because as the residual velocity approaches 0, the residual penetrator tends to exit the rear of the target at angles which approach 90° (normal) to the rear surface of the target. If the target is tilted forward (top toward the gun), the residual penetrator flies upward, away from the original shot line, downward if the target is tilted backward. Sometimes the deviation angle from the shot line (exit angle) is greater than the angle of obliquity—observed with HHA targets. Therefore, account must be taken of the relative position of the x-ray tube, the likely location of the residual penetrator based on the vertical component of the residual velocity, and the x-ray film location in order to insure capturing the image on the film.

3.6 Selecting the Amount of Propellant. The type of propellant and the amount should be recorded.

Variations in striking velocity are achieved by varying the amount of propellant that is packed in the cartridge before loading the gun. The amount of propellant depends mainly on the type of propellant used (that is, its burning rate) and on the mass of the launch package (sabot assembly plus penetrator).

The relationship between the striking velocity and the amount of propellant needed for a particular launch mass is reasonably linear over a wide range of velocities (typical powder

curves are shown in Figures 7 and 8). Therefore, a powder curve can be established by firing two or three shots. The curve can then be used to estimate the propellant needed for a particular shot. For a particular test series, points are added to the powder curve as the test progresses and may mean that the curve must be redrawn to reflect actual conditions.

There are a number of factors involved, any of which will affect the powder curve. One of these factors is the effectiveness of the sabot/bore interface providing a good seal so that the burning propellant gases do not bypass the launch package while traveling within the barrel. This is affected by the wear on the bore caused by each shot and by the diameter of the sabot assembly. Another factor is how well the volume of the cartridge case not taken up by the propellant is packed (the burning rate of the propellant varies directly with the pressure it experiences).

3.7 Witness Pack/Panel. Information about the behind target fragment pattern must sometimes be recorded (depends on the purpose of the test). This information involves not only the distribution pattern of the fragments but also the mass and velocity of individual fragments. A witness pack or panel placed behind the target is frequently used to obtain this information.

It is possible to obtain this information from flash radiographs if orthogonal views are made behind the target—not easily done with oblique angle targets. This method has more problems associated with it than the witness pack method and is not frequently used other than to obtain the mass and velocity of the residual penetrator (Arbuckle, Herr, and Ricchiazzi 1973; Zook and Merrit 1983).

A single panel placed behind the target will provide the distribution pattern of the fragments and allows estimating the size of individual fragments from the size of the hole made in the panel. Estimates of the velocity and the mass of individual fragments can be made by using a witness pack rather than a single panel. Estimates of the mass and velocity can then be made by examining the size of the hole and the depth within the witness pack that a fragment produces. The evaluation of the witness pack for any particular shot is quite tedious and usually requires quite a bit of time. Therefore, it is used only when required for a

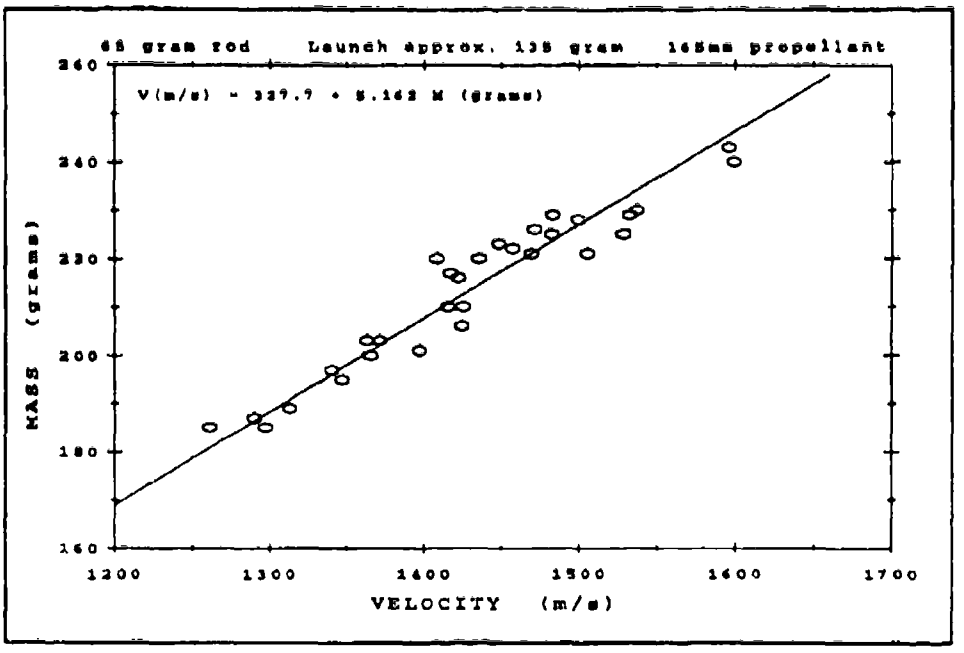

Figure 7. Sample Powder Curve for 165-mm Propellant.

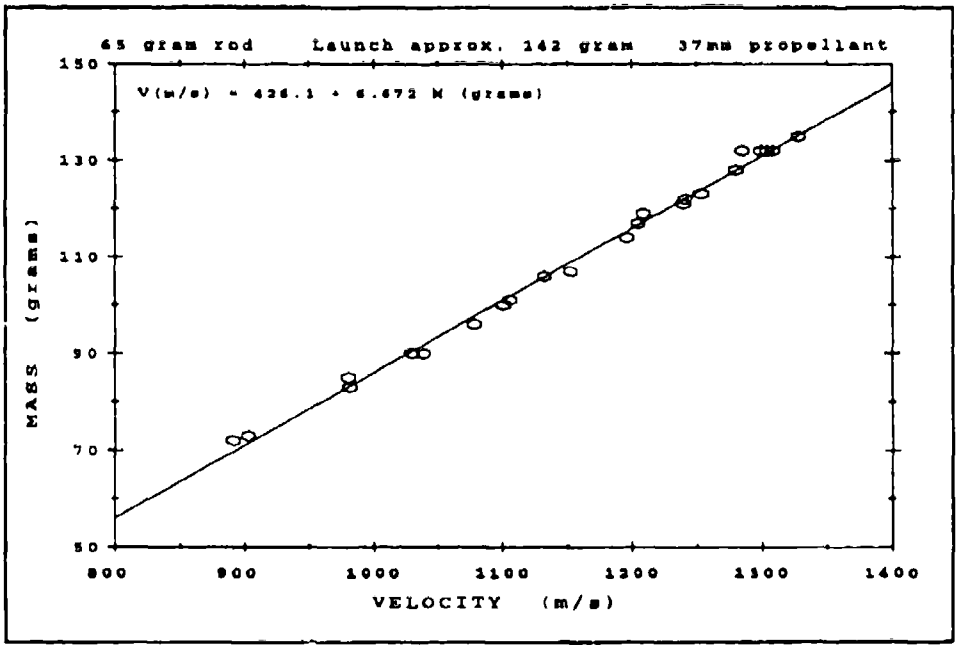

Figure 8. Sample Powder Curve for 37-mm Propellant.

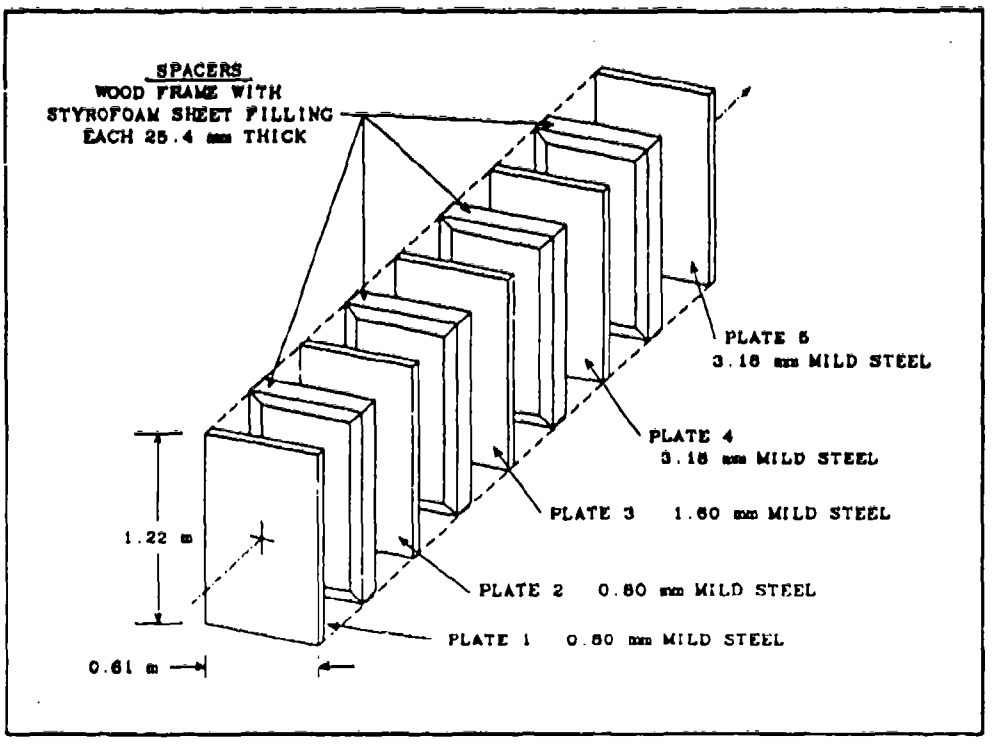

Figure 9. Typical Witness Pack.

particular program. Figure 9 shows a breakout of the components which make up the typical witness pack which is used for small-caliber (up through 25 mm) penetrator shots.

4. THE EVENT

4.1 Projectile in Flight. Sabots are used in production munitions when subcaliber penetrator (the penetrator diameter is less than the gun bore diameter) packages are fired. In this case, the penetrator must be stabilized in flight. This is usually achieved by designing the penetrator with tail fins. Stabilization is sometimes achieved by spinning the penetrator (projectile). Spin stabilization does not work for large L/D subcaliber penetrators (L/D > ~10).

For terminal ballistic research purposes, the distance between gun and target is short (less than 100 ft in interior ranges). Fin or spin stabilization cannot be achieved in a short flight distance. So, the sabot assembly is designed to give a large likelihood of minimal yaw (and pitch) to the rod penetrator. While the projectile is travelling down the gun barrel, the pusher plate is the principal stabilizer. The carrier is designed with a 45° beveled forward edge

(beveled inward) so that, exterior to the gun, the aerodynamic forces acting on the bevel will force the petals of the carrier to separate early in flight. In some cases, sabot separation is accelerated by firing through a thin sheet of foam, although passing through the foam often has a destabilizing effect.

The pusher plate follows along behind the penetrator and usually impacts the target at the entrance hole made by the penetrator. Analysis of the appearance of the entrance hole should take this into account. If it is desirable to eliminate the effect of the pusher plate impact, a deflector set up in front of the target will cause the pusher plate to deviate from the shot line. One method is to position the edge of a metal block so that the pusher plate clips the block. A method which has been tried is to use a metal plate with a hole large enough to allow the penetrator to pass through but not large enough for the pusher plate. This method is not generally successful because the penetrator becomes destabilized in passing through the hole, even though care is taken to align the hole with the shot line.

4.2 Impact. At medium to high striking velocities (above a few hundred meters per second) impact, metal penetrators impacting metal targets produce a brilliant light source during the penetration process. For this reason, optical cameras cannot be used to record the actual penetration process. That is why ballisticians have resorted to flash radiographs. The film used in the flash radiograph is protected from exposure to the light source by being placed in a cassette which is made from either wood or cardboard. The x-rays can easily penetrate through the film cassette and expose the film (generally, the exposure is enhanced by using an image intensifier screen directly in front of the film). Images are formed whenever the x-ray radiation is attenuated by absorption in intervening material such as the metal penetrator or metal target.

Metallic penetrators which strike "soft" metallic targets such as 2S-O aluminum (~BHN 25) can deform but do not lose mass to the penetration process at low to moderate striking velocities (under 1,000 m/s). This mode of penetration is called constant mass penetration. If the penetrator has a pointed nose, there might not be any observable deformation of the penetrator, in which case, the penetration is that of a rigid body.

When penetrator mass does not contribute directly to penetration, the penetrator is said to have eroded. Erosion may occur at high striking velocities for impacts against "soft" targets and is likely to occur at all striking velocities above about 100 m/s when the penetrator impacts on "hard" targets such as RHA (BHN > 200). The residual penetrator may be reduced to as little as one-tenth of the originally mass (and length) when penetrating thick targets as illustrated for a tungsten alloy L/D = 15 penetrator in Figure 10. Below the residual penetrators in the figure is the corresponding profile of the hole made in the target. Below 500 m/s striking velocity, the dimple made in the target appears to be the result of having performed a Brinell hardness test, yet the penetrator will have lost up to 50% of its length, depending on the impact velocity. Above 1,500 m/s striking velocity (not shown), WA and DU penetrators impacting thick RHA are eroded to less than one diameter in length for all L/D > 1/8. Recent experimental data suggest that penetrator disks of L/D ≤ 1/8 do not erode if they impact flat on.

When erosion occurs, penetrator material forced to flow radially and constrained by target cavity walls will be diverted backward. Conceptually, the penetrator turns inside out. Generally, the eroded mass breaks up into small particles and is not recoverable. Sometimes the mass forms a liner along the sides of the hole. For some penetrator materials (e.g., tungsten-tantalum and DU), a recoverable tube is formed at moderate striking velocities. For some penetrator materials interacting with "hard" targets, the penetrator may fracture—breaking up into small pieces—rather than "eroding." In other cases, the residual penetrator may be bent into an S shape if it is too ductile.

One factor which affects penetration performance is the orientation of the penetrator relative to the flight path. In general, maximum performance occurs when the penetrator is aligned with the flight path. It is said to have yaw when it is not aligned. In Roecker and Grabarek (1986), data are presented for an L/D = 30 tungsten alloy (W6 which is 94%W) impacting laminated and solid RHA targets. For normal impact at a nominal 1,340 m/s and 1,500 m/s, penetration is reduced as in the following.

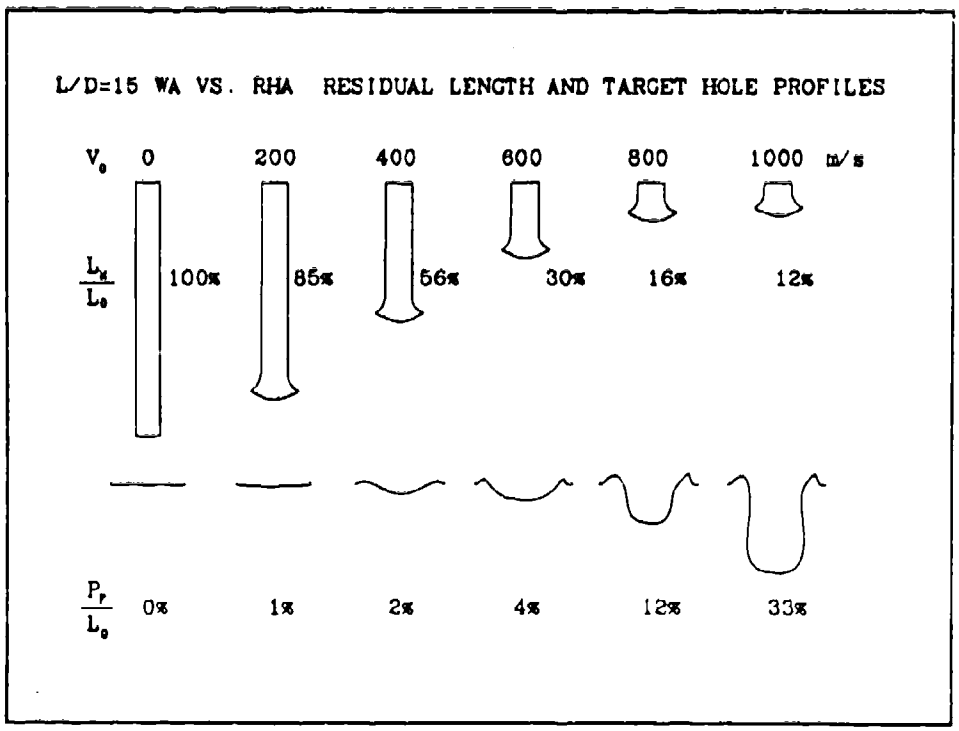

Figure 10. Erosion of Tungsten Alloy Penetrators Impacting RHA.

yaw angle (%)	% of penetration at 0° yaw
0	100
1	98
2	91
3	81
4	71

Data are also shown for oblique impacts of 60°, 65°, and 70.5°. These data suggest that if the pitch (yaw angle in the vertical plane) of the penetrator is away from the target surface (effectively increasing the obliquity), penetration is degraded quite rapidly. Penetration is not degraded as rapidly when the pitch is into the target (effectively reducing the obliquity). Taking the 65° obliquity case, for example, penetration is about 79% with a pitch of -1.5° or +3.0° where the minus pitch is away from the target. For the 70.5° obliquity, penetration is degraded very little for pitch angles from -0.5° to +2.0°.

For normal impact (0° obliquity), an explanation for the effect of yaw on penetration performance is presented in Bjerke et al. (1991). They present evidence to support the theory that a critical yaw angle exists for each penetrator/target configuration. For yaw angles less than the critical yaw angle, there is no degradation in penetration performance. The critical yaw angle is that angle of yaw which allows the side of the penetrator to interact with the wall of the cavity being formed. The equation to compute this critical yaw angle (attributed to Silsby, Roszak, and Giglio-Tos 1983) is as follows:

$$\gamma_{cr} = \sin^{-1}\left[\frac{D_h - D_p}{2L}\right], \tag{1}$$

where D_h is the entrance diameter of the hole in the target (measured in the plane of the original target surface), D_p is the penetrator diameter, and L is the penetrator length.

The hole diameter can be computed from the ratio D_h/D_p, which can be approximated by the following equation:

$$\frac{D_h}{D_p} \approx 1 + \frac{V}{3} + \frac{V^2}{8}. \tag{2}$$

The equation given in the report differs primarily in the value calculated for V = 0, which is 1.1524 in the report rather than 1. V represents the striking velocity in kilometers per second. Since the hole diameter in the target is dependent on material properties of both the penetrator and the target, Equation 2 applies to WA vs. RHA only. A more general solution, which is dependent on material properties, is the following:

$$\frac{D_h}{D_p} = \sqrt{1 + \frac{(\lambda - 1)\rho_p (V_0 - U_0)^2 + \rho_t U_0^2}{2H}}, \tag{3}$$

$$U_0 = \frac{V_0 - \sqrt{(\mu V_0)^2 + 2(1 - \mu^2)\frac{H - Y}{\rho_p}}}{1 - \mu^2} \quad \text{for } \mu \neq 1, \tag{4}$$

$$U_0 = \frac{V_0}{2} - \frac{H - Y}{\rho_p V_0} \quad \text{for } \mu = 1 , \tag{5}$$

where V_0 is the striking velocity, ρ_p and ρ_t are the penetrator and target densities, respectively, H is the target resistance, Y is the penetrator flow stress, $\mu^2 = \rho_t/\rho_p$, and $\lambda = 3.6$ (λ depends to some extent on the size of the hole made in the target). For example, using MKS units, let $V_0 = 1{,}500$ m/s, $\rho_p = 17{,}300$ kg/m^3, $\rho_t = 7{,}850$ kg/m^3, $H = 5.5 \times 10^9$ pascals, and $Y = 1.9 \times 10^9$ pascals, then $\mu^2 = 0.4538$, $U_0 = 701$ m/s, and $D_h/D_p = 1.99$. With Equation 2, the result is 1.78 and using the equation from the report, the result is 1.95 for V = 1.5 km/s. Neither Equation 2 or 3 accurately reflects the hole diameter obtained experimentally at low striking velocities (below ~400 m/s for WA vs. RHA).

Returning to Bjerke et al. (1991), once the critical angle is computed, the degradation in penetration can be computed from the following:

$$P' = P_{max} \cos\left(\frac{11.46\,\gamma}{\gamma_{cr}}\right), \tag{6}$$

where P_{max} is the penetration for a WA penetrator with yaw angles less than γ_{cr}. (Note: The cosine function should be evaluated with the argument in degrees.) For a DU penetrator, the equation to be used is as follows:

$$P' = P_{max} \cos\left(\frac{9.45\,\gamma}{\gamma_{cr}}\right). \tag{7}$$

Nonzero yaw will also affect the performance against finite thickness targets. The yaw on impact as observed from the flash radiographs in experimental work should be taken into account when deciding what residual velocity data should be used in evaluating a velocity ballistic limit. What adjustments can be made to the residual velocity to make it equivalent to what would be obtained with 0° yaw has not been determined yet.

5. RADIOGRAPHIC ANALYSIS

5.1 The Magnification Factor (K Factor). The x-ray radiation which is produced by the x-ray tube emanates as though from a point source. That is, the space that the radiation travels in appears to be a cone with the tip of the cone (apex) located at the source end of the x-ray tube. Since the projectile is located between the x-ray tube and the film at the time the x-ray tube flashes, the image that is produced on the film is larger than the projectile. The closer the projectile is to the film, the less will be the magnification. From the geometry of the range setup, the magnification factor (K factor) can be calculated from distances measured on the film. These values can then be multiplied by the K factor to produce adjusted values which represent the actual location of the projectile in space.

The following is a derivation of the K factor based on the diagrams shown in Figures 11 and 12. Figure 11 represents one station in which there are two x-ray tubes—one horizontal and one vertical. A three-dimensional view is shown in Figure 12 (Grabarek and Herr 1966).

Let X_{hf} and Y_{hf} ⇒ X-ray tube head to film distances in X and Y directions, respectively,

X_{ff} and Y_{ff} ⇒ Fiducial line (z-axis direction) to the orthogonal film plane distance.

X_1 and Z_h ⇒ Coordinates of an image point on the horizontal (X-Z plane) film.

Y_1 and Z_v ⇒ Coordinates of a corresponding image point on the vertical (Y-Z plane) film.

X_p, Y_p, and Z_p ⇒ Actual physical coordinates of the point in space.

The origin of the coordinate system is located at the point of intersection of both film planes with the X-Y plane in which both x-ray tubes are located. The following equations are derived based on the geometry:

$$\frac{Y_{hf}}{X_1 - X_{ff}} = \frac{Y_p}{X_1 - X_p}, \tag{8}$$

$$\frac{X_{hf}}{Y_1 - Y_{ff}} = \frac{X_p}{Y_1 - Y_p}, \tag{9}$$

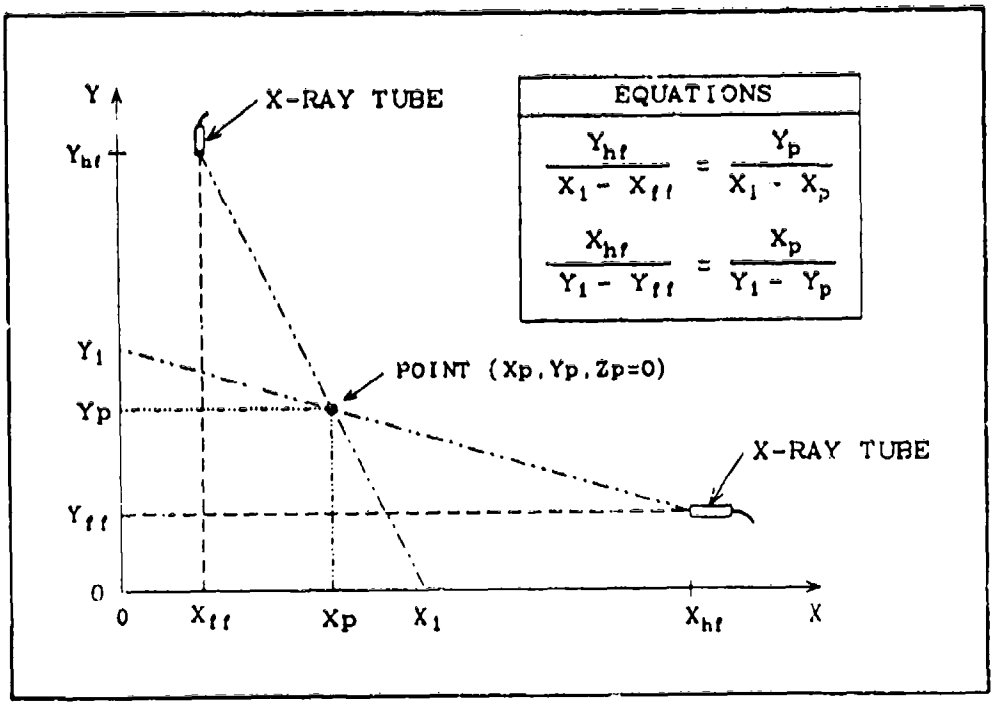

Figure 11. K-Factor Derivation Schematic (Two-Dimensional View).

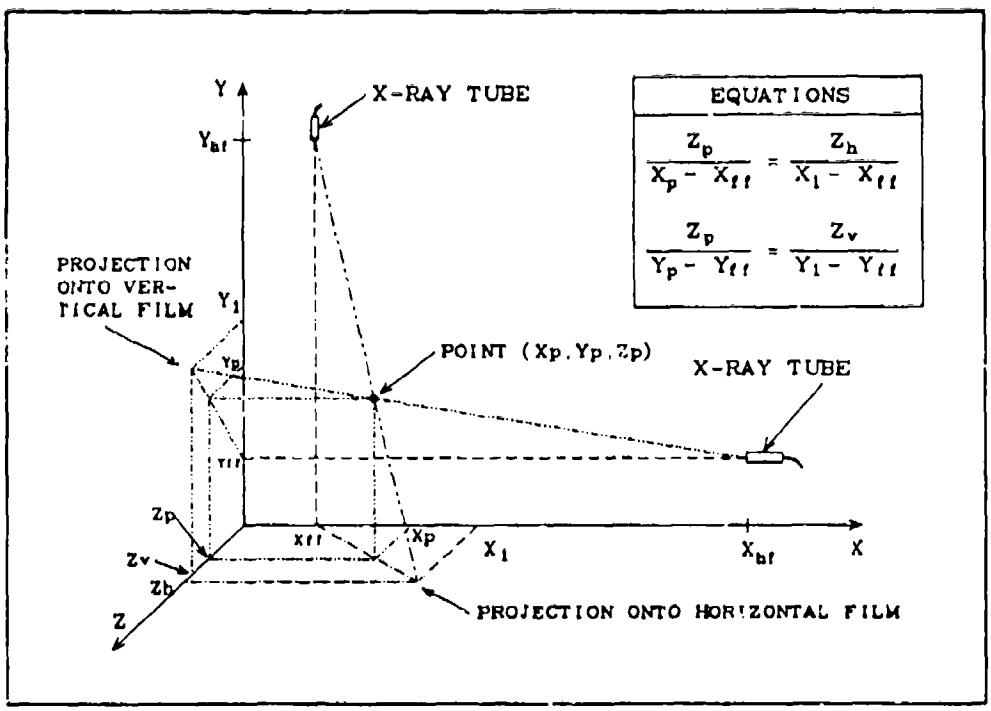

Figure 12. K-Factor Derivation Schematic (Three-Dimensional View).

$$\frac{Z_p}{X_p - X_{ff}} = \frac{Z_h}{X_1 - X_{ff}} , \tag{10}$$

$$\frac{Z_p}{Y_p - Y_{ff}} = \frac{Z_v}{Y_1 - Y_{ff}} . \tag{11}$$

Solving Equation 8 for X_p and substituting in Equation 9 yields the following:

$$\frac{X_{hf}}{Y_1 - Y_{ff}} = \frac{Y_{hf} X_1 + Y_p X_{ff} - Y_p X_1}{Y_{hf} Y_1 - Y_{hf} Y_p} . \tag{12}$$

Cross multiplying, expanding, and then solving for Y_p,

$$Y_p = \frac{X_{hf} Y_{hf} Y_1 + Y_{hf} Y_{ff} X_1 - Y_{hf} X_1 Y_1}{X_{hf} Y_{hf} + X_{ff} Y_1 + Y_{ff} X_1 - X_{ff} Y_{ff} - X_1 Y_1} . \tag{13}$$

The magnification factor in the Y-Z plane (vertical plane) can be defined as follows:

$$K_v = \frac{Z_p}{Z_v} , \quad \text{or using Equation 11,} \quad K_v = \frac{Y_p - Y_{ff}}{Y_1 - Y_{ff}} . \tag{14}$$

Replacing Y_p of Equation 14 with the right side of Equation 13 and collecting terms,

$$K_v = \frac{X_{hf} Y_{hf} - Y_{hf} X_1 + Y_{ff} X_1 - X_{ff} Y_{ff}}{X_{hf} Y_{hf} - (X_1 - X_{ff})(Y_1 - Y_{ff})} . \tag{15}$$

The magnification factor in the horizontal plane (X-Z plane) can be found in a similar manner. That is, solve Equation 8 for Y_p and substitute in Equation 9. Cross multiply, expand, and solve for X_p. Use Equation 9 to find an expression for K_h, which is as follows:

$$K_h = \frac{X_p - X_{ff}}{X_1 - X_{ff}} . \tag{16}$$

Substitute the expression for X_p to obtain the following:

$$K_h = \frac{X_{hf} Y_{hf} - X_{hf} Y_1 + X_{ff} Y_1 - X_{ff} Y_{ff}}{X_{hf} Y_{hf} - (X_1 - X_{ff})(Y_1 - Y_{ff})} . \tag{17}$$

It is easier to measure on the film the distances X_1-X_{ff} and Y_1-Y_{ff}. Therefore, let

$$X = X_1 - X_{ff} \text{ and } Y = Y_1 - Y_{ff} . \tag{18}$$

Then the vertical magnification factor may be expressed as follows:

$$K_v = \frac{Y_{hf}(X_{hf} - X_{ff}) - (Y_{hf} - Y_{ff}) X}{X_{hf} Y_{hf} - X Y} , \tag{19}$$

and the horizontal magnification factor is as follows:

$$K_h = \frac{X_{hf}(Y_{hf} - Y_{ff}) - (X_{hf} - X_{ff}) Y}{X_{hf} Y_{hf} - X Y} . \tag{20}$$

The sign convention is that the X distance is positive if further away from the vertical film plane than the fiducial line on the horizontal film and negative if the point is closer than the fiducial line. Similarly, the Y distance is positive if the point on the vertical film is further away from the horizontal film plane than the fiducial line on the vertical film and negative if closer.

If $X_{hf} = Y_{hf}$, $X_{ff} = Y_{ff}$, and $X = Y$, then the horizontal and vertical magnification factors have identical values. Assuming that X_{hf} and Y_{hf} are both 60 in and that X_{ff} and Y_{ff} are both 8 in, then $K_h = K_v = 0.8667$ when X and Y are both 0.

To make the adjustment to the X, Y, and Z values measured on the film, those values are multiplied by the appropriate K factor to obtain the coordinates of that point in the physical space bounded by the film planes and the respective x-ray tubes. The velocity can be

computed based on the distance calculated in physical space and the time delay between the x-ray tube flashes at adjacent stations. Also, the angle of travel can be determined.

The magnification factor is usually computed for only one x-ray station in front of the target and then used for all adjustments from film measurements to physical space coordinates. This x-ray station must have two tubes which are orthogonal to each other and an image of the projectile obtained in both film planes. For oblique angle impacts, it is not feasible to have a vertical x-ray tube at the station directly in front and the station directly in back of the target since the target blocks the view. The other reason that the magnification factor is computed only once is that the penetrator is assumed to exit the target in the same vertical plane as it entered the target and the magnification factor does not change.

From the film that was in the vertical plane, a point on the image is selected, which can be identified on the image from the film in the horizontal plane. For example, the center of the front end or a point can be assumed to be the center of mass. The distance from the fiducial wire image, which is parallel to the shot line, to the selected point is the Y value (positive if above the fiducial, negative if below). From the film that was in the horizontal plane, the X value is measured in the same way (positive if the point is further away from the vertical film than the fiducial wire image, and negative if closer). The values are substituted in Equation 19 to obtain the vertical magnification factor. The distances X_{hf}, Y_{hf}, X_{vf}, and Y_{vf} must, of course, be known and measured in the same units as used for X and Y. A typical value for K_v is 0.8667, as mentioned before.

5.2 Striking Velocity. Measurements on the radiographic film are made using a transparent plastic ruler which is calibrated in two hundredths of an inch (or 1/2 mm). Working with the film which was vertical at station 1, a point is selected which is located on the image of the projectile (for example, the center point of the front tip). Measurements are made with respect to the fiducial line images which were directly in front of the x-ray tube at station 1. The distance Y_1 is measured from the horizontal fiducial line image to the selected point on the projectile image. If the selected point is above the horizontal fiducial line, the measurement is positive, otherwise, it is negative. The Z_1 value is the measurement from the vertical fiducial line to the selected point on the projectile image. This value is positive if the selected point is further from the gun than the vertical fiducial line image, negative if closer.

The same procedure is followed for the images related to station 2 to obtain Y_2 and Z_2. Letting Z_{hs} represent the separation between stations 1 and 2 in the Z direction, K_v represent the magnification factor evaluated from the equation in Section 5.1, and Δt represent the time delay between the flashes at stations 1 and 2, the striking speed can be calculated as follows:

$$\Delta Y_d = K_v (Y_2 - Y_1) , \tag{21}$$

$$\Delta Z_d = K_v (Z_2 - Z_1) + Z_{hs} , \tag{22}$$

$$V_s = \frac{\sqrt{\Delta Y_d^2 + \Delta Z_d^2}}{\Delta t} , \tag{23}$$

where V_s is the striking speed. Strictly speaking, the X value from the horizontal film should be adjusted and included in Equation 23, but it has such little effect on calculating the velocity that it is neglected. Since measurements are usually done in inches, the result of Equation 23 must be divided by 12 to convert to feet, and since the time delay is usually recorded in microseconds, the result must be multiplied by 1,000,000. This will give the speed in feet per second. To convert feet per second to meters per second, the result must be multiplied by 0.3048. The conversion factor, 0.3048, is an exact value (i.e., no error is introduced in making the conversion).

5.3 Yaw and Pitch. It is unusual for the projectile to fly perfectly straight. The projectile is said to have pitch if it is tilted up or tilted down. It has yaw if it is turned sideways any amount with respect to the flight path. Sometimes, yaw is used in a loose sense and includes the pitch. In this case, the distinction is made between horizontal yaw and vertical yaw. The angle which the projectile's center axis makes with the flight line is called total yaw. How total yaw can be calculated from horizontal yaw and pitch will be shown later.

The method for determining the yaw or pitch from the film used in a system where there is certainty that the fiducial lines are aligned with respect to the gun, shc ne, and the x-ray tubes is as follows. A line is drawn either on the centerline of the projectile image or along

one edge and extended until it intersects a fiducial wire image which is perpendicular to the flight path direction. A protractor is then used for measuring the angle (in degrees) made by the intersection of the line drawn and the fiducial. For pitch, the angle is positive if the projectile is tilted up, negative if tilted down. For horizontal yaw, the angle is positive if the projectile is twisted to the right when looking toward the direction of travel and negative if to the left.

Accurate measurements of the yaw and pitch are dependent on how well the fiducial wires are aligned after installing the film cassettes. Extra care must be taken when installing the film cassettes because the fiducial wires frequently catch on the surface of the cassette and get misplaced. Also, the wire that is used is similar to piano wire and can develop kinks. This makes it difficult, when examining the x-ray film, to determine how the fiducial wire image would have been if the wire had been straight.

A method for determining the yaw and pitch which is independent of the fiducial lines is the following. Establish a point representing the center of mass on each image (see the next subsection for mathematically determining the location of the center of mass). Draw a straight line connecting the center of mass of each image. Draw a line parallel to the side of an image and determine the angle that this line makes with the line drawn through the centers of mass. This can be done with a protractor, or possibly more accurately, by measuring distances as shown in Figure 13 and calculating the arc tangent (easily done with a scientific calculator—arc tangent is usually abbreviated by ATN or by $\tan^{-1}$). An angle computed in radians can be converted to degrees by multiplying the value in radians by 180/3.14159 ($= 180/\pi$).

Yaw and pitch are important considerations when trying to analyze shots made against targets which are at oblique angles to the shot line (not perpendicular). Penetration performance may be enhanced slightly if the angle formed by the centerline of the projectile and the target impact surface is slightly less than angle of obliquity. Otherwise, penetration performance is degraded because there is more projectile area presented to the target. The longer the projectile, the more critical this is. The worst performance for long projectiles will occur when the projectile impacts sideways (90° yaw or 90° pitch for 0 obliquity targets).

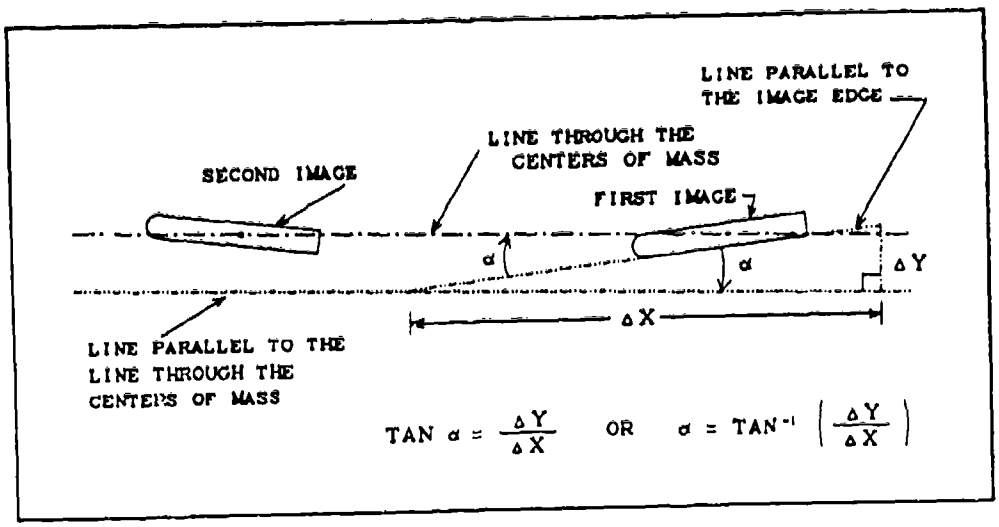

Figure 13. Pitch or Yaw Calculation Without Fiducial Wire Reference.

The total yaw angle may be computed from the two components—yaw and pitch. Figure 14 shows the identification of the angles. In this figure, the angle α is the pitch, the angle β is the horizontal yaw, and the angle γ is the total yaw angle (angular deviation of the nose of the penetrator from the flight path determined at the center of mass of the projectile). The trigonometric identities are as follows:

$$\text{TAN}(\alpha) = \frac{Y}{X}, \tag{24}$$

$$\text{TAN}(\beta) = \frac{Z}{X}, \tag{25}$$

and

$$\text{TAN}(\gamma) = \frac{\sqrt{Y^2 + Z^2}}{X}. \tag{26}$$

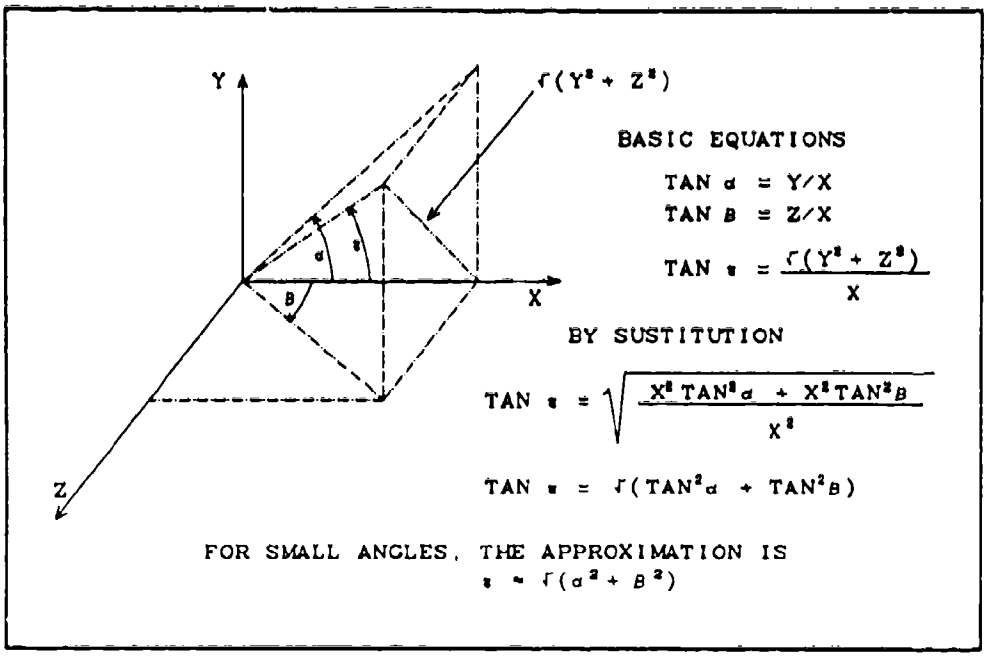

Figure 14. Combining Pitch and Yaw to Obtain Total Yaw Angle.

By substitution,

$$\mathrm{TAN}(\gamma) = \frac{\sqrt{(X\,\mathrm{TAN}(\alpha))^2 + (X\,\mathrm{TAN}(\beta))^2}}{X} . \qquad (27)$$

The X^2 may be extracted from the argument of the square root function which will cancel the X in the denominator. The result is as follows:

$$\mathrm{TAN}(\gamma) = \sqrt{(\mathrm{TAN}(\alpha))^2 + (\mathrm{TAN}(\beta))^2} . \qquad (28)$$

When the angles are small—less than 2°, the following approximation may be made;

$$\gamma = \sqrt{\alpha^2 + \beta^2} . \qquad (29)$$

For a description of the influence of the yaw angle on penetration performance, refer to Section 4.2.

5.4 Center of Mass. The center of mass of a physical object is the geometric point within the object which behaves as though all of the mass were concentrated at that point when the object is subjected to external forces. A more rigorous definition is the following:

> If an arbitrary set of forces acts on a rigid body, the center of mass of the body will move as if all of the mass and all of the forces were concentrated at the center of mass (Ference, Lemon, and Stephenson 1956).

For a sphere of uniform density (homogeneous) or a sphere made up of concentric shells, each shell made of material of uniform density, the center of mass is the center of the sphere. The center of mass for a right circular cylinder of uniform density is the midpoint (L/2, D/2), where L is the length and D is the diameter.

The center of mass of an object made up from several different geometric shapes can be found by first finding the center of mass of each individual geometric shape. Then the individual centers of mass are combined, as will be demonstrated in the following section contributed by Graham F. Silsby.

5.4.1 Location of the Center of Mass of a Hemispherical Nosed Right Circular Cylinder.

Symbols:
- L ⇒ overall length of rod
- D ⇒ diameter of rod
- m ⇒ mass
- ρ ⇒ density (assumes rod is of uniform density)
- v ⇒ volume
- z ⇒ distance measured from the tail end toward the nose.

Subscripts (see Figure 15):
- c ⇒ cylinder
- cm ⇒ center of mass
- i ⇒ ith term
- h ⇒ hemisphere.

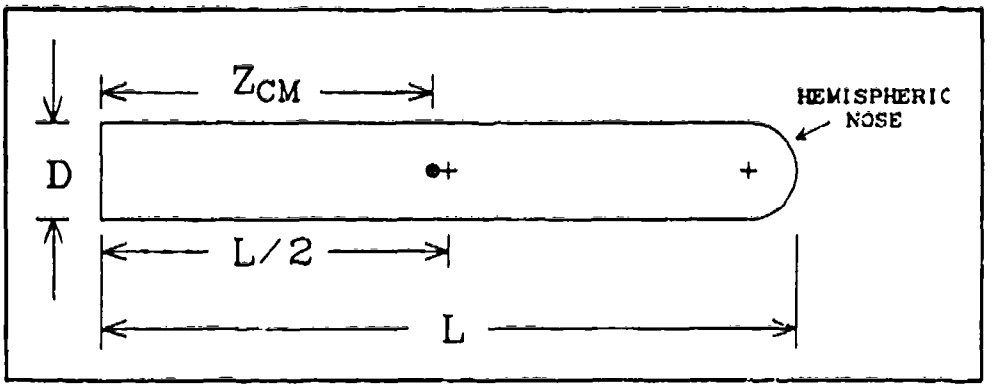

Figure 15. Location of Center of Mass of a Hemispheric Nose Rod.

Derivation: By definition, for any solid comprised of different geometric sections of uniform density,

$$z_{cm} = \frac{\sum z_i m_i}{\sum m_i} = \frac{\sum z_i \rho v_i}{\sum \rho V_i} = \frac{\sum z_i v_i}{\sum v_i},$$

where the subscript i denotes the ith section. For the right circular cylinder portion, the center of mass relative to its base (noting that L is the overall length of the heminosed rod) is as follows:

$$z_c = \frac{1}{2}\left(L - \frac{D}{2}\right).$$

The volume of the right circular cylinder portion is as follows:

$$v_c = \frac{\pi D^2}{4}\left(L - \frac{D}{2}\right).$$

For a hemisphere, the center of mass relative to its base is as follows (Oberg, Jones, and Holbrook 1979):

$$\frac{3}{8}\,\frac{D}{2}.$$

The center of mass of the hemispheric nose portion relative to the tail end of the rod is as follows:

$$z_h = L - \frac{D}{2} + \frac{3D}{16}.$$

The volume of the hemisphere is as follows:

$$v_h = \frac{2}{3}\,\frac{\pi D^3}{8} = \frac{\pi D^3}{12}.$$

Therefore,

$$z_{cm} = \frac{\frac{1}{2}\left(L - \frac{D}{2}\right)\frac{\pi D^2}{4}\left(L - \frac{D}{2}\right) + \left(L - \frac{D}{2} + \frac{3D}{16}\right)\left(\frac{\pi D^3}{12}\right)}{\frac{\pi D^2}{4}\left(L - \frac{D}{2}\right) + \frac{\pi D^3}{12}}.$$

Cancel out $\pi D^2/4$ and consolidate separate terms. Then,

$$z_{cm} = \frac{\frac{1}{2}\left(L - \frac{D}{2}\right)^2 + \left(L - \frac{5D}{16}\right)\frac{D}{3}}{L - \frac{D}{6}}.$$

Substituting D (L/D) for L and simplifying results in the following:

$$z_{cm} = D\left[\frac{\frac{1}{2}\left(\frac{L}{D} - \frac{1}{2}\right)^2 + \frac{1}{3}\left(\frac{L}{D} - \frac{5}{16}\right)}{\frac{L}{D} - \frac{1}{6}}\right],$$

which is valid for all $L/D \geq 1/2$.

Example: Let L = 195 mm and D = 6.5 mm so that L/D = 30. Then,

$$z_{cm} = 6.5\left[\frac{\frac{(29.5)^2}{2} + \frac{29.6875}{3}}{29.8333}\right] = 96.96\ .$$

Since L/2 = 195/2 = 97.5, the center of mass is 0.54 mm toward the tail end from the center point of the overall length. The following will show that for all L/D > 3, the center of mass is located very near D/12, behind the center point of the overall length.

Let $$\Delta = \left(\frac{L}{2} - z_{cm}\right).$$

Substituting the expression for z_{cm} and simplifying results in the following:

$$\Delta = D\left(\frac{\frac{L}{D} - \frac{1}{4}}{12\frac{L}{D} - 2}\right) = D\left(\frac{1 - \frac{1}{4\frac{L}{D}}}{12 - \frac{2}{\frac{L}{D}}}\right).$$

In the limit, as L/D goes to infinity, Δ goes to D/12. This is shown in Table 4.

For short hemispheric nose rods, the center of mass is near the midpoint of the overall length. For long rods, the center of mass is near the midpoint of the cylindrical portion of the rod. The cylinder midpoint is always D/4 behind the center of the overall length. Therefore, the displacement between the center of mass and the overall midpoint increases with overall length

5.4.2 Location of the Center of Mass of a Conical Nosed Right Circular Cylinder.

Symbols:
- L ⇒ overall length of rod
- D ⇒ diameter of rod
- N ⇒ length of the conic nose (cone height)
- m ⇒ mass
- ρ ⇒ density (assumes rod is of uniform density)

Table 4. Displacement (Δ) of Center of Mass to the Rear of the Midpoint of the Overall Length of a Hemispheric Nosed Rod

L/D	Δ
1/2	0.0625 D
1	0.0750 D
2	0.0795 D
3	0.0809 D
4	0.0815 D
5	0.0819 D
10	0.0826 D
20	0.0830 D
30	0.0831 D
40	0.0832 D
50	0.0832 D
∞	0.08333333... D

v ⇒ volume

z ⇒ distance measured from the tail end toward the nose.

Subscripts (see Figure 16): c ⇒ cylinder

cm ⇒ center of mass

i ⇒ ith term

cc ⇒ circular cone.

Derivation: For the right circular cylinder portion, the center of mass relative to its base (noting that L is the overall length of the conic-nosed rod) is as follows:

$$z_c = \frac{L - N}{2}.$$

The volume of the right circular cylinder portion is as follows:

$$v_c = \frac{\pi D^2}{4}(L - N).$$

For a cone, the center of mass relative to its base is as follows (Gray 1972):

$$\frac{N}{4}.$$

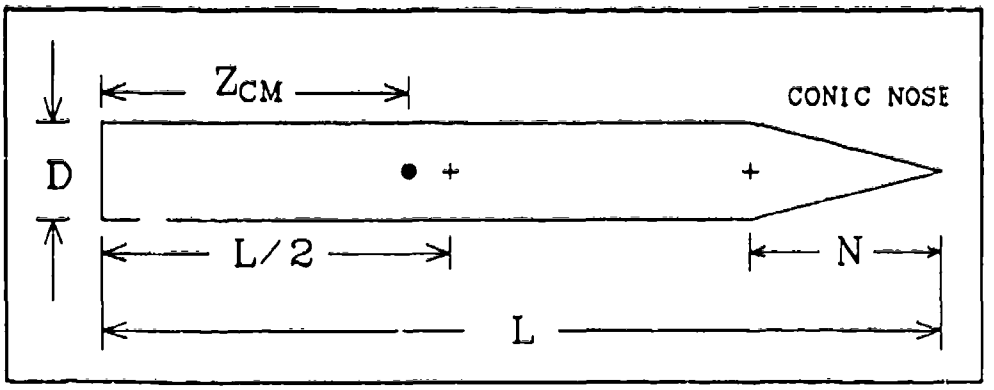

Figure 16. Location of Center of Mass of a Conic Nose Rod.

The center of mass for the conic nose portion relative to the tail end of the rod is as follows:

$$z_{cc} = (L - N) + \frac{N}{4} = L - \frac{3N}{4} .$$

The volume of the cone is as follows:

$$v_{cc} = \frac{\pi D^2}{4} \frac{N}{3} .$$

Therefore,

$$z_{cm} = \frac{\frac{L - N}{2}\left(\frac{\pi D^2}{4}(L - N)\right) + \left(L - \frac{3N}{4}\right)\frac{\pi D^2}{4}\frac{N}{3}}{\frac{\pi D^2}{4}(L - N) + \frac{\pi D^2}{4}\frac{N}{3}} .$$

Cancel out $\pi D^2/4$ and consolidate separate terms. Then,

$$z_{cm} = \frac{6L^2 - 8LN + 3N^2}{12L - 8N} .$$

which is valid for all $L > N$ and for $L = N$ if $N > 0$. Let $\Delta = \left(\frac{L}{2} - z_{cm}\right)$.

Substituting the expression for z_{cm} and simplifying results in the following:

$$\Delta = \frac{4LN - 3N^2}{12L - 8N}.$$

Dividing the numerator and denominator by D results in the following:

$$\Delta = \frac{4\frac{L}{D}N - 3\frac{N^2}{D}}{12\frac{L}{D} - 8\frac{N}{D}}.$$

In the limit, as L/D goes to infinity, Δ goes to $\frac{N}{3}$;

as N goes to 0, Δ goes to 0; and

as L goes to N, Δ goes to $\frac{N}{4}$.

Some additional values for Δ are listed in Table 5.

5.4.3 Location of the Center of Mass of a Conical Frustum Nosed Right Circular Cylinder. For rods which have conic-shaped noses, the nose is not usually a full cone. Generally, the tip end is cut off. The name given to that geometry is frustum of the cone. This is illustrated in Figure 18.

Symbols: L ➡ overall length of rod

D ➡ diameter of rod

n ➡ length (height) of the frustum of the cone

d ➡ diameter of the tip end of the frustum

m ➡ mass

ρ ➡ density (assumes rod is of uniform density)

Table 5. Displacement (Δ) of Center of Mass to the Rear of the Midpoint of the Overall Length of a Conical Nosed Rod for Selected L/D

	Δ						
L/D	general	N=D	N=2D	N=3D	N=4D	N=5D	N=10D	N=20D
1	$\frac{4N-3N^2/D}{12-8N/D}$	0.25D	—	—	—	—	—	—
2	$\frac{8N-3N^2/D}{24-8N/D}$	0.31D	0.50D	—	—	—	—	—
3	$\frac{12N-3N^2/D}{36-8N/D}$	0.32D	0.60D	0.75D	—	—	—	—
4	$\frac{16N-3N^2/D}{48-8N/D}$	0.32D	0.62D	0.88D	1.00D	—	—	—
5	$\frac{20N-3N^2/D}{60-8N/D}$	0.33D	0.64D	0.92D	1.14D	1.25D	—	—
10	$\frac{40N-3N^2/D}{120-8N/D}$	0.33D	0.65D	0.97D	1.27D	1.56D	2.50D	—
20	$\frac{80N-3N^2/D}{240-8N/D}$	0.33D	0.66D	0.99D	1.31D	1.62D	3.12D	5.00D
30	$\frac{120N-3N^2/D}{360-8N/D}$	0.33D	0.66D	0.99D	1.32D	1.64D	3.21D	6.00D
40	$\frac{160N-3N^2/D}{480-8N/D}$	0.33D	0.66D	0.99D	1.32D	1.65D	3.25D	6.25D
50	$\frac{200N-3N^2/D}{600-8N/D}$	0.33D	0.66D	1.00D	1.32D	1.65D	3.27D	6.36D
∞	$\frac{N}{3}$	0.33D	0.67D	1.00D	1.33D	1.67D	3.33D	6.67D

v ➡ volume

z ➡ distance measured from the tail end toward the nose.

Subscripts (see Figure 17): c ➡ cylinder

cm ➡ center of mass

i ➡ ith term

f ➡ frustum of the cone.

The center of mass of the cylindrical portion is $\frac{L-n}{2}$.

The volume of the cylindrical portion is $\frac{\pi D^2}{4}(L-n)$.

The center of mass of a frustum of a cone along the center axis is as follows (Gray 1972):
The center of mass of the frustum nose relative to the base of the rod is as follows:

$$z_f = L - n + \frac{n}{4}\frac{((D+d)^2 + 2d^2)}{((D+d)^2 - Dd)}.$$

The volume of the frustum of a circular cone is as follows:

$$v_f = \frac{\pi n}{3}\left(\frac{D^2 + Dd + d^2}{4}\right).$$

Setting

$$Q_1 = \frac{L-n}{2}\left(\frac{\pi D^2}{4}(L-n)\right)$$

and

$$Q_2 = \left(L - n + \frac{n}{4}\frac{((D+d)^2 + 2d^2)}{((D+d)^2 - Dd)}\right)\frac{\pi n}{3}\left(\frac{D^2 + Dd + d^2}{4}\right),$$

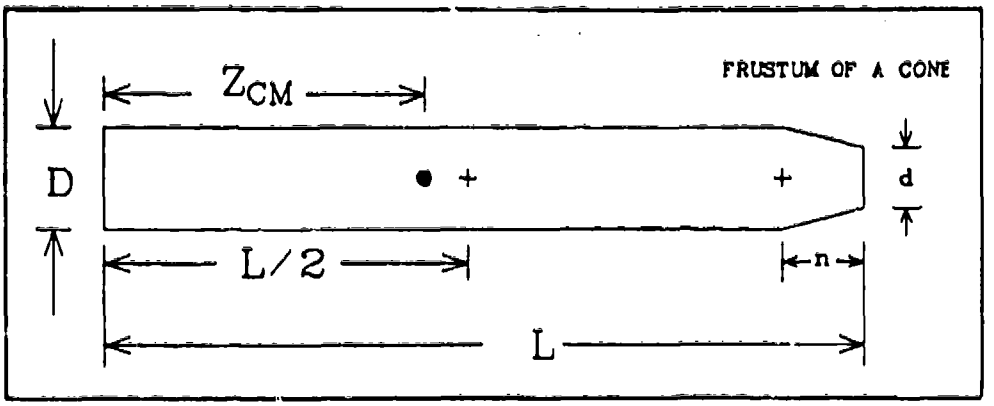

Figure 17. Location of Center of Mass of a Conic Frustum Nose Rod.

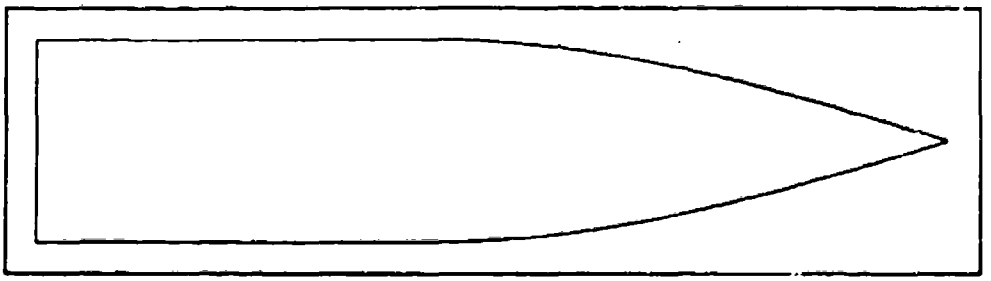

Figure 18. Ogival Nose Shape.

the center of mass of the conic frustum nose rod is as follows:

$$z_{cm} = \frac{Q_1 + Q_2}{\frac{\pi D^2}{4}(L - n) + \frac{\pi n}{3}\left(\frac{D^2 + Dd + d^2}{4}\right)}.$$

Expanding and consolidating terms results in:

$$z_{cm} = \frac{6L^2D^2 + (d-D)nL(8D + 4d) - n^2(3D + d)}{12D^2L + n(d - D)(8D + 4d)}.$$

This equation may be evaluated for a particular case. However, the larger the value of d, the closer the center of mass point will be to the midpoint than had the nose been the full cone. In other words, the value from the table for the full cone represents an extreme with respect to the value for any frustum of the cone.

A similar analysis may be made for a penetrator with an ogival nose. The equation for the ogive of a penetrator with nose length N is as follows:

$$r = R\cos\left(\frac{\pi n}{2N}\right),$$

where R is the maximum radius of the penetrator (at the base of the nose) and r is the distance from the center axis of the penetrator to the curved surface at point n where n = 0 at the base and n = N at the tip (see Figure 18 for an example of an ogival nose penetration shape).

To a close approximation, the curvature of the ogive is given by the arc of a circle of radius R_{circ} where the center of the circle lies on an extended line from the base of the nose section. The radius of the circle is given by the following:

$$R_{circ} = \frac{R^2 + N^2}{2R},$$

as shown in Figure 19.

5.5 Penetrator Residual Velocity. In general, more effort is required to determine the residual velocity than the striking velocity. The projectile has a definite known shape, and the image on the film in front of the target may readily be identified, as shown schematically in Figure 20. During the penetration process, the penetrator is deformed and loses mass through "erosion." Generally, enough of the tail end of the penetrator emerges from the target intact and undeformed so that the residual penetrator can be identified. In addition to the residual penetrator, there will be images of numerous other fragments, some of which are penetrator material, but most are target material.

Analysis of the images behind the target becomes more difficult if the time delays for the sequence of flashes behind the target are ill chosen. The fragment front forms an expanding cone with the apex of the cone at the exit point on the rear surface of the target. If the time delay to the first flash behind the target is too short, the fragments will be close together (including the residual penetrator) so that it will be impossible to pick out the image of the residual penetrator. If the time delay to the first flash behind the target is too long, the

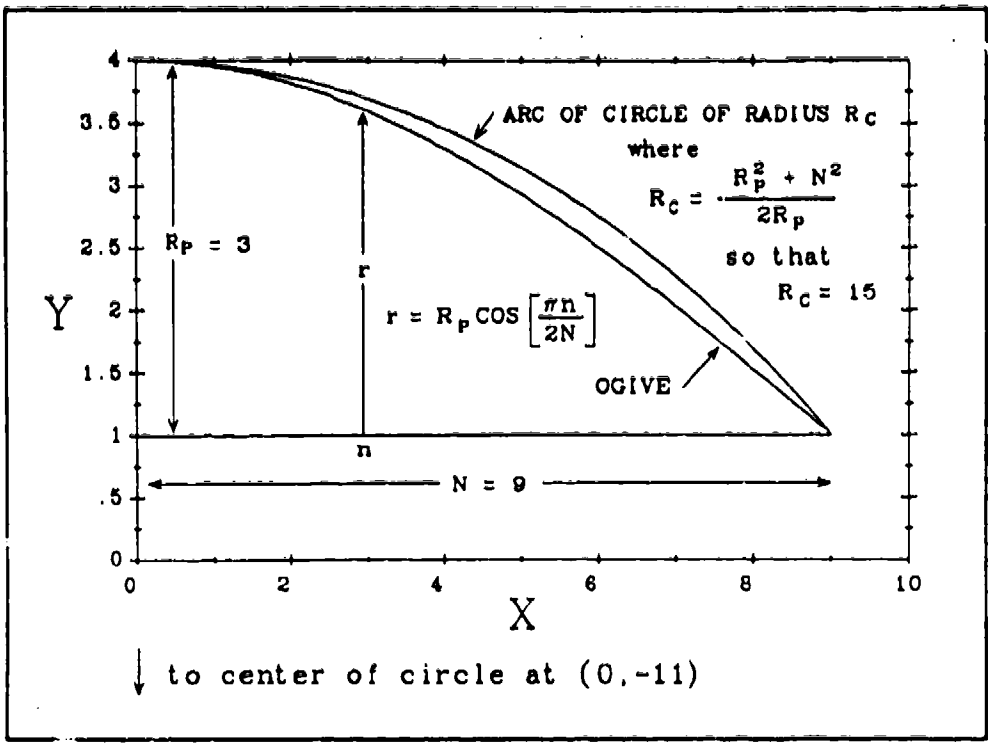

Figure 19. Comparison of an Ogive to the Arc of a Circle.

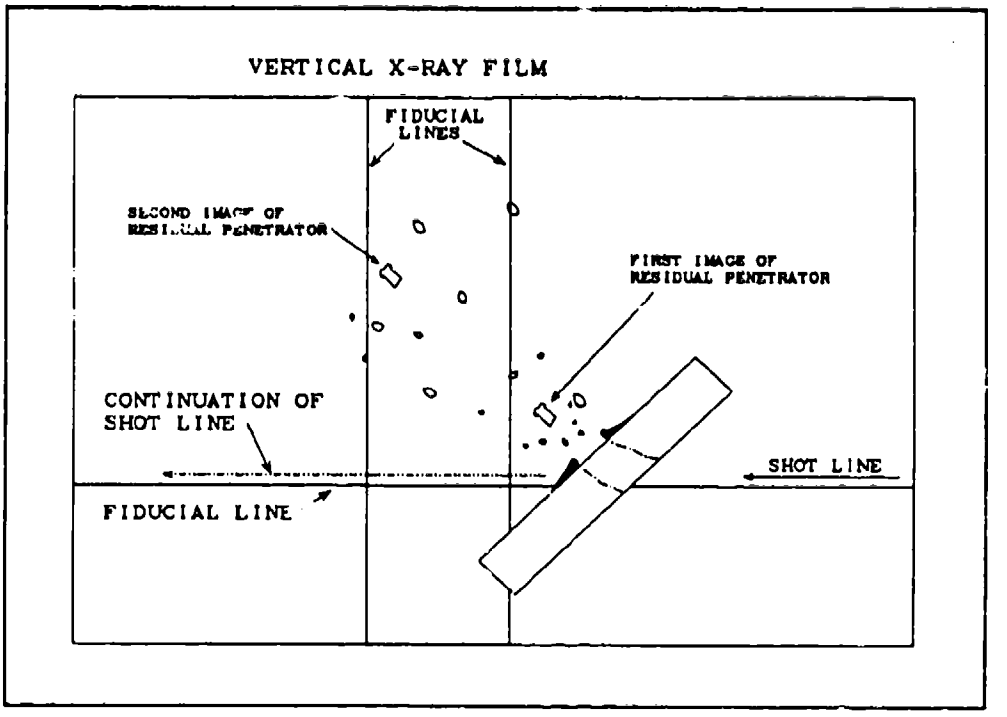

Figure 20. Typical Behind Target Fragment Pattern for Oblique Impact.

fragments may have spread out so that it becomes difficult to identify which flash produced the image, especially if the time delay between flashes behind the target is short.

Once the images of the residual penetrator produced by the first and second flashes behind the target have been identified, the procedure for calculating the residual velocity is the same as that to calculate the striking velocity. The film coordinates are adjusted using the K factor that was used in calculating the striking velocity. The assumption is made that the residual penetrator does not deviate from the vertical plane through the shot line. That is, it is not deflected either right or left while emerging from the target. It is reasonable to expect that in most cases, this assumption is valid.

5.6 Penetrator Residual Mass and Exit Angle. The mass of the residual penetrator can be estimated within a few percent from the image on the film if the image is well defined. The simplest way is to take the ratio of the length of the image of the residual penetrator to the length of the "striking" image and multiply by the original penetrator mass. An alternative method is to take the measured length on the film and multiply by the K factor, then divide by the original length and multiply by the mass. The calculation must be reduced if the penetrator has a long nose.

The exit angle is the angle that the path of the residual penetrator (after leaving the target) makes with the original shot line. To get residual velocity, there should be images from two x-ray stations. With two images of the residual penetrator at different times, it is possible to readily determine the path that the penetrator took (see Figure 21 for an illustration). The exit angle is positive if the residual penetrator's flight path rises above the original shot line, negative if below.

5.7 Multiple Plate Targets. In order to be able to calculate velocities of the residual penetrator between the plates of multiple-plate targets, the plates must be sufficiently spaced apart to allow at least two x-ray tubes to be positioned beside each other, each tube directed at the space between the plates. For target arrays which are normal to the shot line, the tubes may be either horizontal or vertical. For oblique target arrays (plates are either tilted forward or tilted backwards), the tubes must be positioned horizontally. The target plates will "hide" the residual penetrator from vertically positioned tubes.

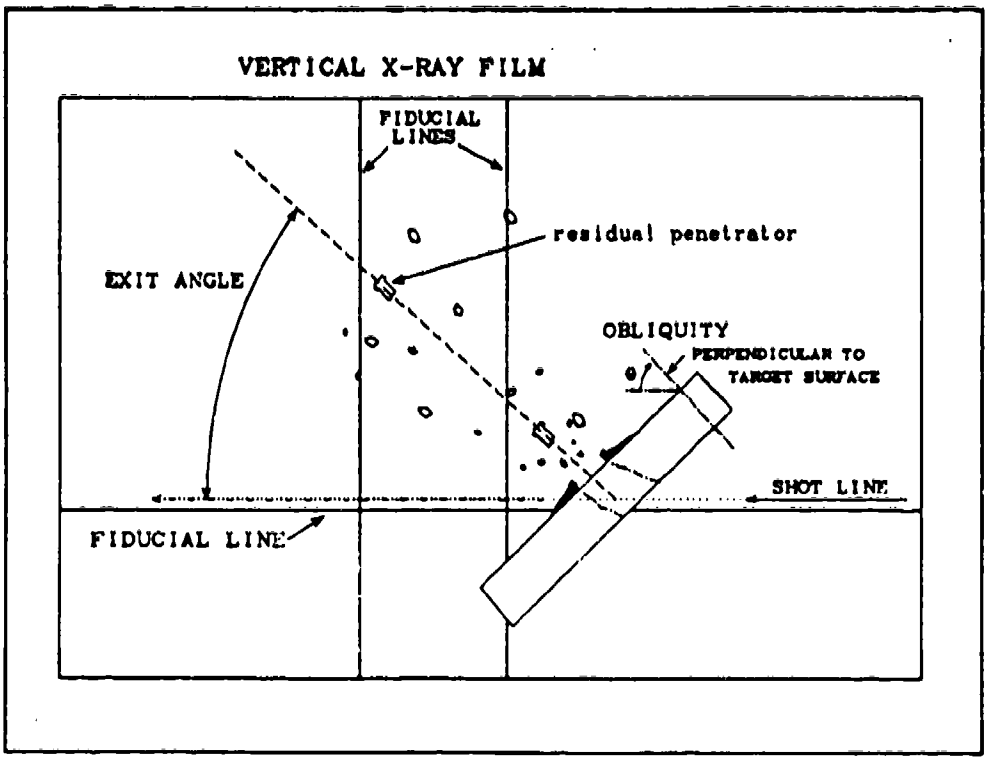

Figure 21. Target Obliquity and Penetrator Exit Angle.

Triggering these tubes is accomplished by additional trigger screens and associated delay units or by delay generators which are initiated by earlier events. Selecting the time delays in the latter case is difficult because an estimate of the penetration time for each target plate and an estimate of the residual velocity behind each plate must be made.

The method of calculating the residual mass and velocity from the x-ray film is the same as that for single-plate targets.

6. TARGET PLATE MEASUREMENTS (AFTER FIRING THE SHOT)

The hole made by the penetrator should be marked with the shot number or some other unique identification.

The following measurements should be made:

(1) Distance from edge of entrance to nearest target edge.

(2) Front crater: width (diameter if normal impact); length (if oblique impact).

(3) Entrance: width (diameter if normal impact); length (if oblique impact).

Perforated Target

(4) Distance from edge of exit to nearest target edge.

(5) Exit: width (diameter if normal impact); length (if oblique impact).

(6) Rear crater: width (diameter if normal impact); length (if oblique impact).

Nonperforated Target

(7) Normal depth of penetration.

(8) Line-of-sight depth (oblique impact).

(9) Height of rear bulge.

(These are explained in more detail in the remainder of this section.)

In addition, comments should be recorded concerning anything that is unusual.

6.1 Perforated Targets.

6.1.1 Normal Impact.

• The shortest distance from the edge of the hole to the nearest edge of the target for both entrance and exit should be recorded. (This is particularly important if the distance is less than two projectile diameters because of the likelihood that the edge has influenced the penetration process.)

• The length and width of the entrance hole and of the exit hole at the target surface should be recorded (see Figure 22).

• Comments should be recorded concerning anything that is unusual.

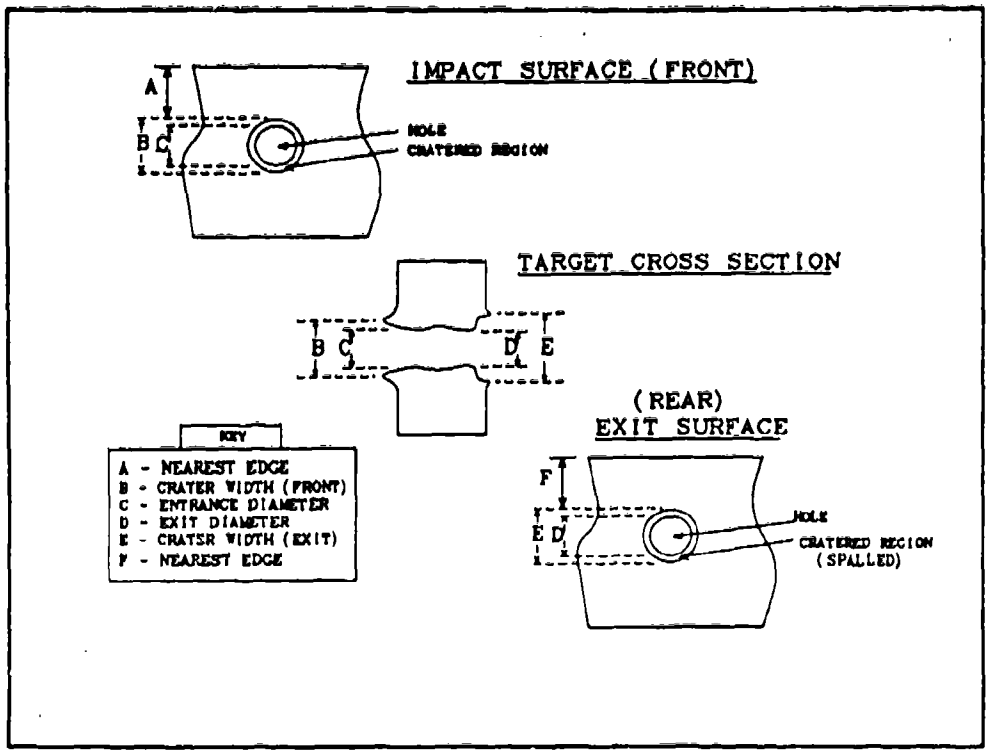

Figure 22. Perforated Target Measurements (Normal Impact).

6.1.2 Oblique Impact.

• The shortest distance from the edge of the hole to the nearest edge of the target for both entrance and exit should be recorded. (This is particularly important if the distance is less than two projectile diameters because of the likelihood that the edge has influenced the penetration process.)

• The length and width of the entrance hole and of the exit hole at the target surface should be recorded (see Figure 23).

• Comments should be recorded concerning anything that is unusual.

6.2 Semi-Infinite and Nonperforated Targets. In order for a target to be considered semi-infinite, it must be of sufficient thickness so that shock waves reaching the rear surface do not noticeably affect the penetration performance (the rear surface must not change shape). A thickness which is twice the normal depth of penetration generally qualifies as semi-infinite.

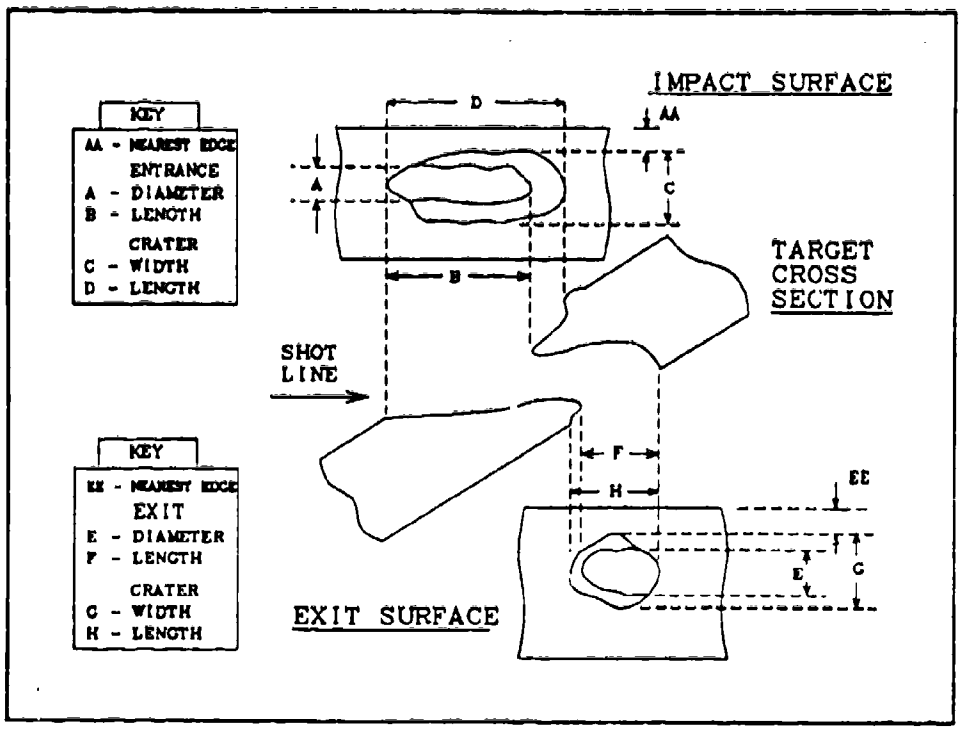

Figure 23. Perforated Target Measurements (Oblique Impact).

For each shot, the rear surface of the target should be examined and its condition recorded–especially if there is any hint of a bulge being formed. The following comments also apply to nonperforated targets.

6.2.1 Normal Impact.

• The shortest distance from the edge of the hole to the nearest edge of the target for the entrance should be recorded. (This is particularly important if the distance is less than two projectile diameters because of the likelihood that the edge has influenced the penetration process.)

• The length and width of the entrance hole at the target surface should be recorded.

• An estimate should be made of the depth of penetration. To get an accurate measurement of the depth of penetration, it is necessary to have the target plate cut (cross

sectioned) along the centerline of the hole since it is likely that the residual penetrator is stuck at the bottom of the hole.

• The rear surface of the target should be examined for fracture, bulge, etc. Measurements should be made and noted.

• Comments should be recorded concerning anything that is unusual (see Figure 24).

6.2.2 Oblique Impact.

• The shortest distance from the edge of the hole to the nearest edge of the target for the entrance should be recorded. (This is particularly important if the distance is less than two projectile diameters because of the likelihood that the edge has influenced the penetration process.)

• The length and width of the entrance hole at the target surface should be recorded.

• An estimate should be made of the depth of penetration. To get an accurate measurement of the depth of penetration, it is necessary to have the target plate cut (cross sectioned) along the centerline of the hole since it is possible that the residual penetrator is stuck at the bottom of the hole and because the hole can be measured by laying the ruler on the cross-sectioned surface.

• The rear surface of the target should be examined for fracture, bulge, etc. Measurements should be made and noted (see Figure 25).

• Comments should be recorded concerning anything that is unusual.

7. WITNESS PACK/PANEL MEASUREMENTS

Requirements for a particular firing program may include collecting information about the behind-target fragment distribution with respect to mass and velocity. If all that is required in regard to the behind-target fragments is the distribution pattern and only rough estimates of

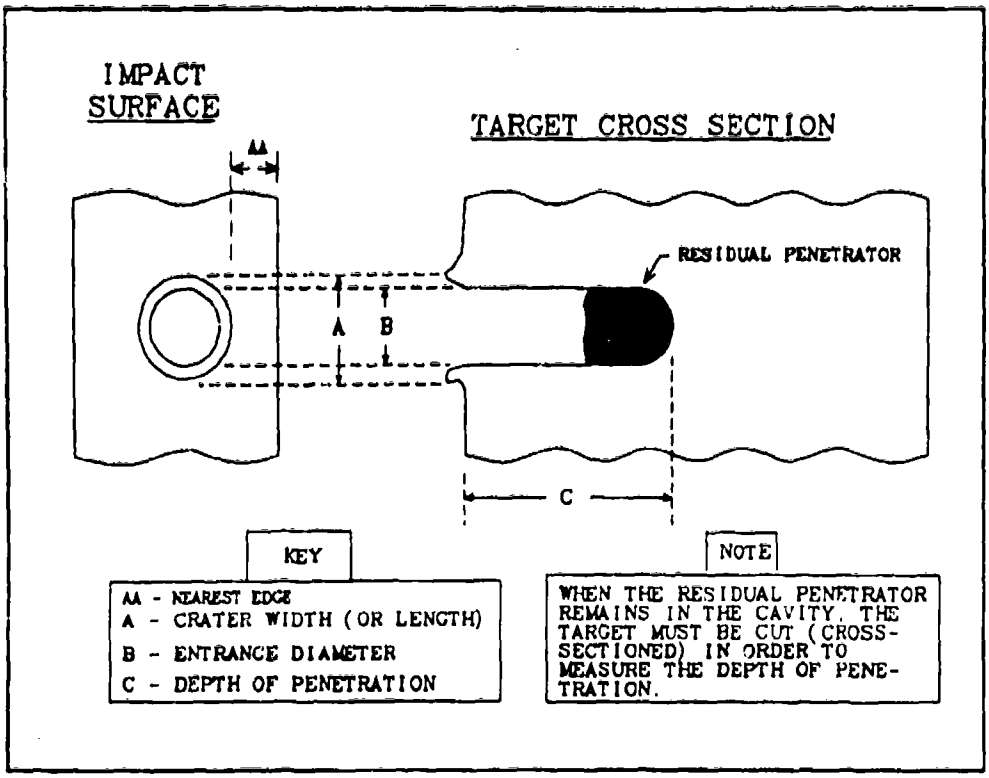

Figure 24. Semi-Infinite Target Measurements (Normal Impact).

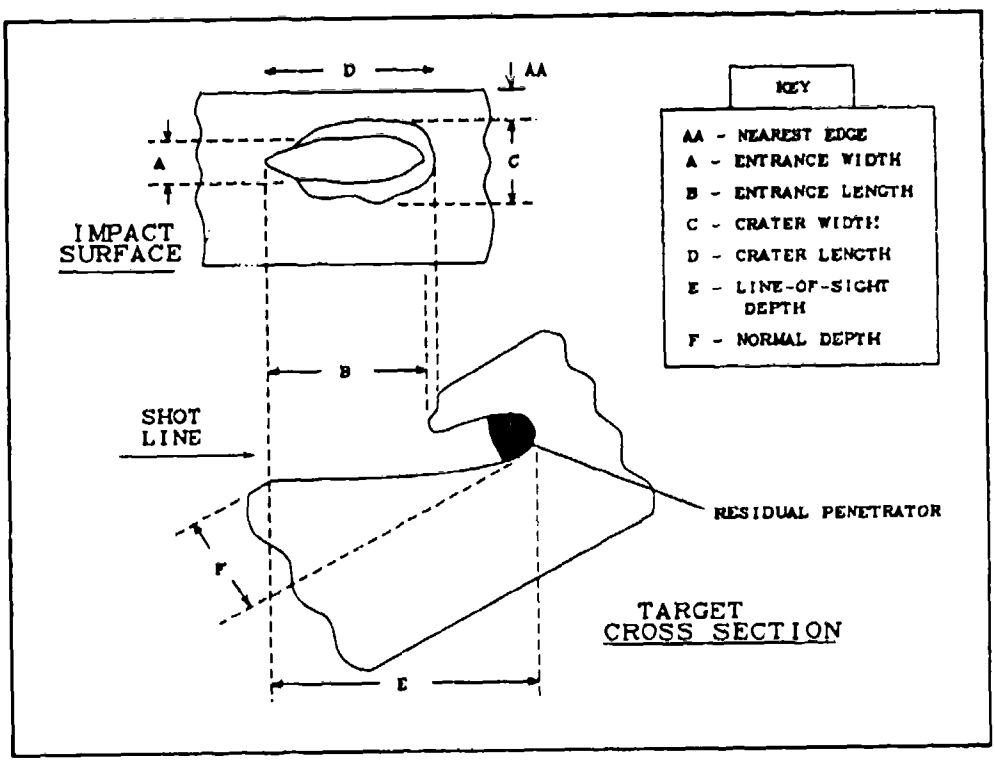

Figure 25. Semi-Infinite Target Measurements (Oblique Impact).

mass and velocity, then a witness panel (for example, an 1/8-in thick panel of 2020ST aluminum) will generally suffice (sometimes, a sheet of mild steel may be required in the case of "hot" penetrators). The pattern can be determined from the holes and indentations made in the panel. Mass and velocity can be roughly estimated from the size of the holes.

In order to obtain more accurate estimates of the mass and velocity distributions, it is necessary to use a witness pack. In this case, mass can be estimated from the size of the holes, and velocity can be estimated from the depth of penetration into the witness pack (see Figure 26 for an exploded view of a typical witness pack). In either case (panel or pack), the shot line should be projected onto the surface of the witness unit and marked. This serves as the origin of the coordinate system to which distance measurements will be made (see Figure 27).

Then the coordinates of each hole and its size are recorded in a systematic fashion (e.g., begin at upper left corner, go across to the right, and then drop to the next row).

The equation used by the Vulnerability and Lethality Division (VLD) to estimate the mass of a fragment is as follows:

$$M = \left(\frac{A}{k}\right)^{\frac{2}{3}},$$

where M is the fragment mass, A is the size of the hole, and k is a shape factor (an empirical constant). The velocity of the fragment is estimated by using the Thor equations for residual velocity and mass.

$$V_r = V_s - 10^{c1} \left[\sec(\theta)\right]^{c2} M_s^{c3} V_s^{c4} (eA)^{c5},$$

$$M_r = M_s - 10^{k1} \left[\sec(\theta)\right]^{k2} M_s^{k3} V_s^{k4} (eA)^{k5},$$

where V_r is residual velocity, V_s is striking velocity, sec is the secant function, θ is the target obliquity, M_s is the striking mass, e is the target thickness, A is the area of the hole, M_r is the residual mass, and c^1, c^2, c^3, c^4, c^5, k^1, k^2, k^3, k^4, and k^5 are empirical constants. The impirical constants are dependent on the fragment material and on the target material (Project Thor 1961, 1963). Assumptions are made about the striking velocity and mass and about the

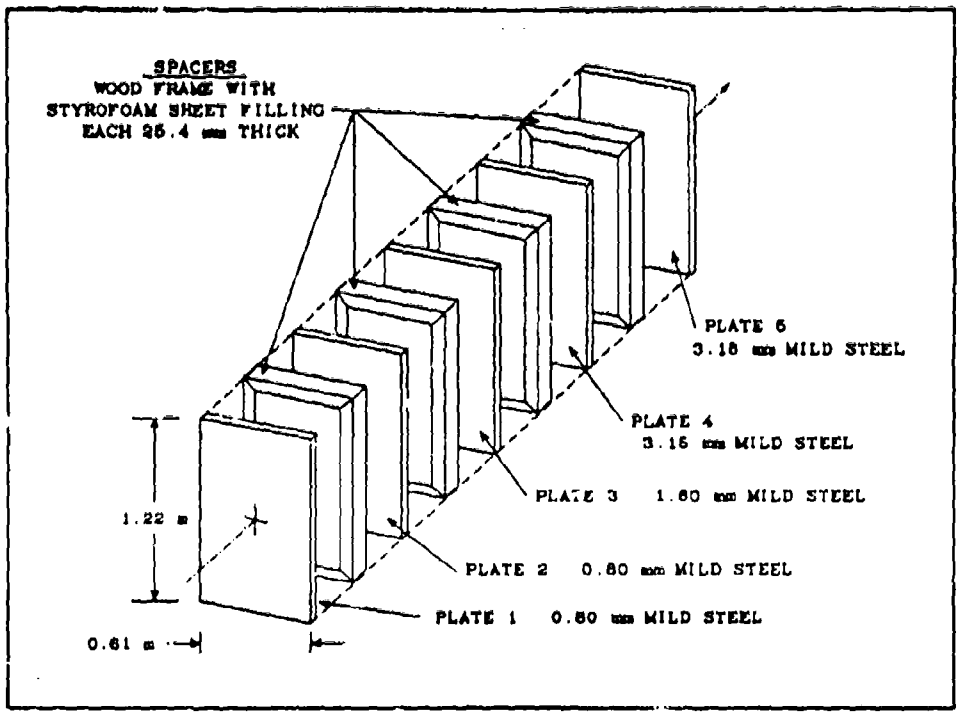

Figure 26. Typical Witness Pack.

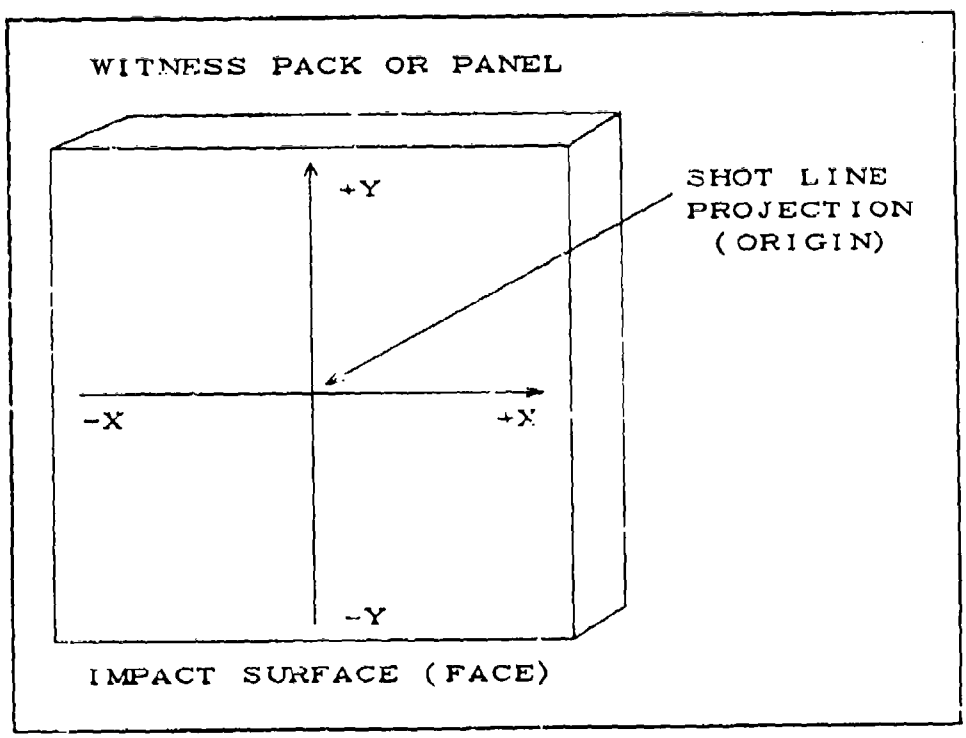

Figure 27. Witness Pack Coordinate System.

residual mass of the fragment. So, this methodology for estimating fragment mass and velocity is very prone to error.

8. VELOCITY, THICKNESS, AND OBLIQUITY BALLISTIC LIMITS

8.1 Definitions. The most frequent test of performance for a penetrator is comparing the highest striking velocity which produces a penetration (sometimes referred to as a partial penetration) or, alternatively, the lowest striking velocity which produces a perforation (not necessarily the same value, but is close) when fired against a specified target configuration. This velocity is called the ballistic limit for that penetrator against that target. There are several definitions for determining what qualifies as a penetration and a perforation (Zukas et al. 1982). There is the Army criterion which defines a perforation to be any case where any or all of the penetrator exits the rear surface; the protection criterion which requires that a witness plate placed behind the target be perforated to qualify as a perforation; and the Navy criterion which defines a perforation as any case in which light can be seen through the hole (Figure 28).

The Army defines the value of the velocity ballistic limit to be the velocity at which there is a 50% probability in perforating the target (V_{50}). The method of determining the V_{50} is discussed in Section 8.2. Additional discussion of the velocity ballistic limit can be found in Misey (1978).

Since vehicles are frequent targets for KE rounds and most vehicles present a variation in target thickness and obliquity depending on the orientation of the vehicle in relation to a gun system which is attacking, it is of interest to determine at what obliquity a particular target should be placed to just defeat the projectile. This value of obliquity is the obliquity ballistic limit. Since the Greek letter theta (θ) is frequently used to denote obliquity, the obliquity ballistic limit is often referred to as the "theta fifty" (the obliquity at which there is a 50% chance of getting through, symbolically, θ_{50}).

8.2 V_{50} Method for Velocity Ballistic Limit. The V_{50} method establishes a striking velocity which is purported to have a 50% probability of perforating the target. The most widely used criterion is called the "six-round ballistic limit." Enough shots are fired so that there are three

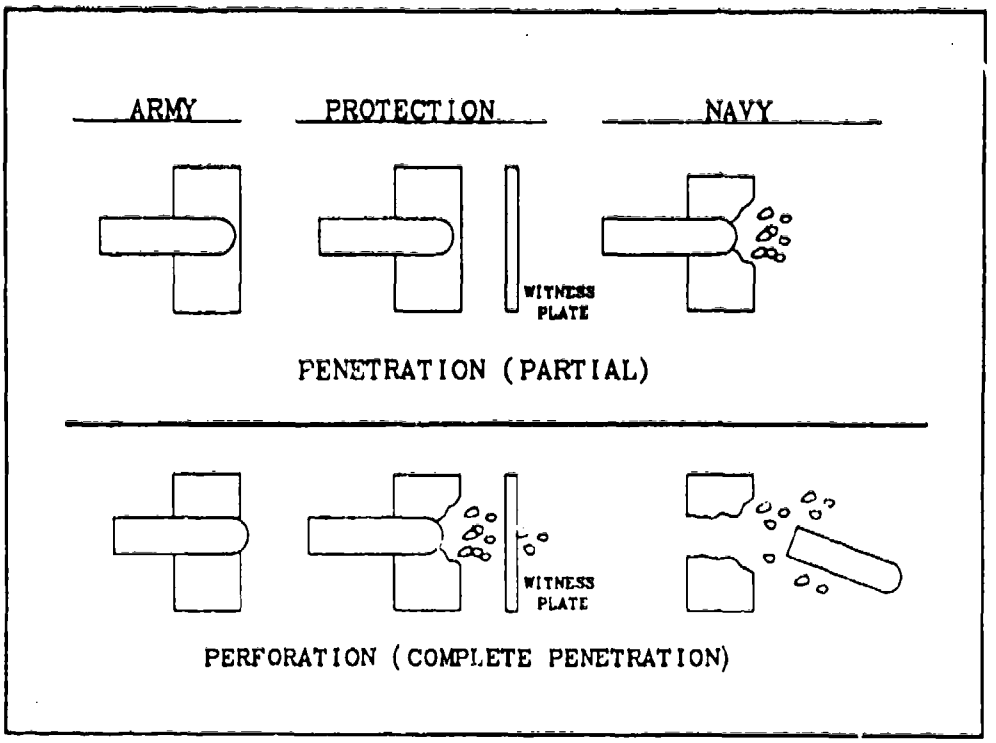

Figure 28. Penetration (Partial) and Perforation Criteria.

penetrations (partials) and three perforations which all lie within a range of 125 ft/s (38 m/s). Then an arithmetic average (sum divided by the number of values) of these six values is calculated. The resulting value is the V_{50}. The protection criterion for the result of a shot to be called a perforation is that a perforation be made by a fragment from the target or the penetrator in a witness panel (usually 0.020-in Dural aluminum → 2024ST aluminum) which is placed 6 in behind the target.

An example of calculating the V_{50} is as follows. Assume the following set of experimental data.

Striking (m/s)	Result
1,523	Perforation
1,508	Penetration (partial)
1,533	Perforation
1,505	Perforation
1,499	Penetration (partial)
1.507	Penetration (partial)

The spread is 1,533–1,499 = 34 m/s (112 fps), so this set of values qualifies for a V_{50} calculation. The sum is 9,075. Dividing by 6 yields an average value of 1,512.5 which would be rounded off to 1,512. Therefore, the V_{50} would be 1,512 m/s.

There are alternatives to the six-round limit velocity. If the number of projectiles is limited, a two-round or four-round ballistic limit velocity may be reported. In some cases, it may be necessary to increase the range over which the velocities lie (e.g., 10-round ballistic limit within 250 fps). In any case, the number of shots used in making the calculation should be an even number, half of which are penetrations and the rest perforations. The ballistic limit reported should identify the number of shots and the velocity spread.

8.3 Method of Maximum Likelihood. Golub and Grubbs (1956) describe a method of obtaining the most likely value for the intercept when the values involved occur in a zone of mixed results (an overlap of successes and failures). In applying this method to evaluating the ballistic limit velocity, two requirements must be met. First, there must be at least one penetration (partial) that lies above the lowest perforation—the zone of mixed results. Secondly, all the values to be used in calculating the ballistic limit must be close together --that is, the zone of mixed results must be small.

The following example reported in the article illustrates the method. Assume the following set of data.

Velocity (fps)	Condition of Impact
2,453	Perforation
2,433	Penetration (partial)
2,423	Perforation
2,415	Penetration (partial)
2,415	Penetration (partial)

In this set, a partial penetration (V = 2,433) occurs above a perforation (V = 2,423). This set qualifies as a zone of mixed results. When firing at an impact velocity close to the limit velocity, a number of factors can affect the outcome. For example, the partial might have occurred because the yaw (or pitch) on impact was greater than for the perforation. The

target or the penetrator might have had slightly different material properties which affected the outcome.

The procedure to evaluate this set of data is as follows:

(1) Calculate the arithmetic average (denoted as μ) as an initial estimate of the most likely intercept value; $\mu = (2{,}453 + 2{,}433 + 2{,}423 + 2{,}415 + 2{,}415)/5 = 12{,}139/5 = 2{,}427.8$ fps.

(2) Calculate a sigma (σ) on this estimate. This is done as follows:

- Sum the squares of the differences between each value and μ.

$(2{,}453 - 2{,}427.8)^2 + (2{,}433 - 2{,}427.8)^2 + (2{,}423 - 2{,}427.8)^2 + (2{,}415 - 2{,}427.8)^2 + (2{,}415 - 2{,}427.8)^2 = 1{,}012.8.$

- Take the square root of the previous sum divided by the number of values.

$$\sigma = \sqrt{\frac{1012.8}{5}} = 14.23236.$$

(3) Group the penetrations together separately from the perforations and calculate the following quantities:

	V_i	t_i	t_i^2	t_i^3
penetrations (partials)	2,433	0.36536	0.13349	0.04877
	2,415	-0.89936	0.80885	-0.72745
	2,415	-0.89936	0.80885	-0.72745
perforations	2,453	1.77061	3.13506	5.55097
	2,423	-0.33726	0.11375	-0.00384

where t_i is the quantity $(V_i - \mu)/\sigma$ and V_i is the indicated value in the second column.

(4) The next step involves consulting Tables 6 and 7. The lookup value is the t_i value from step 3. For the penetrations (partials), if t_i is negative, then consult Table 6, otherwise Table 7. For the perforations, if t_i is negative, then consult Table 7, otherwise Table 6. The value selected, z/q or z/p, should be an interpolated value unless the lookup value is specified in the table explicitly.

	V_i	z/q	$(z/q)^2$	$(z/q)^3$
penetrations (partials)	2,433	1.044	1.08994	1.13789
	2,415	0.326	0.10628	0.03465
	2,415	0.326	0.10628	0.03465

	V_i	z/p	$(z/p)^2$	$(z/p)^3$
perforations	2,453	0.087	0.00757	0.00066
	2,423	1.024	1.04858	1.07374

(5) Calculate the following (Σ means to sum):

[1] $\Sigma(z/q) - \Sigma(z/p) = (1.044 + 0.326 + 0.326) - (0.087 + 1.024) = 0.585.$

[2] $\Sigma t_i(z/q) - \Sigma t_i(z/p) = (0.36536)(1.044) + (-0.89936)(0.326) + (-0.89936)(0.326)$
$- \{ (1.77061)(0.087) + (-0.33726)(1.024) \} = -0.01364.$

Table 6. Ratio of the Standardized Normal Density Function to the Cumulative Standardized Normal Distribution

$\frac{z(t)}{p(t)}$

t	0.00	0.01	0.02	0.03	0.04	0.05	0.06	0.07	0.08	0.09
0.0	0.798	0.792	0.785	0.779	0.773	0.766	0.760	0.754	0.748	0.741
0.1	0.735	0.729	0.723	0.717	0.711	0.705	0.699	0.693	0.687	0.681
0.2	0.675	0.669	0.663	0.657	0.652	0.646	0.640	0.634	0.629	0.623
0.3	0.617	0.612	0.606	0.600	0.595	0.589	0.584	0.578	0.573	0.567
0.4	0.592	0.556	0.551	0.546	0.540	0.535	0.530	0.525	0.519	0.514
0.5	0.509	0.504	0.499	0.494	0.489	0.484	0.479	0.474	0.469	0.464
0.6	0.459	0.454	0.449	0.445	0.440	0.435	0.430	0.426	0.421	0.417
0.7	0.412	0.407	0.403	0.398	0.394	0.389	0.385	0.381	0.376	0.372
0.8	0.368	0.363	0.359	0.355	0.351	0.346	0.342	0.338	0.334	0.330
0.9	0.326	0.322	0.318	0.314	0.310	0.306	0.303	0.299	0.295	0.291
1.0	0.288	0.284	0.280	0.277	0.273	0.269	0.266	0.262	0.259	0.255
1.1	0.252	0.249	0.245	0.242	0.239	0.235	0.232	0.229	0.226	0.223
1.2	0.219	0.216	0.213	0.210	0.207	0.204	0.201	0.198	0.195	0.193
1.3	0.190	0.187	0.184	0.181	0.179	0.176	0.173	0.171	0.168	0.165
1.4	0.163	0.160	0.158	0.155	0.153	0.150	0.148	0.146	0.143	0.141
1.5	0.139	0.137	0.134	0.132	0.130	0.128	0.126	0.124	0.121	0.119
1.6	0.117	0.115	0.113	0.111	0.110	0.108	0.106	0.104	0.102	0.100
1.7	0.098	0.097	0.095	0.093	0.092	0.090	0.088	0.087	0.085	0.083
1.8	0.082	0.080	0.079	0.077	0.076	0.074	0.073	0.072	0.070	0.069
1.9	0.068	0.066	0.065	0.064	0.062	0.061	0.060	0.059	0.058	0.056
2.0	0.055	0.054	0.053	0.052	0.051	0.050	0.049	0.048	0.047	0.046
2.1	0.045	0.044	0.043	0.042	0.041	0.040	0.039	0.038	0.038	0.037
2.2	0.036	0.035	0.034	0.034	0.033	0.032	0.031	0.031	0.030	0.029
2.3	0.029	0.028	0.027	0.027	0.026	0.025	0.025	0.024	0.024	0.023
2.4	0.023	0.022	0.022	0.021	0.020	0.020	0.019	0.019	0.019	0.018
2.5	0.018	0.017	0.017	0.016	0.016	0.016	0.015	0.015	0.014	0.014
2.6	0.014	0.013	0.013	0.013	0.012	0.012	0.012	0.011	0.011	0.011

Table 6. Ratio of the Standardized Normal Density Function to the Cumulative Standardized Normal Distribution (Continued)

t	0.00	0.01	0.02	0.03	0.04	0.05	0.06	0.07	0.08	0.09
2.7	0.010	0.010	0.010	0.010	0.009	0.009	0.009	0.009	0.008	0.008
2.8	0.008	0.008	0.008	0.007	0.007	0.007	0.007	0.007	0.006	0.006
2.9	0.006	0.006	0.006	0.005	0.005	0.005	0.005	0.005	0.005	0.005
3.0	0.004	0.004	0.004	0.004	0.004	0.004	0.004	0.004	0.003	0.003
3.1	0.003	0.003	0.003	0.003	0.003	0.003	0.003	0.003	0.003	0.002
3.2	0.002	0.002	0.002	0.002	0.002	0.002	0.002	0.002	0.002	0.002
3.3	0.002	0.002	0.002	0.002	0.002	0.001	0.001	0.001	0.001	0.001
3.4	0.001	0.001	0.001	0.001	0.001	0.001	0.001	0.001	0.001	0.001
3.5	0.001	0.001	0.001	0.001	0.001	0.001	0.001	0.001	0.001	0.001
3.6	0.001	0.001	0.001	0.001	0.001	0.001	0.000	0.000	0.000	0.000

$$z(t) = \frac{1}{\sqrt{2\pi}} \exp\left(-\frac{t^2}{2}\right); \; p(t) = \int_{-\infty}^{t} z(t)\, dt .$$

Note: See text for conditions where this table is applicable.

Table 7. Ratio of the Standardized Normal Density Function of the Complimentary Cumulative Standardized Normal Distribution

$$\frac{z(t)}{p(t)}$$

t	0.00	0.01	0.02	0.03	0.04	0.05	0.06	0.07	0.08	0.09
0.0	0.798	0.804	0.811	0.817	0.824	0.830	0.836	0.843	0.849	0.856
0.1	0.803	0.869	0.876	0.882	0.889	0.896	0.902	0.909	0.916	0.923
0.2	0.929	0.936	0.943	0.950	0.957	0.964	0.970	0.977	0.984	0.991
0.3	0.998	1.005	1.012	1.019	1.026	1.033	1.040	1.047	1.054	1.062
0.4	1.069	1.076	1.083	1.090	1.097	1.105	1.112	1.119	1.126	1.134
0.5	1.141	1.148	1.156	1.163	1.171	1.178	1.185	1.193	1.200	1.207
0.6	1.215	1.222	1.230	1.237	1.245	1.253	1.260	1.268	1.275	1.283

Table 7. Ratio of the Standardized Normal Density Function of the Complimentary Cumulative Standardized Normal Distribution (Continued)

t	0.00	0.01	0.02	0.03	0.04	0.05	0.06	0.07	0.08	0.09
0.7	1.290	1.298	1.306	1.313	1.321	1.329	1.336	1.344	1.352	1.360
0.8	1.367	1.375	1.383	1.391	1.399	1.406	1.414	1.422	1.430	1.438
0.9	1.446	1.454	1.461	1.469	1.477	1.485	1.493	1.501	1.509	1.517
1.0	1.525	1.533	1.541	1.549	1.557	1.565	1.573	1.581	1.590	1.598
1.1	1.606	1.614	1.622	1.630	1.638	1.646	1.655	1.663	1.671	1.679
1.2	1.687	1.696	1.704	1.712	1.720	1.729	1.737	1.745	1.754	1.762
1.3	1.770	1.779	1.787	1.795	1.804	1.812	1.820	1.829	1.838	1.846
1.4	1.854	1.862	1.871	1.879	1.888	1.896	1.905	1.913	1.922	1.930
1.5	1.938	1.947	1.955	1.964	1.972	1.981	1.990	1.998	2.007	2.015
1.6	2.024	2.033	2.041	2.050	2.058	2.067	2.076	2.084	2.093	2.102
1.7	2.110	2.119	2.128	2.136	2.145	2.154	2.162	2.171	2.180	2.188
1.8	2.197	2.202	2.215	2.223	2.232	2.241	2.250	2.258	2.267	2.276
1.9	2.285	2.294	2.303	2.311	2.320	2.329	2.338	2.346	2.355	2.364
2.0	2.373	2.381	2.390	2.399	2.408	2.417	2.426	2.435	2.444	2.453
2.1	2.462	2.470	2.479	2.488	2.497	2.506	2.515	2.524	2.533	2.542
2.2	2.551	2.560	2.569	2.578	2.587	2.596	2.605	2.614	2.623	2.632
2.3	2.641	2.650	2.659	2.668	2.677	2.687	2.696	2.705	2.714	2.723
2.4	2.732	2.741	2.750	2.759	2.768	2.777	2.786	2.795	2.805	2.814
2.5	2.823	2.832	2.841	2.850	2.859	2.868	2.878	2.887	2.896	2.905
2.6	2.914	2.923	2.932	2.942	2.951	2.960	2.969	2.978	2.987	2.997
2.7	3.006	3.015	3.024	3.033	3.043	3.052	3.061	3.070	3.079	3.089
2.8	3.098	3.107	3.116	3.126	3.135	3.144	3.153	3.163	3.172	3.181
2.9	3.190	3.200	3.209	3.218	3.227	3.237	3.246	3.255	3.265	3.274
3.0	3.283	3.292	3.302	3.311	3.320	3.330	3.339	3.348	3.358	3.367
3.1	3.376	3.386	3.395	3.404	3.413	3.423	3.432	3.441	3.451	3.460
3.2	3.470	3.479	3.488	3.498	3.507	3.516	3.526	3.535	3.544	3.554
3.3	3.563	3.573	3.582	3.591	3.601	3.610	3.620	3.629	3.638	3.648
3.4	3.657	3.667	3.676	3.685	3.695	3.704	3.714	3.723	3.732	3.742
3.5	3.751	3.761	3.770	3.780	3.789	3.799	3.808	3.817	3.827	3.836

Table 7. Ratio of the Standardized Normal Density Function of the Complimentary Cumulative Standardized Normal Distribution (Continued)

t	0.00	0.01	0.02	0.03	0.04	0.05	0.06	0.07	0.08	0.09
3.6	3.846	3.855	3.865	3.874	3.884	3.893	3.902	3.912	3.921	3.931
3.7	3.940	3.950	3.959	3.969	3.978	3.988	3.997	4.007	4.010	4.026
3.8	4.035	4.045	4.054	4.064	4.072	4.083	4.092	4.102	4.111	4.121
3.9	4.130	4.140	4.149	4.159	4.169	4.178	4.188	4.197	4.206	4.216
4.0	4.226	4.235	4.245	4.254	4.264	4.273	4.283	4.292	4.302	4.312

$$z(t) = \frac{1}{\sqrt{2\pi}} \exp\left(-\frac{t^2}{2}\right); \; q(t) = 1 - \int_{-\infty}^{t} z(t)\, dt \; .$$

Note: See text for conditions where this table is applicable.

Similarly, calculate the following:

[3] $\Sigma t_i(z/q) - \Sigma(z/q)2 - \Sigma t_i(z/p) - \Sigma(z/p)2$ divided by σ.

[4] $\Sigma t_i^2(z/q) - \Sigma t_i(z/q)^2 - \Sigma(z/q) - \Sigma t_i^2(z/p) - \Sigma t_i(z/p)^2 + \Sigma(z/p)$ divided by σ.

[5] $\Sigma t_i^3(z/q) - 2\Sigma t_i(z/q) - \Sigma t_i^2(z/q)^2 - \Sigma t_i^3(z/p) + 2\Sigma t_i(z/p) - \Sigma t_i^2(z/p)^2$ divided by σ.

(6) The values computed in step (5) are used in the following set of simultaneous equations to solve for changes to be made in the estimated values for μ and σ. Steps (3) through this step are repeated using the revised values until the resulting calculation of this step is within an acceptable tolerance value.

$[1] = -([3]\,\Delta\mu + [4]\,\Delta\sigma)$.

$[2] = -([4]\,\Delta\mu + [5]\,\Delta\sigma)$.

Here the bracketed values are replaced by the corresponding value calculated in step (5). Then, $\Delta\mu$ and $\Delta\sigma$ can be determined from the following symbolic equations:

$$\Delta\mu = \frac{[2][4] - [1][5]}{[3][5] - [4][4]} .$$

$$\Delta\sigma = \frac{[2][3] - [1][4]}{[4][4] - [3][5]} .$$

The estimated intercept value (μ) and its corresponding σ is adjusted by adding the value for $\Delta\mu$ and $\Delta\sigma$, respectively.

$$\text{New } \mu = \text{old } \mu + \Delta\mu.$$
$$\text{New } \sigma = \text{old } \sigma + \Delta\sigma.$$

As indicated previously, steps (3) through (6) are repeated until the value for $\Delta\mu$ is small enough (less than 0.01, for example).

(7) The following table summarizes the values for the first four iterations. Since $\Delta\mu$ is less than 0.01, the sequence is terminated.

[1]	[2]	[3]	[4]	[5]	$\Delta\mu$	$\Delta\sigma$
0.58065	-0.01331	-0.16674	-0.01213	-0.09126	3.560	-0.619
-0.03110	0.14215	-0.16436	0.06129	-0.14622	0.205	1.058
-0.00509	0.02336	-0.15707	0.05304	-0.11325	0.044	0.227
-0.00018	0.00085	-0.15558	0.05151	-0.10716	0.002	0.009

The final μ = 2,427.8 + 3.560 + 0.205 + 0.044 + 0.022 = 2,431.611, and σ = 14.232 -0.619 + 1.058 + 0.227 + 0.009 = 14.097. Therefore, the ballistic limit velocity would be

reported as being 2,432 ft/s (since the input values were fps) with a sigma of 15 fps (rounding up the calculated value).

It is possible to further calculate a statistical σ on the average values (μ) and a σ on the σ. Refer to Golub and Grubbs (1956) if this is desired.

The previous method is very sensitive to how the values are distributed about the mean value. Values below or above one sigma from the mean are likely to cause a problem in evaluating a realistic final mean value.

The values in Tables 6 and 7 may be computed by using the following approximation where T_I is the lookup value and P_x is the tabulated value. Positive values generate Table 6, and negative values generate Table 7. The ABS function forces the argument value to be a positive value. The EXP is the exponential function.

$$T_x = \text{ABS}\,(T_I)\ .$$

Note: if $T_x > 5$, then T_x is set to 5.

$$Q_1 = C_1\ \text{EXP}\left(\frac{-T_x^2}{2}\right).$$

$$Q_2 = \Big(\Big(\Big(\Big((C_7T_x + C_6)T_x + C_5\Big)T_x + C_4\Big)T_x + C_3\Big)T_x + c_2\Big)T_x + 1\ ,$$

where

C1 = 0.3989422804
C2 = 0.0498673470
C3 = 0.0211410061
C4 = 0.0032776263
C5 = 0.0000380036
C6 = 0.0000488906
C7 = 0.0000053830.

$$\text{If } T_1 \text{ is positive, then } Q_3 = 1 - \frac{1}{2\,Q_2^{16}} .$$

$$\text{If } T_1 \text{ is negative, then } Q_3 = \frac{1}{2\,Q_2^{16}} ,$$

$$P_x = \frac{Q_1}{Q_3} .$$

The value of C1 is equal to $\frac{1}{\sqrt{2\pi}}$. The previous approximation is reported in Herr and Grabarek (1978). Also refer to Golub and Grubbs (1950) and Hagan and Visnaw (1970) for more information.

8.4 Lambert/Jonas Method for Velocity Ballistic Limit. Another method for caiculating the velocity ballistic limit is to fit the striking velocity and residual velocity data for a penetrator-target configuration to the following equation:

$$V_R = A \left(V_S^p - V_L^p \right)^{\frac{1}{p}} , \tag{30}$$

where V_R is the residual velocity, V_S is the striking velocity, V_L is the ballistic limit velocity (to be determined), and A and p are empirical constants (Lambert and Jonas 1976). The reason for using this method for evaluating the ballistic limit is that it generally reduces the number of shots that need to be fired. For a six-round V_{50}, a minimum of six shots has to be fired, of which half must be perforations and the rest penetrations and all within a limited velocity range. To achieve this when firing newly designed penetrators with only six shots would be unusual. However, with only three shots which yield residual velocities, of which one is less than 500 m/s, a reasonably good prediction of the velocity ballistic limit can be made by fitting to Equation 30.

In applying this equation to experimental data, A is restricted to the range $0 < A \leq 1$, and p is restricted to the range $1 \leq p \leq 8$. The fit to the data is obtained by selecting a value for V_L, beginning with the lowest perforation and then allowing p to increment beginning at 1 and stepping by 0.05. For each set of V_L and p, A is determined by a least squares fit to the

perforation data. The value for V_L is then decremented by one until the set of values which minimize the least squares error is found. The least squares fitting procedure is terminated prematurely if the selected value for V_L has been decremented down to the highest penetration.

This method for evaluating the ballistic limit does not require any penetration data (partials). The equation is too sensitive to the convergence point to permit using a nonlinear least squares technique to obtain a solution.

If only one perforation point is available, then the value 1 is assigned to A and a reasonable value for p is selected based on any data sets for the same penetrator and target obliquity, which are more complete.

A method for estimating the values for A, p, and V_L apriori is given in Lambert (1978).

This method is the following. Setting $z = \frac{T}{D}\left[\sec(\theta)\right]^{0.75}$, where T is the target thickness, D is the penetrator diameter, θ is the target obliquity, and sec is the secant function, the value for A can be estimated from the following:

$$A = \frac{M}{M + \frac{M'}{3}}, \quad \text{where } M' = \rho_t \frac{\pi D^3}{4} z . \tag{31}$$

M is the penetrator mass, and $\rho_t = 7.85$ (value used in report is 7.8). Note that M' is related to the mass of a plug of the target plate with the same cross-sectional area as the penetrator. The value for p may be estimated from $p = 2 + \frac{z}{3}$. This equation is probably not applicable in general because it is possible to get unrealistically large values for thick targets.

Finally, the ballistic limit velocity for RHA targets may be estimated from the following:

$$V_L = 4{,}000 \left(\frac{L}{D}\right)^{0.15} \sqrt{\left[z + \mathrm{EXP}\,(-z) - 1\right] \frac{D^3}{M}} ,$$

where EXP is the exponential function and L, D, and T are in centimeters, M is grams, and V_L in m/s. A discussion of the rationale behind these equations is given in Zukas et al. (1982).

8.5 Thickness Ballistic Limit. In experimental work, a firing program will generally call for obtaining a velocity ballistic limit for a particular target configuration. However, it is also possible to have a particular striking velocity specified (for example, the expected velocity at a specified distance from a particular gun) and then ask what thickness of target is required to just stop the penetrator. Since plates used for targets are available only in discrete thicknesses, it is not feasible to obtain a thickness ballistic limit directly through experiment. A good estimate can be made graphically if velocity ballistic limits both above and below the specified striking velocity are available.

8.6 Obliquity Ballistic Limit θ_{50}. The θ_{50} is determined in a manner similar to the V_{50}, except that the striking velocity is held constant (as near as possible) and the obliquity is varied around the value at which the penetrator will just perforate the target. A standard definition of the number of shots needed for a θ_{50} doesn't exist. An acceptable condition would be three penetrations and three perforations within a 10° spread in obliquity and with the striking velocity within 25 m/s. In any case, the criteria used should be reported so that at some future time, verification can be made if necessary. Refer to Figure 29, which shows that the θ_{50} lies between θ_2 where perforation occurs and θ_1 where only penetration occurs and that $\theta_1 > \theta_2$.

9. PENETRATION/PERFORATION EQUATIONS AND THEORY

9.1 Symbols. The equations described in this section will use symbols to represent parameters which are defined as in the following.

A - empirical constant, or area
B - empirical constant, or area
C - empirical constant, or area
D - penetrator diameter
E - Young's modulus
F - force

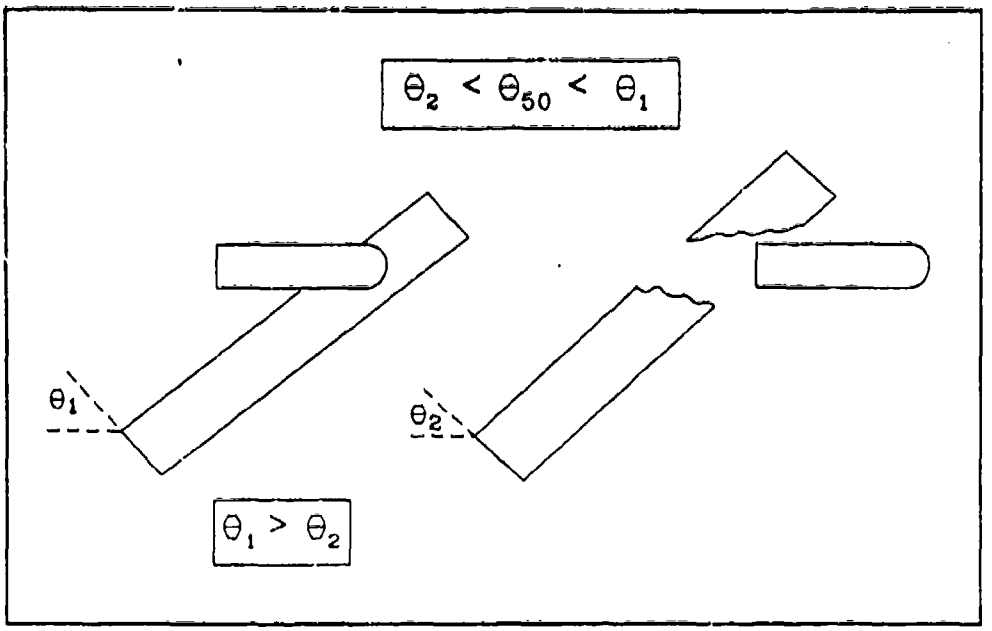

Figure 29. Effect of Obliquity on Ballistic Limit.

G - Shear modulus

H - Material resistance of target (units of pressure)

L - penetrator length

M - penetrator mass

P - penetration (semi-infinite)

Q - plug/shear portion

T - target thickness or a calculated limit thickness

U - velocity (penetration interface)

V - velocity (penetrator) $\rightarrow V_L$ ballistic limit

W - weight, target areal density

Y - material flow stress (units of pressure) - in some cases, Y can represent the yield strength of the material

a - dimensionless constant

b - dimensionless constant

c - dimensionless constant

d - dimensionless constant

e - dimensionless constant

f - length/diameter ratio (fineness ratio)

g - a Grabarek's constant

h - normalized crater/hole cross section

k - dimensionless constant

l " "

m " "

n " "

t - time

u - instantaneous velocity

v - instantaneous velocity

w - instantaneous velocity

The following, when used as subscripts, will have the indicated meaning.

L - limit

p - parameter related to the penetrator

r,R - residual

s,S - striking

t - parameter related to the target

0 - initial value

50 - probability is 50%

Characters from the Greek alphabet have the following meanings.

alpha (α) - empirical constant or angle

beta (β) - empirical constant or angle

theta (θ) - angle of obliquity

pi (π) - ratio of circle circumference to diameter (3.141592654...)

rho (ρ) - material density

9.2 Engineering Models.

9.2.1 Purely Empirical Equations. Numerous empirical (constants evaluated from experimental data) equations have been used to describe penetrator performance for KE projectiles. Some equations are purely empirical and are quite limited in making predictions, while others are based on physics principles. The latter are more likely to give good predictions, but the ultimate equation, which is applicable in all cases, has not been found. An example of the purely empirical equations are the well known THOR equations described in Project THOR (1961, 1963) and Johnson and Mioduski (1966). These equations have the following form:

$$V_R = V_S - A\,(TA_p)^a\, M^b\, V_S^c\, [\sec(\theta)]^d\,, \tag{32}$$

where V_R is the residual velocity, V_S is the striking velocity, T is the target thickness, A_p is the penetrator cross-sectional area, M is the penetrator mass, sec is the secant function, θ is the target obliquity, and A, a, b, c, and d are empirical constants; and

$$M_R = M_S - B\,(TA_p)^k\, M^l\, V_S^m\, [\sec(\theta)]^n\,, \tag{33}$$

where M_r is the residual velocity, M_s is the striking mass, and B, k, l, m, and n are empirical constants. The values of the empirical constants are highly dependent on the set of data used to evaluate the constants. Therefore, predictions of events involving conditions which lie outside the set of data are not reliable. The values of the empirical constants are also dependent on the units used for the parameters. A modification of Equation 32 is described in Zook, Slack, and Izdebski (1983), which equates the loss of KE (assuming no loss in mass) to the second term of the right side of Equation 32. This equation is as follows:

$$\frac{1}{2}\, M_p\, (V_S^2 - V_R^2) = KT^a\, A_p^b\, M_p^c\, V_S^d\, [\sec(\theta)]^e\,. \tag{34}$$

This equation gives the curvature in the V_S - V_R curve that is observed in most experimental data as the residual velocity approaches 0.

Another empirical approach to penetration performance is described in Appendix E of Lambert (1978).

The method described in the report for estimating the values for A, p, and V_L in the equation

$$V_R = A\left(V_S^p - V_L^p\right)^{\frac{1}{p}}$$

is as follows. Set

$$z = \frac{T}{D}\left[\sec(\theta)\right]^{0.75},$$

where T is the target thickness, D is the penetrator diameter, θ is the target obliquity, and sec is the secant function. The value for A can be estimated from the following:

$$A = \frac{M}{M + \frac{M'}{3}}, \quad \text{where } M' = \rho_t \frac{\pi D^3}{4} z,$$

M is the penetrator mass, and $\rho_t = 7.85$ (value used in report is 7.8). Note that M′ is related to the mass of a plug of the target plate with the same cross-sectional area as the penetrator. The value for p may be estimated from the following:

$$p = 2 + \frac{z}{3}.$$

This equation is probably not applicable in general because it is possible to get unrealistically large values for thick targets.

Finally, the ballistic limit velocity for RHA targets may be estimated from the following:

$$V_L = 4{,}000\left(\frac{L}{D}\right)^{0.15}\sqrt{\left[z + \mathrm{EXP}(-z) - 1\right]\frac{D^3}{M}},$$

where EXP is the exponential function and L, D, and T are in centimeters, M in grams, and V_L in m/s. A discussion of the rationale behind these equations is given in Zukas et al. (1982).

9.2.2 Semiempirical Equations. A step above purely empirical equations is relating nondimensional quantities (Baker, Westine, and Dodge 1973). Ratios are formed based on the parameters involved in such a way that the numerator has the same units as the denominator, and, therefore, the ratios are dimensionless. Such ratios are as follows:

$$\frac{L}{D} \quad \frac{\text{penetrator length}}{\text{penetrator diameter}},$$

$$\frac{T}{D} \quad \frac{\text{target thickness}}{\text{penetrator diameter}},$$

$$\frac{\rho_p}{\rho_t} \quad \frac{\text{penetrator density}}{\text{target density}},$$

and

$$\frac{\frac{1}{2}\rho_p V^2}{H} \quad \frac{\text{penetrator KE per unit volume}}{\text{target resistance}}.$$

The first equation of Grabarek's equations (to be covered more fully in Section 9.2.5) is based on a relationship of three of the previous ratios—the first, second, and last.

$$\frac{\frac{1}{2}\rho_p V_L^2}{H} = \frac{\left(\frac{T}{D}\left[\sec(\theta)\right]^{\beta}\right)^{\alpha}}{\frac{L}{D}}. \tag{35}$$

By letting $\frac{1}{2} H\pi = A$ and $\rho L \frac{\pi D^2}{4} = M$, Equation 35 becomes

$$V_L = \sqrt{A \frac{D^3}{M} \left(\frac{T}{D} [\sec(\theta)]^\beta \right)^\alpha} , \tag{36}$$

which is Grabarek's single-plate equation.

Most penetration equations which have some physical basis may similarly be reduced to a relationship of dimensionless ratios. For example, the equation reported in Zook (1977) is derived from an expression for the resistive force experienced by the penetrator. In compact form, this equation is as follows:

$$T = \frac{4M}{\pi D^2 \rho_t} f(V_S, V_R, H, \rho_t) . \tag{37}$$

This equation does not consider oblique impacts. The expression for the function $f(V_S, V_R, H, \rho_t)$ is made up of quantities which are dimensionless ratios and, therefore, the function is dimensionless. For a right circular cylinder, Equation 37 may be rearranged to the following:

$$\frac{T}{D} = \left(\frac{L}{D} \frac{\rho_p}{\rho_t} \right) f(V_S, V_r, H, \rho_t) , \tag{38}$$

by substituting $\rho_p L \frac{\pi D^2}{4}$ for M and dividing both sides by D.

One word of caution when applying the equation in MR 2797 to new data—that equation works well only for penetrators which have an L/D ratio of nearly 1 (as in the report). For penetrators with L/D ratios greater than 1, a different expression, which includes the length parameter, must be used for the force equation unless the penetrator strength exceeds that of the target and the penetrator does not lose mass as a result of the interaction. A satisfactory force equation which can be integrated and is applicable to penetrators with high L/D ratios which erode during the penetration process has not yet been found. However, a penetration model which can be applied to both eroding and noneroding penetrators will be described in Section 9.2.4.

9.2.3 Semitheoretical Equations. Some of the penetration equations have a physical rationale. The usual starting point is to define an expression for the resistive force acting on the penetrator by the target. The simplest assume the resistive force to be a constant as follows (proposed by Robinson [circa 1742] and Euler [circa 1750]):

$$F = A . \tag{39}$$

From physics, the force is equal to the mass multiplied by the acceleration. In this case, the penetrator is being decelerated (minus sign). Therefore,

$$F = -Ma = A . \tag{40}$$

From calculus, the acceleration a can be expressed as dv/dt or as (dv/dx)(dx/dt) which is equal to v (dv/dx). Therefore,

$$-Mv \frac{dv}{dx} = A . \tag{41}$$

Integrating this expression with the limits $v = V_0$ when $x = 0$ and $v = 0$ when $x = P$ and assuming M and D to be constant, yields the following relationship:

$$\frac{1}{2} MV_0^2 = A P . \tag{42}$$

The left-hand side of this equation is the KE of the penetrator on impact. The right-hand side is proportional to the volume of the crater made in the target (set $A = A_h H$, where A_h is an average hole cross-sectional area and H is the target resistance). The concept of volume of the crater being proportional to the work done in creating the crater has been attributed to Morin (1833) and to Martel (1897).

More complicated expressions for the force equation have been proposed.

$$F = A + BV , \tag{43}$$

$$F = A + BV^2 \quad \text{(Poncelet [circa 1830])}, \tag{44}$$

$$F = BV + CV^2 \quad \text{(Resal [circa 1895])}, \tag{45}$$

and

$$F = A + BV + CV^2 . \tag{46}$$

The previous equations are expressed without the cross-sectional area, A_p, as part of the equation. However, it is known that the resistive force is a function of the cross-sectional area. When A_p is treated as a constant, the result will represent an average force. The aerodynamic force acting on a projectile in air is known to have the following form:

$$F = \frac{1}{2} C_d A_p \rho_{(air)} V^2 , \tag{47}$$

where C_d is the drag coefficient and $\rho_{(air)}$ is the density of air. The drag coefficient is not constant but varies with the velocity of the projectile. However, for velocities below the speed of sound in air (approximately 1,100 fps), known as Mach 1, the drag coefficient is nearly constant. Above about Mach 1.5 (one and a half times the speed of sound in air), the drag coefficient decreases almost linearly with increasing speed. See Figure 30 for typical drag coefficient curves.

Integration of the aerodynamic force equation with respect to range yields the following equation, assuming C_d to be constant:

$$V = V_0 \exp\left(\frac{-C_d A_p \rho_{(air)} R}{2M}\right), \tag{48}$$

where V_0 is the velocity at the range R = 0 and exp is the exponential function. For a given value of R, the resulting velocity may be calculated. The result is NOT valid for velocities above Mach 0.8, except that above Mach 1.5; C_d may be considered constant only over small changes in speed. If R is in meters, then M must be in kilograms, A_p in square meters, and $\rho_{(air)}$ in kilograms per cubic meter. The density of air under standard conditions (sea level, no

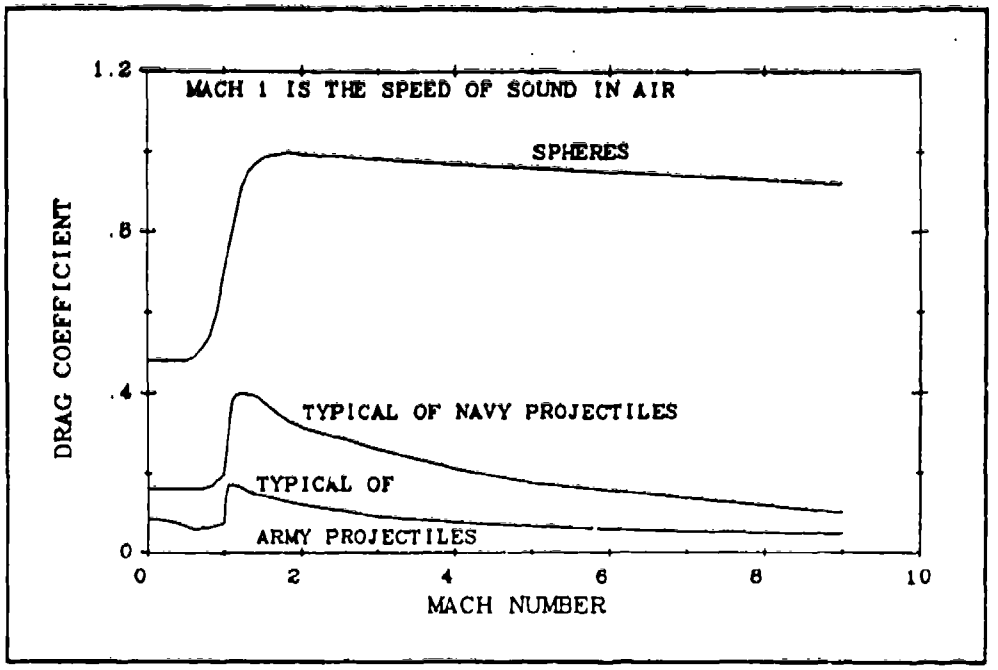

Figure 30. Typical Drag Coefficient Curves.

humidity, and 70° F) is approximately 1.229 kg/m^3 (Johnson 1972; Backman and Goldsmith 1978).

9.2.4 A Finite Thickness Target Model. Recent analysis of perforation performance indicates that perforation involves two stages—a penetration phase in which the action taking place is the same as if the target were semi-infinite and a breakout phase in which the expended energy is directed toward fracturing the bulge which forms on the rear surface and accelerating the target material (plug) which breaks free. For long rod penetrators, the depth of penetration is proportional to the length of the penetrator multiplied by the striking velocity raised to a power. The thickness related to the breakout phase is proportional to the diameter of the penetrator. This is represented by the following equation:

$$T = L \cos(\theta) \left(\frac{V_L}{C} \right)^B + AD \ , \qquad (49)$$

where θ is the angle of obliquity, V_L is the ballistic limit for thickness T, and A, B, and C are empirical constants evaluated by fitting at least three velocity ballistic limit values, and cos is

the trigonometric cosine function. When fitting ballistic limit data resulting from more than one penetrator, a better fit for RHA targets might be obtained by modifying the equation to the following:

$$T = \sqrt{LD}\,\cos(\theta)\left(\frac{V_L}{C}\right)^B + AD\,. \tag{50}$$

Values for A range generally from –1 to 2; for B, the range of values is from 1.5 to 3; and for C, the range of values is from 1,000 to 3,000 when T, L, and D are in millimeters and V_L is in meters per second. No method has been found yet to calculate values apriori for A, B, and C, so a fit must be made to experimental data. However, after finding A, B, and C for a particular penetrator vs. target material, reliable estimates of ballistic limits may be made for other thicknesses and obliquities.

9.2.5 Grabarek's Equations. After establishing the ballistic limit (V_L) values for several target thickness/obliquity configurations, a fit may be made to determine the empirical constants in Equation 51. This equation will permit predictions of the ballistic limit for other target configurations. The values of the empirical constants are dependent on the target material and on all characteristics of the penetrator.

$$V_L = \sqrt{\frac{AD^3\left(\frac{T}{D}\left[\sec(\theta)\right]^{\beta}\right)^{\alpha}}{M}}\,. \tag{51}$$

where V_L is the ballistic limit (meters/second), A is an empirical constant, D is the penetrator diameter (mm), M is the penetrator mass (grams), T is the target thickness (mm), θ is the target obliquity, sec is the secant function, and α and β are empirical constants. The values for A range from about 5,000 to 60,000 or more, depending on the material properties of the penetrator and the target. Values for α and β are usually close to 1. If β is less than 1, then the penetrator performs better when fired against an oblique target than would be expected based on line-of-sight thickness (compared to normal impact).

The form of Equation 51 has been reported in Grabarek (1971, 1976) and Herr and Grabarek (1976).

To predict the residual velocity (V_R) for a given striking velocity (V_s) where the ballistic limit is known, the following may be used:

$$V_R = V_L \left(\frac{aX^2 + bX + c\sqrt{X}}{X + 1} \right), \tag{52}$$

where $X = \frac{V_s}{V_L} - 1$, a = 1.1, b = 0.8, and c = 1.65. If the striking velocity is greater than eight times the limit velocity, then the residual velocity is approximately 99% of the striking velocity. The values given for a, b, and c can be used in general. However, as empirical constants, the values are dependent on the penetrator and the target. This equation is reported in Herr and Grabarek (1976).

The residual mass (M_R) may be estimated using the following equation:

$$M_R = MB \left[X \left(\frac{D}{T \sec(\theta)} \right) \left(1 - \frac{kT \sec(\theta)}{L} \right) \right]^g, \tag{53}$$

where B and g are empirical constants, X is that of Equation 52, k is the projectile material factor (a value of 1 may be used, although a value greater than 1 should be used for high-density materials), D is the penetrator diameter, and L is the penetrator length. If the calculation for M_R is negative, then the residual mass is assumed to be 12% of the striking mass. Typical values for B lie in the range of 0.3 to 0.8 and for g, in the range 0.1 to 1.

These three equations may be used to make predictions about penetrator performance when fired against multiple-plate targets. The residual velocity and residual mass become the striking velocity and striking mass for the subsequent plate. Complications due to systematic deflection or misorientation of the penetrator while perforating the target array are not explicitly accounted for. Reasonably good fits to experimental data can be made over only a modest range of velocities and obliquities.

9.3 Theoretical Models.

9.3.1 The Alekseevskii/Tate Penetration Algorithm.

- The Equations. A frequently used algorithm for making quick (compared to hydrocodes), approximate predictions of long rod penetration performance impacting semi-infinite targets is that proposed by Alekseevskii (1966) and independently by Tate (1967, 1969). The justification for the first two of the four basic equations is shown in Figure 31. In these equations, L is the instantaneous length of the penetrator, V is the velocity of the tail end of the penetrator, U is the axial velocity at the interface between the penetrator and the target, and P is the instantaneous depth of penetration.

The erosion rate of the penetrator is as follows:

$$\frac{\Delta L}{\Delta t} = -(V - U) . \tag{54}$$

The minus sign is due to the fact that the erosion rate is decremental. The material which is eroded makes no direct contribution to the penetration.

The penetration rate is $\frac{\Delta P}{\Delta t} = U$. (55)

A schematic representation of the conditions for the third and fourth equation is shown in Figure 32.

The force balance at the base of the penetrator head region when $Y \leq H$ or when $Y > H$ and $U < V$ is as follows:

$$A_p L \rho_p \frac{\Delta V}{\Delta t} = -A_p Y . \tag{56}$$

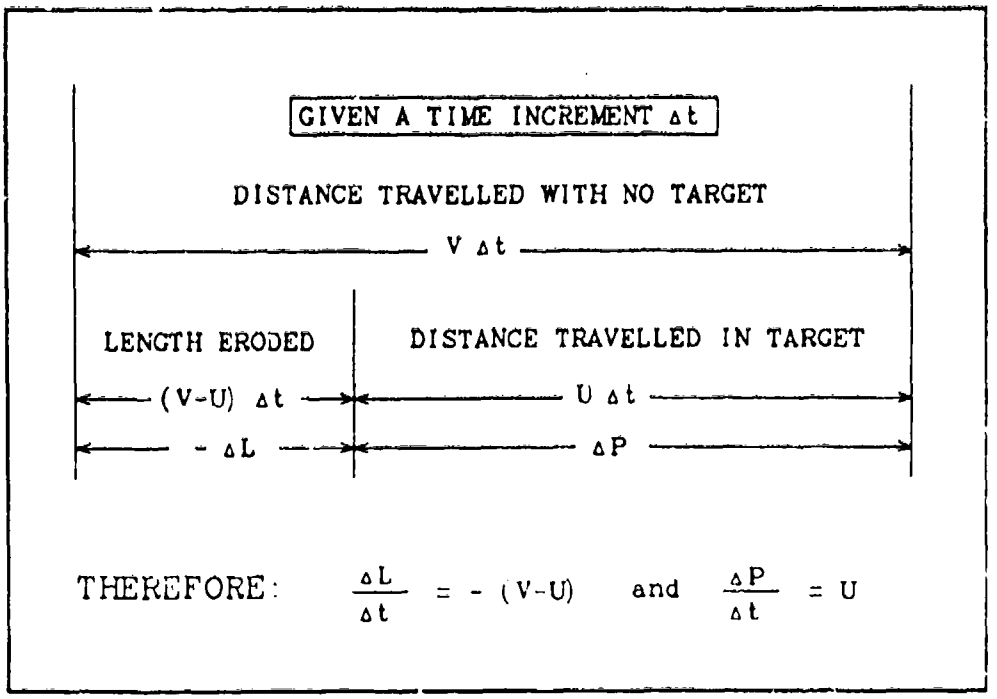

Figure 31. Basis for Equations 54 and 55.

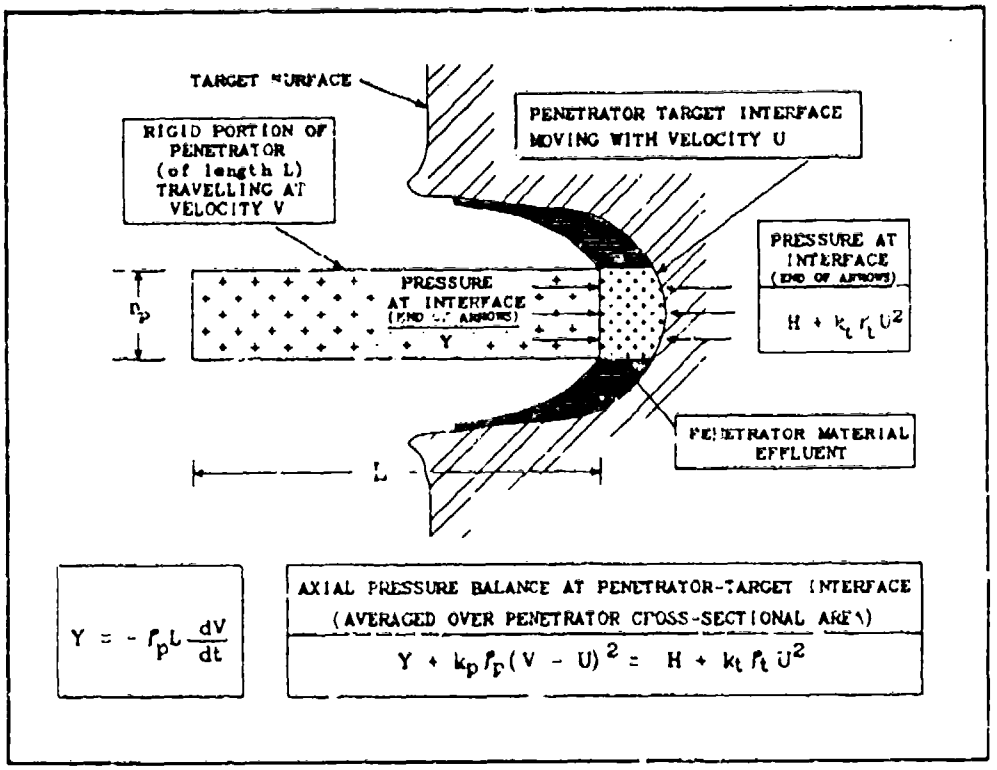

Figure 32. Schematic Illustrating Equations 56 and 58.

A_p is the initial penetrator cross-sectional area, and ρ_p is the penetrator density. When the pressure between the rigid portion of the penetrator and the target interface no longer supports material flow, then the remaining penetrator becomes rigid. Under these conditions,

$$A_p L \rho_p \frac{\Delta V}{\Delta t} = -A_p \left(H + k_t \rho_t V^2 \right), \tag{57}$$

or, equivalently, $Y = H + k_t \rho_t V^2$. In this case, Y is no longer interpreted as flow stress but as the resistive force of the target; k_t is a factor related to the target, and ρ_t is the target density.

The fourth and last of the basic equations is the modified Bernoulli equation, which is the pressure balance across the penetrator-target interface while the penetrator is eroding, and is as follows:

$$Y + k_p \rho_p (V - U)^2 = H + k_t \rho_t U^2 . \tag{58}$$

Equations 56 and 58 are based on the following simplifying assumptions.

(1) The dynamic behavior of the homogeneous penetrator is that of a rigid body up to some pressure Y (the flow stress of the penetrator). Likewise, the homogeneous target acts as a rigid body up to some pressure H (the target resistance). The penetrator material flows like a fluid for pressures at or above Y, and, likewise, the target material flows like a fluid for pressures at or above H.

(2) The retardation of the rigid portion of the long rod penetrator of length L is determined only by the pressure Y, which is the maximum stress level the still rigid rod material can sustain before it begins to act as a fluid.

(3) After an initial impact transient, the penetrator-target interface moves with a velocity U. If the penetrator erodes (becomes shorter than the initial length L_0 while penetrating the target), the rigid portion of the penetrator has a velocity V, while the front end

travels with the velocity U. Relative to the penetrator-target interface, the penetrator travels with a velocity V – U.

These four equations model the penetration process quite well for the time between the end of the initial impact transient (on the order of microseconds for metallic interactions) and the time when the penetrator erodes down to the length of the head region—generally between one radius and one diameter. For long rods, most of the penetration occurs between the two end phases and, therefore, the model is reasonably accurate in predicting depth of penetration. For short rods, most of the time is spent in the final phase, and the basic four-equation model underpredicts the depth of penetration.

The Alekseevskii formulation treats k_t and k_p as shape factors. Tate takes the values for k_p and k_t to both be 1/2, corresponding to the values which appear in the original Bernoulli equation (what follows is based on $k_p = k_t = 1/2$). Equation 58 is a quadratic equation in U and can be solved as follows:

Let $$\mu^2 = \frac{k_t \rho_t}{k_p \rho_p},\ a = 1 - \mu,\ b = -2V, \text{ and } c = V^2 + \frac{Y - H}{k_p \rho_p};$$

then, if $a = 0$, then $$U = -\frac{c}{b}. \tag{59}$$

Otherwise, the discriminant $d = b^2 - 4ac$ must be evaluated.

If $d \geq 0$, then $$U = \frac{-b - \sqrt{d}}{2a}.$$ (If $d = 0$, μ must not be 1.) (60)

If $d < 0$, then $Y \leq H$, then $U = 0$; otherwise, $U = V$. (61)

The interface velocity U has the restriction $0 \leq U \leq V$, and a check must be made to assure that it does not fall outside that range. The upper limit on the value of V when U reaches a

limit on its range can be calculated. When $H \geq Y$ and $V \leq \sqrt{\frac{H - Y}{k_p \rho_p}}$, then $U = 0$ (no penetration occurs, but the projectile continues to erode until $V \rightarrow 0$). When $H \leq Y$ and $V \leq \sqrt{\frac{Y - H}{k_t \rho_t}}$, then $U = V$ (the penetrator behaves as a rigid body). When V is greater than either critical value (depends on relation of H to Y), then both erosion and penetration will occur.

Figures 33 through 35 illustrate the behavior of Equation 58. These figures show the effect of varying Y with respect to H (H remains constant) for three different penetrator densities. In Figure 34, the penetrator and target have the same density. The curve labelled 2 in each of these figures is for $Y = H$. The value of U is the rate at which penetration occurs.

The conclusion may be drawn that if $Y \leq H$, the penetrator will always erode (because $U < V$), and if $Y < H$, there exists a positive value of V where U will go to 0 as explained previously. Below this value of V, no penetration into the target occurs. However, the penetrator continues to erode until V goes to 0. On the other hand, if $Y > H$, there exists a value of V below which the entire penetrator is rigid ($U = V$). Above this value of V, the penetrator erodes.

If Equations 59, 60, and 61 are approximated by $\frac{U}{V} = \frac{1 - \frac{\psi}{V^2}}{1 + \mu}$ where $\mu = \sqrt{\frac{k_t \rho_t}{k_p \rho_p}}$ and $\psi = \frac{H - Y}{k_p \rho_p}$, and if Y and H are assumed to be constants, then these equations can be integrated in closed form for the cases where $Y = 0$, $Y = H$, and $Y = H/(2 + \mu)$. These are the S_1, S_2, and S_3 functions which have been published in Frank and Zook (1987, 1991).

If Equation 54 is set to 0, representing a constant mass (rigid) penetrator (requires $Y > H$), then Equation 57 is applicable and can be integrated in closed form to yield the following:

$$\frac{P_t}{L_0} = \frac{\rho_p}{2k_t \rho_t} \ell n \left[1 + \frac{k_t \rho_t V_0^2}{H} \right]. \qquad (62)$$

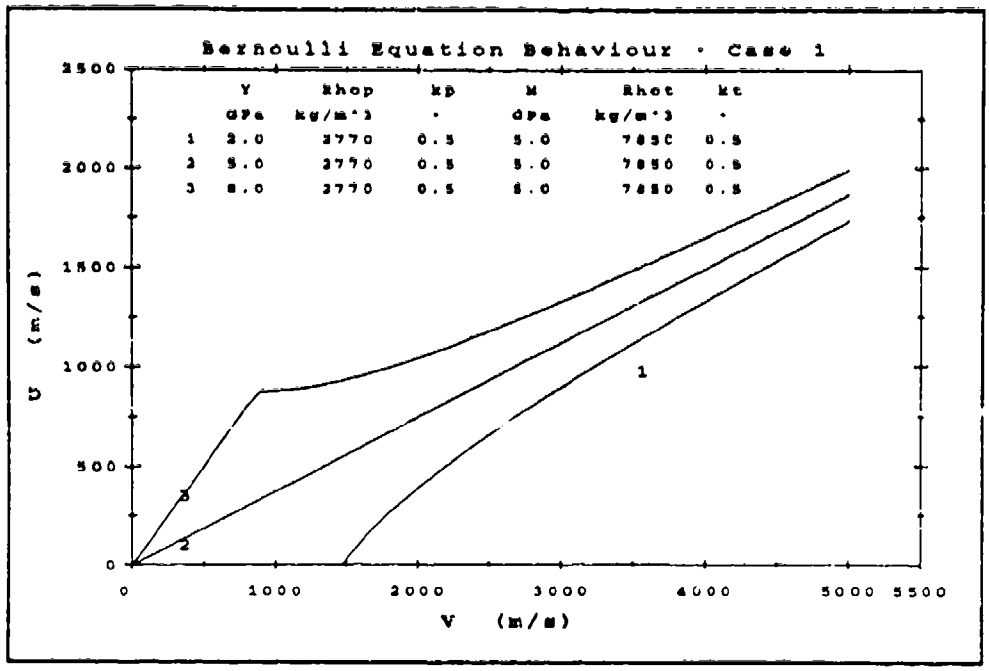

Figure 33. U vs. V for Y = 2, 5, and 8 GPa and ρ_p = 2,770 kg/m^3.

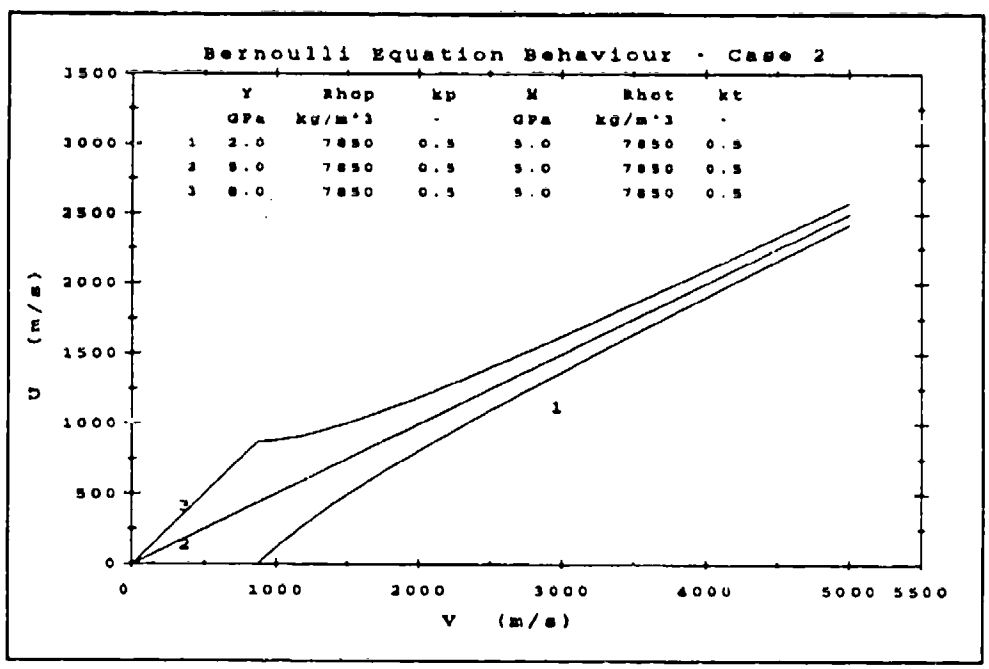

Figure 34. U vs. V for Y = 2, 5, and 8 GPa and ρ_p = 7,850 kg/m^3.

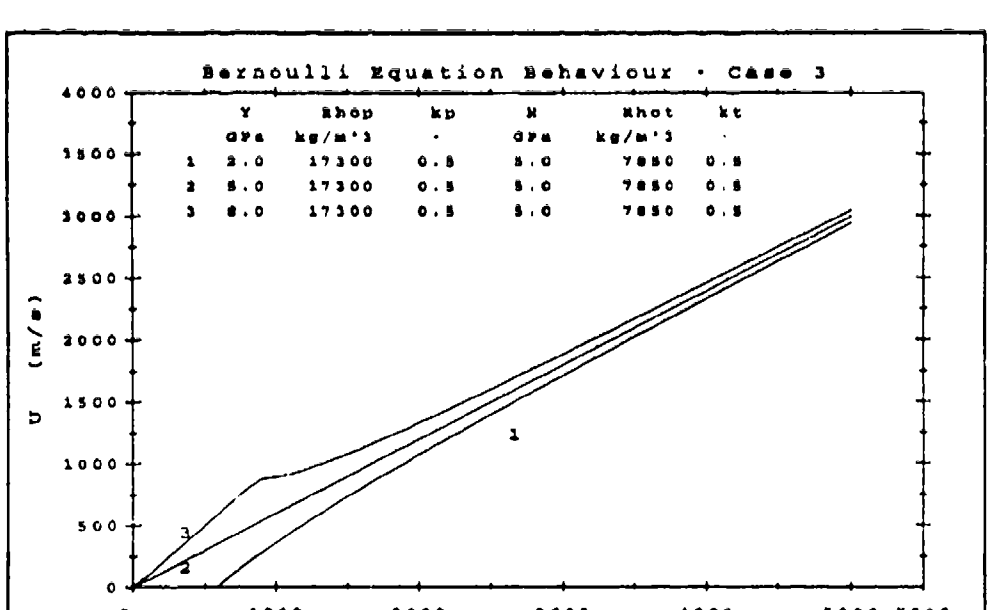

Figure 35. U vs. V for Y = 2, 5, and 8 GPa for ρ_o = 17,300 kg/m^3.

The integration is performed assuming that H is constant. This equation is similar to the S_D function in Frank and Zook (1987, 1991).

The S_D function, combined with one of the S_L functions (S_1, S_2, or S_3) in the equation

$$P_f = (L_o - mD)\, S_L + mD\, S_D ,$$

can be used to generate P/L curves, which compare favorably with experimental data. This approach has been used to make predictions of penetrator performance in a number of studies.

• Determining a Value for Y From Experiment. Y is identified as being the pressure at which the material begins to flow (deform plastically). The value of Y can be determined from low striking velocity experimental data. When a penetrator impacts a target which has greater strength than the penetrator at low speeds (below about 500 m/s for tungsten alloy or DU vs. RHA), the penetrator erodes and any penetration into the target is a few millimeters at most. So the assumption is made that U = 0. Equations 54 and 56 with U = 0 are solved simultaneously for Y and integrated to produce the following:

$$Y = \frac{\frac{1}{2}\rho_p V_0^2}{\ell n\left(\frac{L_0}{L_r}\right)}, \tag{63}$$

where L_r is the measured residual length and L_0 is the initial length. It is necessary to recover the residual penetrator in order to obtain L_r, since it would be difficult to estimate a proper delay time to catch the residual penetrator on x-ray film. Since little or no penetration of the target occurs, the penetrator remains at the target surface until $V \rightarrow 0$.

Figures 36 and 37 show the variation of Y for some penetrator materials. Figure 36 is based on data reported in Wilkins and Guinan (1973). From Figures 36 and 37, it appears that Y may be a function of the striking velocity. However, there was some penetration (less than 8 mm) for the data of Figure 37 and part, if not all, of the variation of Y is not real (Equation 63 assumes 0 penetration). The amount of penetration for the data of Figure 36 was not reported. Since Y is assumed to be constant, the value to be used is the extrapolated value at V = 0.

Equations for computing Y, which are slightly more complex than Equation 63, have been proposed. The first is Taylor (1948). Wilkins and Guinan (1973) offer a similar equation. The added complexity of these equations does not seem to be justified.

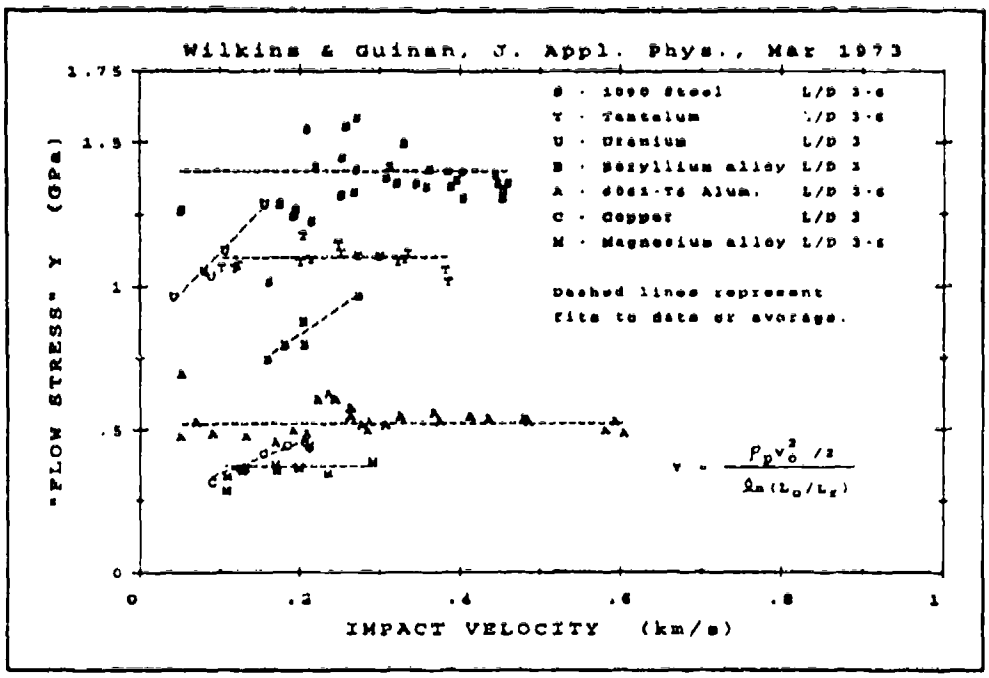

Figure 36. Material Flow Stress Y for Various Materials.

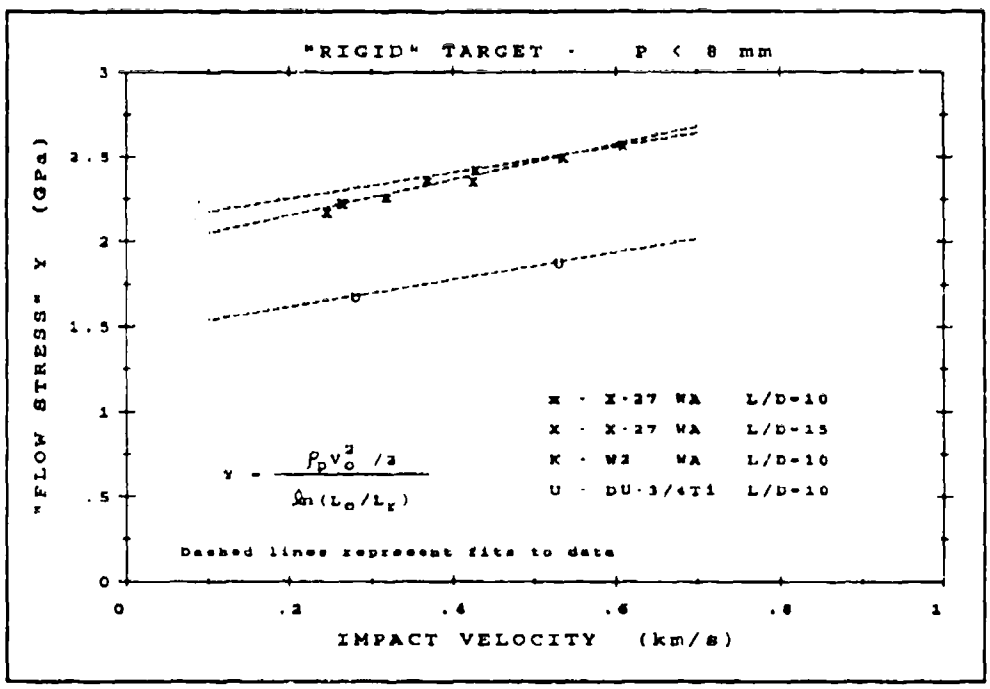

Figure 37. Material Flow Stress Y for Tungsten Alloy and DU.

• Determining a Value for H. The target resistance pressure H deep in the target can be determined from cavitation analysis (Hill 1950; Hopkins 1960; Goodier 1965; Hanagud and Ross 1971; Tate 1986a).

Expanding cylindrical cavity (Hill 1950),

$$H = \frac{Y_{ys}}{\sqrt{3}}\left[1 + \ell n\left(\frac{E}{Y_{ys}\sqrt{3}}\right)\right] + \frac{\pi^2}{18}E_t \,. \tag{64}$$

Expanding spherical cavity
(Hopkins 1960; Goodier 1965)

$$H = \frac{2Y_{ys}}{3}\left[1 + \ell n\left(\frac{2E}{3Y_{ys}}\right)\right] + \frac{2\pi^2}{27}E_t \,. \tag{65}$$

Expanding spherical cavity (Hanagud and Ross 1971),

$$H = \frac{2Y_{ys}}{3}\left[1 - \frac{E_t}{E} + \ell n\left(\frac{2E}{3Y_{ys}}\right)\right] + \frac{2\pi^2}{27}E_t \,. \tag{66}$$

Advancing cavity (Tate 1986a)

$$H = Y_{ys}\left[\frac{2}{3} + \ell n\left(\frac{2E}{3Y_{ys}}\right)\right]. \tag{67}$$

In these equations, Y_{ys} is the target yield strength (identified as Y in Figure 38, E is Young's modulus, and E_t is the slope of the curve from the yield point to the ultimate strength point (assumes a bilinear stress-strain curve). Tables 8 and 9 show relevant material

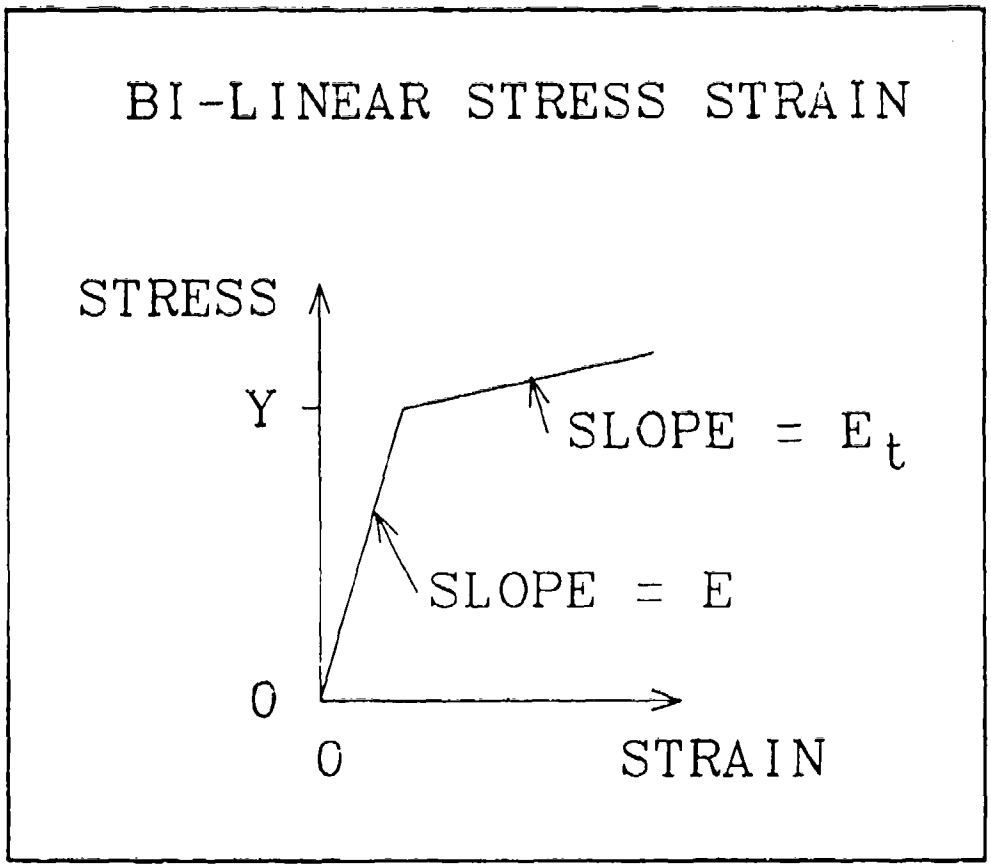

Figure 38. Bilinear Stress-Strain Slope Definitions.

Table 8. Selected Material Properties

Material	Density (kg/m^3)	Yield (GPa)	E (GPa)	E_t (GPa)
RHA 0.5"	7,850	1.23	208	0.64
RHA 1.5"	7,850	0.87	206	0.76
RHA 4.0"	7,850	0.94	206	0.44
HHA (USS,L)	7,850	1.72	214	2.38
Al 7039	2,800	0.41	75	0.55
WA 90%	17,200	1.18	324	2.56

Table 9. Computed Values of Target Resistance

Material	H_1 (GPa)	H_2 (GPa)	H_3 (GPa)	H_4 (GPa)
RHA 0.5"	4.31	5.16	5.16	6.63
RHA 1.5"	3.39	4.07	4.07	4.98
RHA 4.0"	3.41	4.07	4.07	5.31
HHA (USS,L)	6.54	7.95	7.94	8.75
Al 7039	1.64	1.99	1.99	2.24
WA 90%	5.54	6.76	6.75	6.93

H_1 - Equation 64 (Hill 1950).

H_2 - Equation 65 (Hopkins 1960; Goodier 1965).

H_3 - Equation 66 (Hanagud and Ross 1971).

H_4 - Equation 67 (Tate 1986b).

parameters and the resulting calculations for H. The yield, E, and E_1 in the table were obtained from bilinear approximations to stress-strain compression tests performed at the BRL.

The values in Table 9 are the values for H using the values of Table 8 in Equations 64 through 67.

The values for H_4 (the last column) are in close agreement with the values needed in the algorithm to give reasonable agreement with experimental data in the ordnance velocity range (1,000–1,800 m/s).

An alternative method for calculating H based on the BHN and Young's modulus is given by Tate (1986b) and is summarized in Zukas (1991). This method is the following:

$$H = \sigma_{y1}\left(\frac{2}{3} + \ell n\left(\frac{0.57E}{\sigma_{y1}}\right)\right), \quad \text{where} \quad \sigma_{y1} = 4.2 \times 10^6\,\text{BHN} .$$

The dynamic compressive yield stress σ_{yt} has units of pascals using the previous equation (e.g., for BHN = 270, $\sigma_{yt} = 1.13 \times 10^9$ Pa, and assuming E = 206 GPa, then H = 6.0 GPa). An equation is also given for computing Y, but Tate seems to make a distinction between the Y of Equation 37, which he calls σ_{yp}, and the Y of Equation 38 (the modified Bernoulli equation). He indicates that $Y = 1.7\ \sigma_{yp}$ and that $\sigma_{yp} = 4.2 \times 10^6$ BHN Pa.

• Numerical Integration Results. To solve Equations 54 through 58 for any arbitrary value of Y or H requires using a numeric integration scheme. This involves establishing the values for the penetrator length, density, striking velocity, and Y; the target density and H; setting P = 0; and selecting a suitable time step. The differentials are computed for a value of U, resulting from evaluating Equation 58, and L, V, and P are updated. These steps are cycled until $V \rightarrow 0$. The following values were used to create Figures 39 through 46.

$\rho_p = 17{,}300$ kg/m^3, $Y = 1.9 \times 10^9$ pascals, $k_p = 1/2$;
$\rho_t = 7{,}850$ kg/m^3, $H = 5.5 \times 10^9$ pascals, $k_t = 1/2$.

These values remain constant independent of any velocities.

The first set of plots (Figures 39 through 42) show how the velocity ratios V/V_0 and U/V_0 (if $U > 0$ at time 0), the length ratio L_t/L_0, and the depth to initial length ratio P_i/L_0 change with time for striking velocities of 500, 1,000, 1,500, and 2,000 m/s, respectively. The vertical dash-dot line in Figure 40 marks the time when the phase change from a penetration-erosion phase ($0 < U < V$) to an erosion-only phase ($U = 0$) took place. Although the length and diameter values used are shown, these curves apply to any high L/D value ($L/D \geq 15$) because the diameter does not appear in any of the equations.

Figures 43 through 45 show the same velocity and length ratios as in Figures 40 through 42 but plotted as a function of depth normalized by the initial length rather than of time. Note that there is no figure corresponding to Figure 39 because for that case, there was no penetration into the target; although, as will be shown later, penetration of up to about 4 mm (for striking velocities below 500 m/s) is observed experimentally for the penetrator and target material represented by the parameter values used for these plots. These plots look quite similar to the plots as a function of time because the penetration into the target progresses

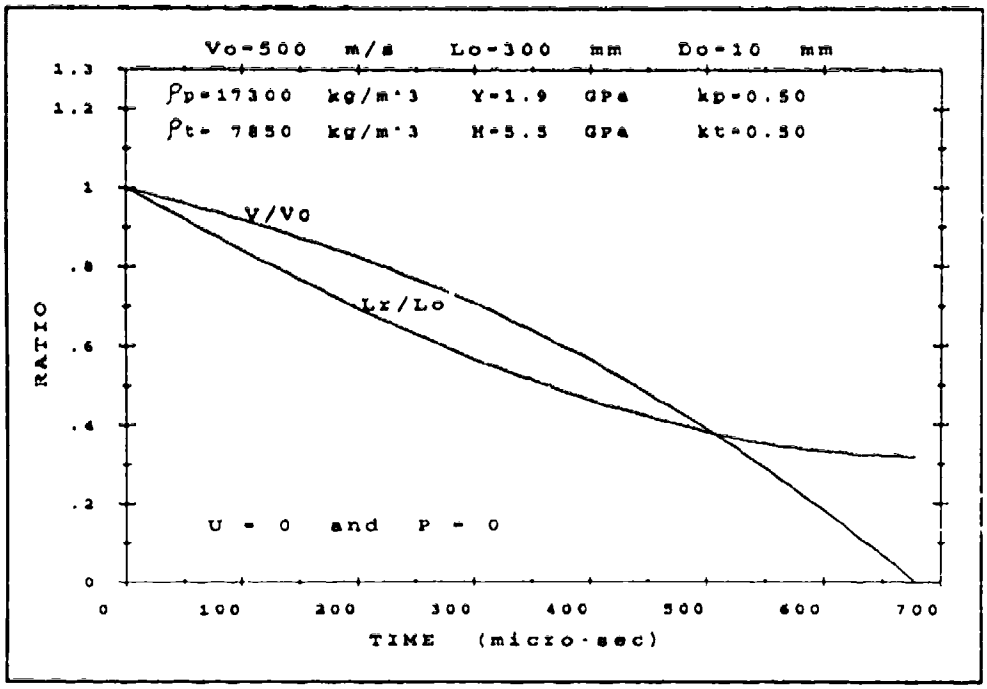

Figure 39. The Ratios as a Function of Time for V_o = 500 m/s.

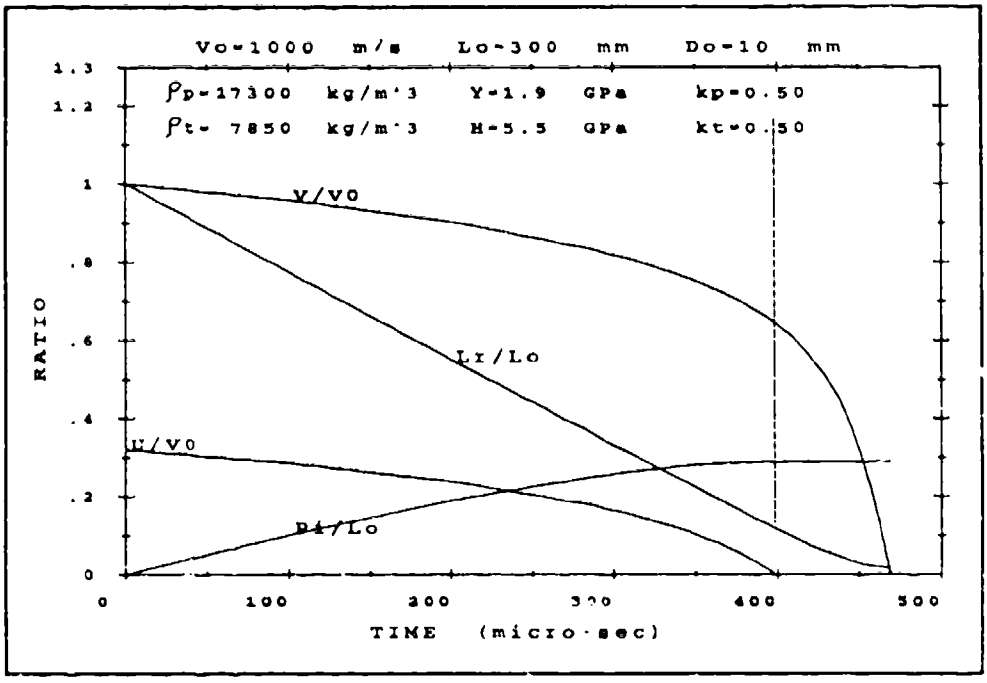

Figure 40. The Ratios as a Function of Time for V_o = 1,000 m/s.

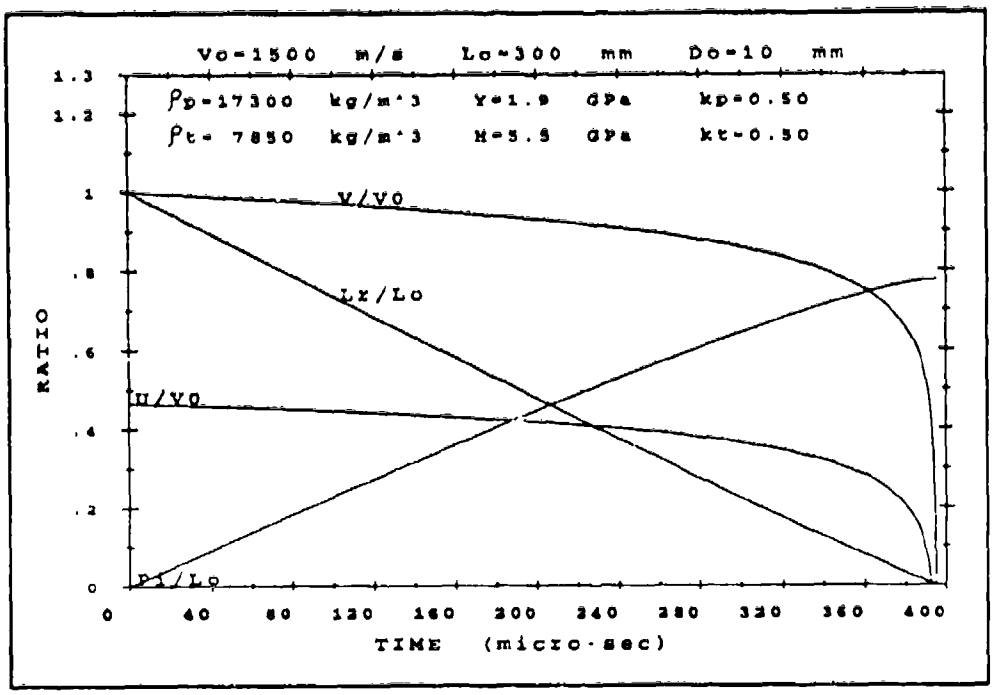

Figure 41. The Ratios as a Function of Time for V_o = 1,500 m/s.

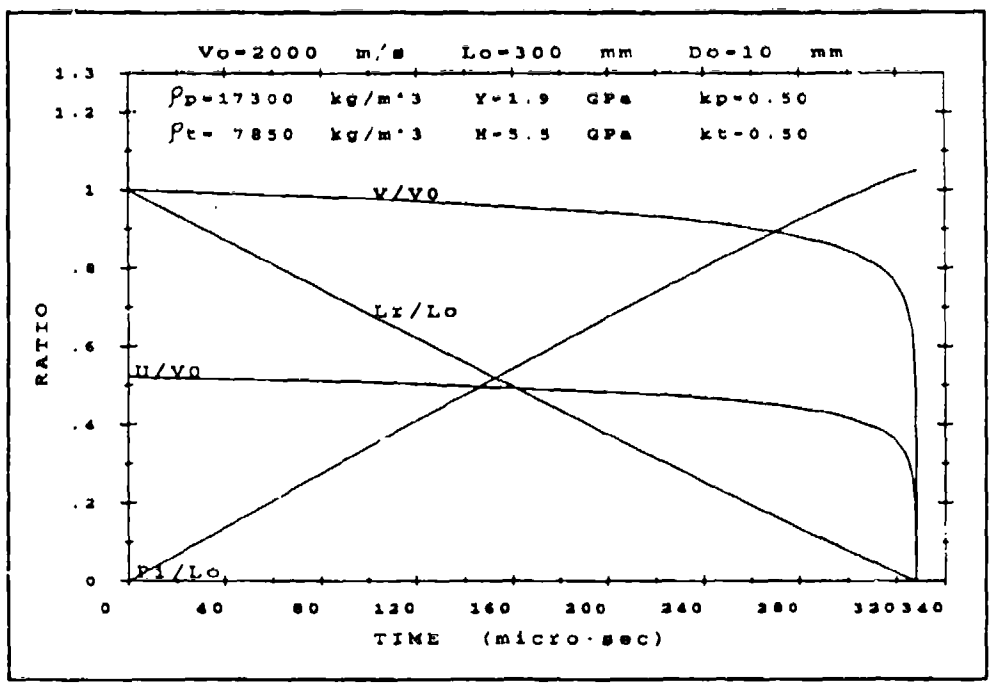

Figure 42. The Ratios as a Function of Time for V_o = 2,000 m/s.

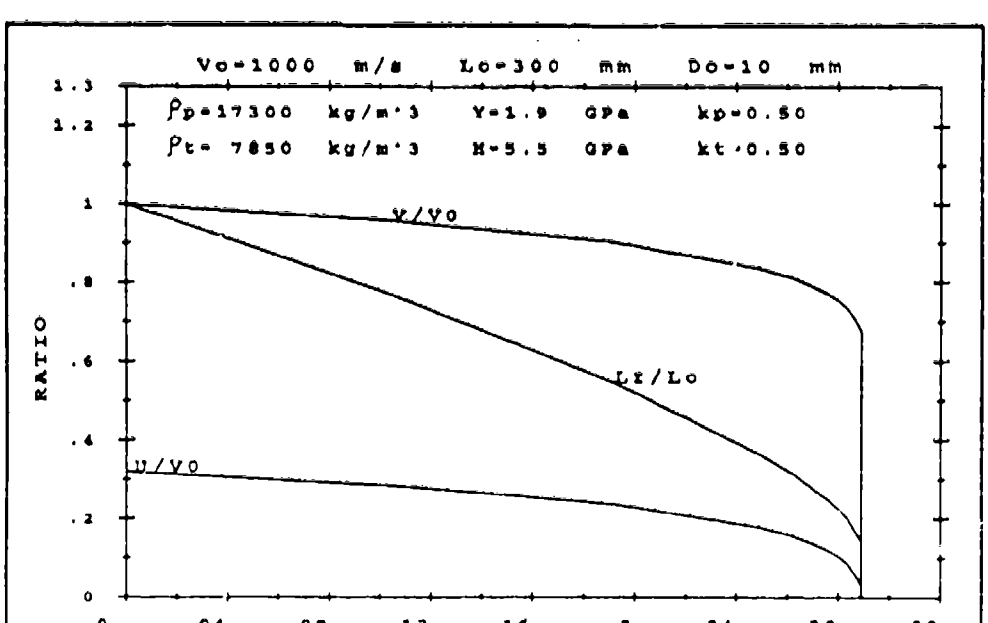

Figure 43. The Ratios as a Function of Normalized Depth of Penetration for V_o = 1,000 m/s.

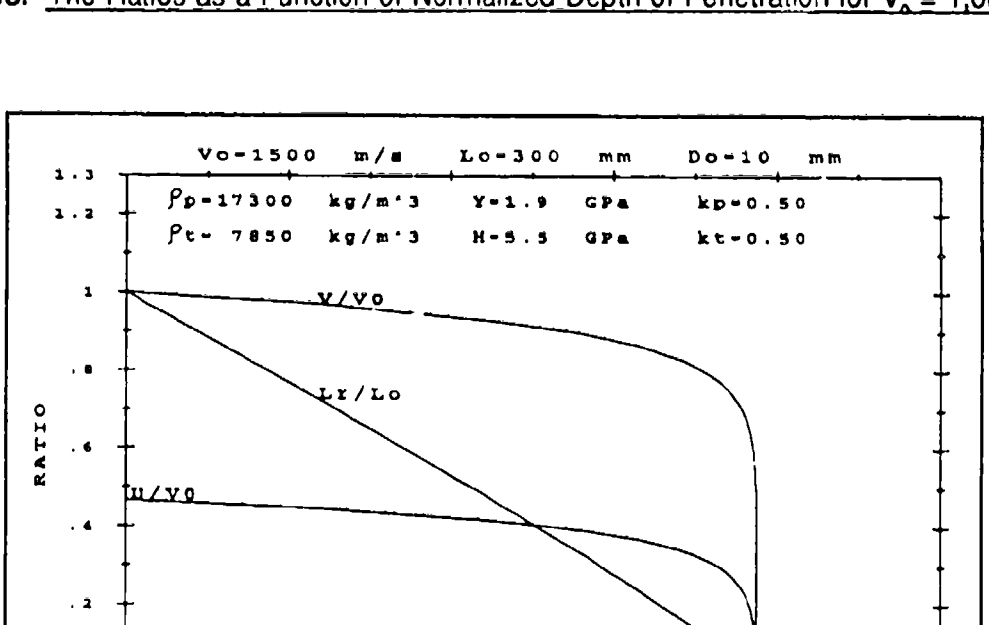

Figure 44. The Ratios as a Function of Normalized Depth of Penetration for V_o = 1,500 m/s.

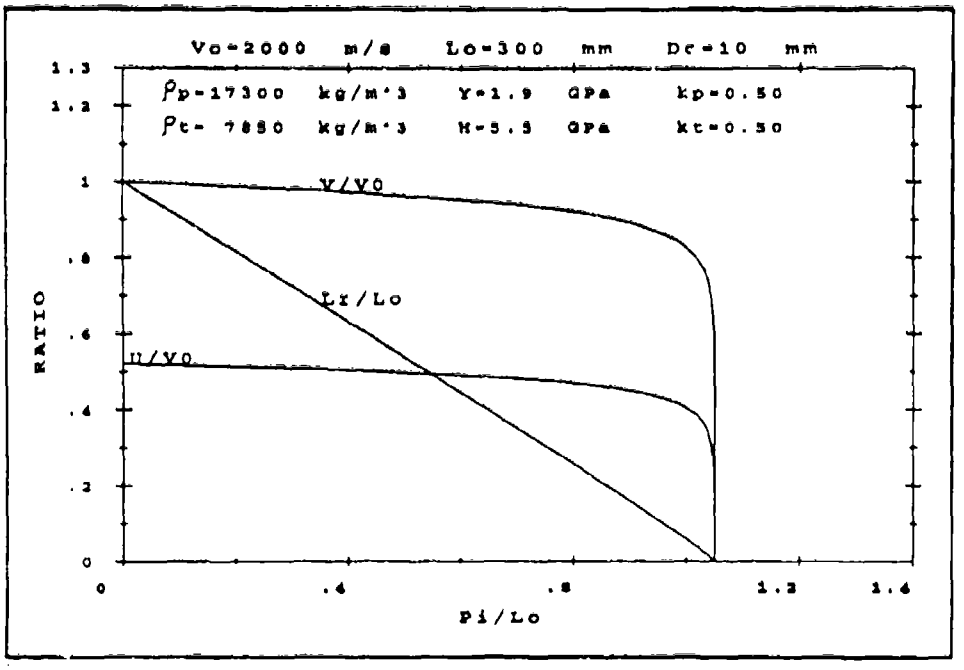

Figure 45. The Ratios as a Function of Normalized Depth of Penetration for V_0 = 2,000 m/s.

almost linearly with time. For the cases of Figures 44 and 45, both U and V go rapidly to 0 as the length approaches 0. This limits the final P/L_0 and appears to be the reason why this algorithm (Equations 56 through 58) applies only to large L/D and, as will be shown in the next section, to striking velocities below about 1,800 m/s.

By running the algorithm through a series of striking velocities, a P/L curve can be generated. The sequence used here is the following:

25 to 100 m/s, stepping by 25 m/s,
200 to 2,000 m/s, stepping by 100 m/s,
2,200 to 3,000 m/s, stepping by 200 m/s, and
3,250 to 5,000 m/s, stepping by 250 m/s.

Figure 46 shows the final depth of penetration normalized by the initial penetrator length (P_f/L_0) as a function of impact velocity for selected values of H and using the Y value (1.9 GPa) from Section 9.3.1. The experimental data represented by the x s are tabulated in

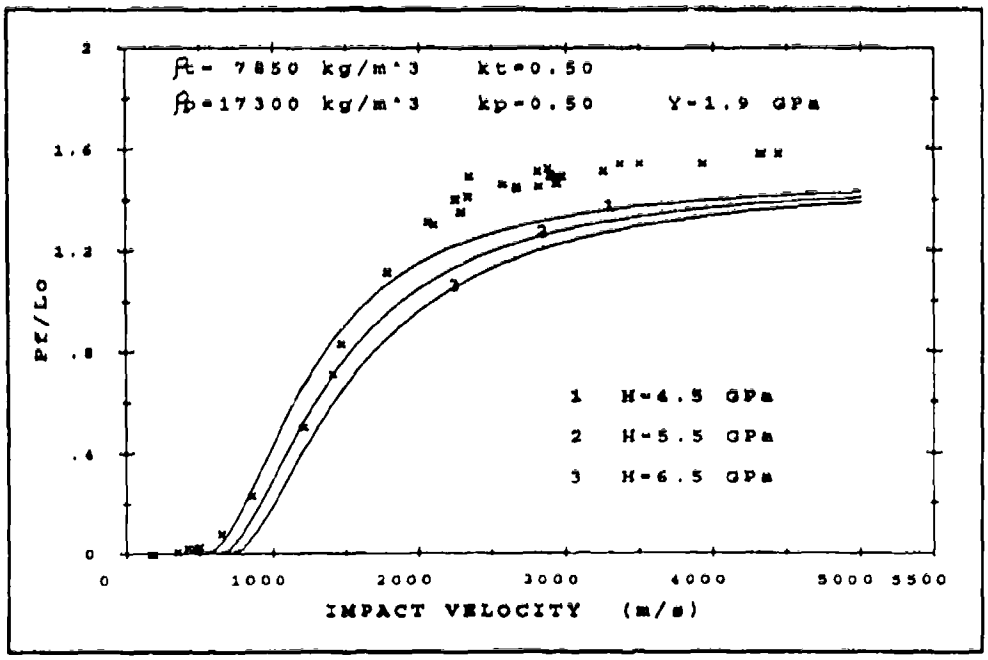

Figure 46. Normalized Depth of Penetration for H = 4.5, 5.5, and 6.5 GPa.

range (1,000–1,800 m/s), the experimental data fall close to the curves labeled 1 (H = 4.5 GPa) and 2 (H = 5.5 GPa).

All three curves fail to represent the experimental data at high striking velocities. One reason for this is illustrated in Figure 47, which shows the residual length normalized by the initial length (L_r/L_0) as a function of striking velocity. The predicted residual length for striking velocities above 1,300 m/s is very close to 0. The value of the target resistance H has little effect on the residual length because it is so much larger than the value for Y. The trend in the experimental data suggests that this aspect of the algorithm is not modeled correctly. When the length approaches 0, the velocity V drops rapidly (per Equation 56) thus limiting the depth of penetration at high velocities as shown in Figure 46.

9.3.2 A Modified Alekseevskii/Tate Penetration Model. It is desirable to have a model which will give reasonable depth of penetration predictions independent of the length of the penetrator. As suggested in the previous section, short penetrators with Y < H impacting at

Table 10. Tungsten Alloy (ρ_p = 17,300 kg/m^3) Penetrators vs. RHA

L_0 / D_0	V_0 (m/s)	P_f / L_0	L_r / L_0
15	245	0.004	0.79
	264	0.002	0.76
	424	0.014	0.52
	495	0.029	—
	544	0.030	—
	577	0.034	0.32
	727	0.085	0.19
	934	0.237	0.14
	1,551	0.84	—
	2,890	1.52	—
	2,980	1.51	—
	2,990	1.50	—
	4,008	1.55	—
20	2,140	1.32	—
	2,180	1.31	—
	2,330	1.41	—
	2,420	1.50	—
	2,900	1.46	—
	2,980	1.50	—
	3,020	1.50	—
23	1,291	0.51	—
	1,494	0.72	—
	1,865	1.12	—
	2,365	1.36	—
	2,409	1.41	—
	2,653	1.47	—
	2,742	1.46	—
	2,746	1.45	—
	3,335	1.53	—
	3,449	1.55	—
	3,580	1.55	—
	4,398	1.59	—
	4,415	1.59	—
	4,525	1.59	—
30	2,960	1.53	—
	3,020	1.47	—
	3,050	1.50	—

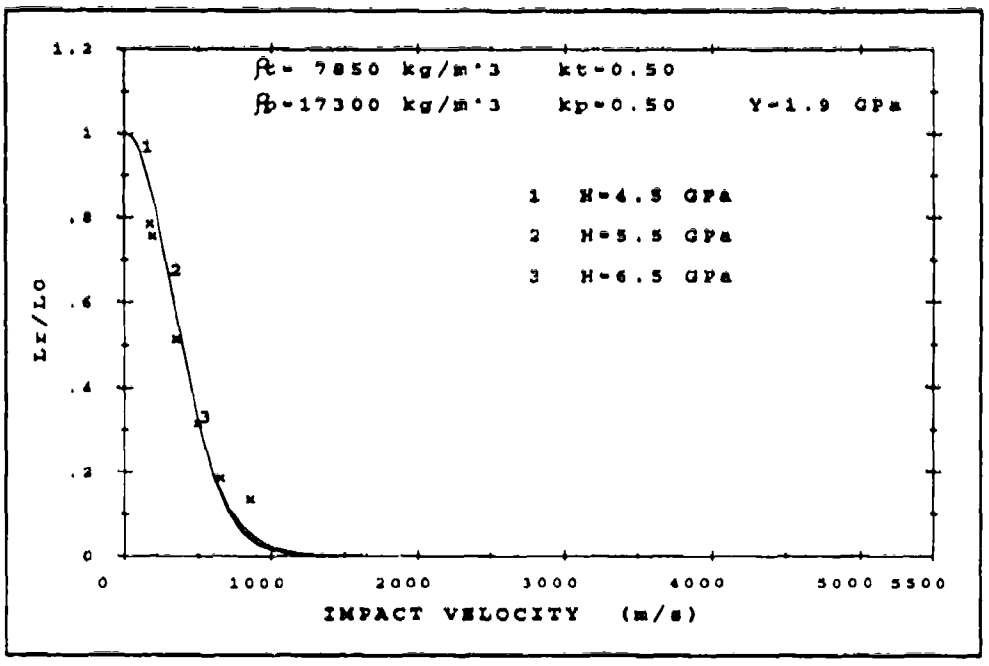

Figure 47. Normalized Residual Length for H = 4.5, 5.5, and 6.5 GPa.

velocities above the Bernoulli cutoff velocity, i.e., $\sqrt{\frac{Y-H}{k_p \rho_p}}$, spend most of the time with the remaining penetrator in the head region. When the tail end of the penetrator is contained in the head region, erosion of the penetrator is greatly reduced. In other words, the penetrator behaves more like a rigid penetrator.

To model this behavior using the one-dimensional model of the previous section, the following equation has been found to produce reasonable results:

$$Y = Y_0 \, EXP\left[\frac{2\,(L_0/L - 1)}{(L_0/D)^{1.2}}\right]. \qquad (68)$$

This equation forces Y to take on exponentially increasing values as the length erodes below approximately one diameter. For L/D < 1 penetrators, the value of Y is initially Y_0, but then begins to increase exponentially immediately. The effect of Y increasing is to reduce the erosion rate. The exponential increase of Y does not have a physical basis—it is simply a

mathematical tool to induce the desired behavior. Figure 48 illustrates how Y varies with length and with L/D. Recent experimental tests with L/D = 1 down to L/D = 1/8 penetrators suggest that what happens physically is that as the length shortens below one diameter, the penetration process changes from a state of uniaxial stress to a state of uniaxial strain. The L/D = 1/8 penetrator impacting the target did not expand radially (did not erode) (Bjerke, Zukas, and Kimsey 1991).

Applying the four basic equations plus Equation 68 results in the curves shown in Figure 49. The data shown are for tungsten alloy L/D = 1, L/D = 10, and L/D = 23 penetrators vs. RHA targets. There is generally good agreement between the predictive curves and the experimental data. Table 11 shows the values plotted for the L/D = 1 and L/D = 10 shots. These shots were all fired in Range 110 of TBD, with the exception of the high velocity L/D = 1 shot (V_0 = 4,881 m/s), which was fired at a range facility located in Tullahoma, TN. The L/D = 23 values are tabulated in a previous table (Silsby 1984).

One reason for saying that the exponential function for Y is not physical is illustrated in Figure 50. This shows that for an L/D = 1 penetrator impacting at 5,000 m/s, the value for the penetration velocity U begins to increase shortly after impact and continues to increase before merging with the velocity V of the rigid portion of the penetrator (the merge point is marked by a vertical dash-dot line). There is no physical basis for U to increase.

9.3.3 Other Modifications to the Alekseevskii/Tate Penetration Model. From Figures 40 to 42, it can be seen that U, although nearly constant, varies with time, especially as $U \rightarrow 0$. Therefore, it seems reasonable that there should be a term included in Equation 58 that contains dU/dt. Since Equation 58 is a pressure balance equation, the coefficient of dU/dt should have units of mass/area. The equation would then be rearranged to solve for dU/dt, giving four differential equations to solve simultaneously. This equation is as follows:

$$\frac{M_x}{A_p}\frac{dU}{dt} = Y + k_p \rho_p (V - U)^2 - \left(H + k_t \rho_t U^2\right).$$

It is not clear how to identify the mass M_x involved. One theory is that since some of the mass in the target ahead of the penetrator-target interface gains momentum shortly after

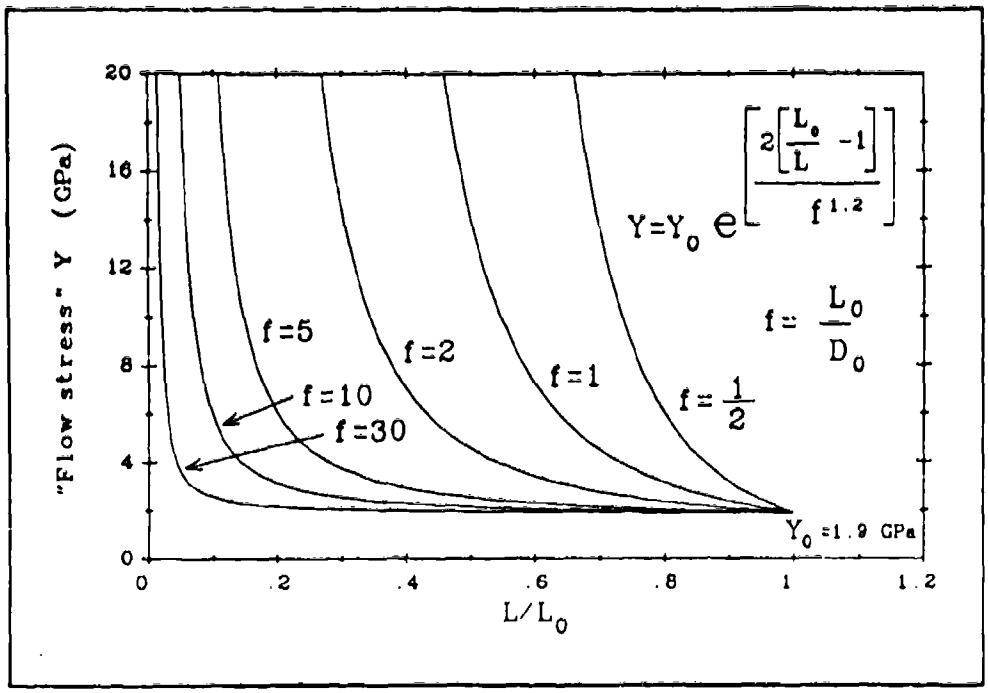

Figure 48. Flow Stress Y as a Function of L and L/D.

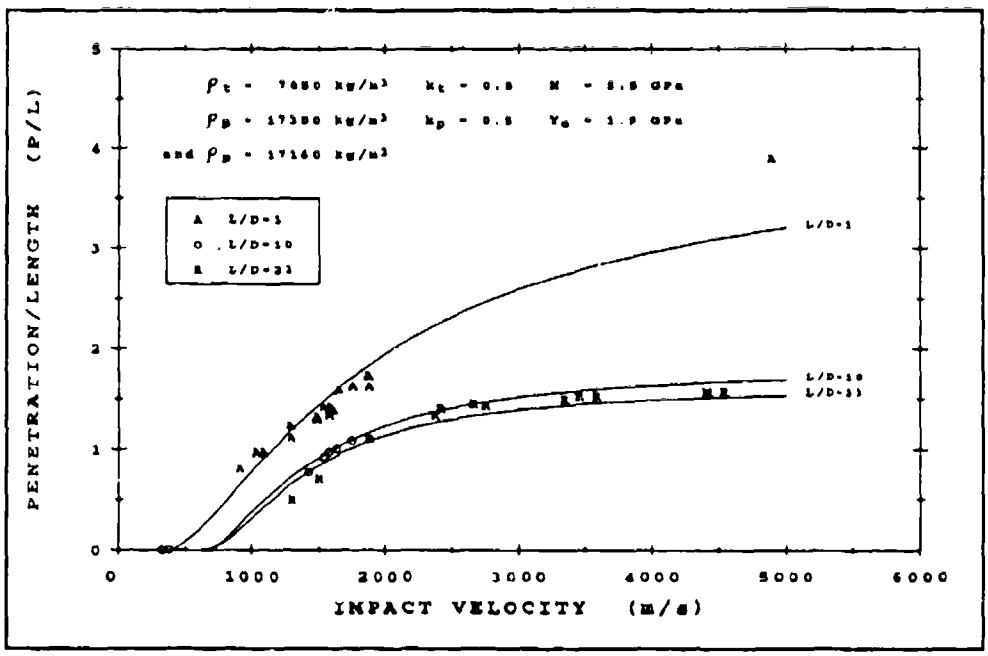

Figure 49. Penetration Normalized by Length (P/L) Curves Generated Using the Basic Four-Equation Alekseevskii/Tate Model With Y Varying Exponentially With Length and L/D.

Table 11. Depth of Penetration for L/D = 1 and 10 Tungsten Alloy Penetrators vs. RHA

L_0 / D_0	V_0 (m/s)	P_1 / L_0	L_0 / D_0	V_0 (m/s)	P_1 / L_0
1	906	0.82	1	1,748	1.64
1	1,027	0.98	1	1,853	1.75
1	1,078	0.98	1	1,864	1.74
1	1,283	1.25	1	1,867	1.64
1	1,286	1.13	1	4,881	3.91
1	1,480	1.34	10	318	0.014
1	1,481	1.31	10	369	0.018
1	1,527	1.44	10	1,419	0.79
1	1,572	1.36	10	1,526	0.93
1	1,573	1.41	10	1,530	0.94
1	1,578	1.44	10	1,567	0.99
1	1,600	1.41	10	1,626	1.02
1	1,642	1.61	10	1,740	1.10

impact, that an equivalent target mass moving with velocity U should be used. In this theory, the effective mass is that of a hemisphere which results in $\frac{M_x}{A_p} = \frac{1}{3}\rho_t D_0$. Applying this in the algorithm, it is assumed that the mass exists at the moment of impact (otherwise, dU/dt is infinite). Since the dU/dt term now involves the penetrator diameter, the predictions made by the model will vary with penetrator diameter. Exercising the basic four-equation model with only this modification shows that the shorter L/D penetrators yield a larger P/L than high L/D penetrators. This is the correct direction, but the variation is much too small compared to experiment. Another possibility for the mass M_x is the mass of the penetrator in the head region.

Assuming one diameter, $\frac{M_x}{A_p} = \rho_p D$. This also involves the penetrator diameter and gives similar results. Since the selection of a definition for M_x is arbitrary, no plots are shown.

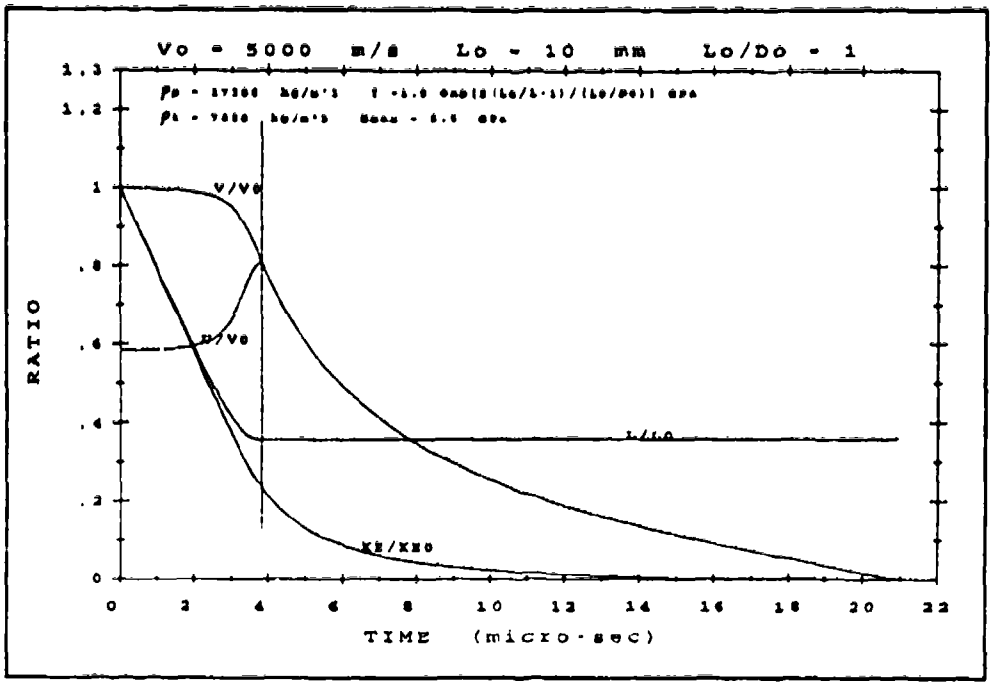

Figure 50. Ratios as a Function of Time for an L/D = 1 Penetrator at 5,000 m/s.

Another theory which introduces the penetrator diameter is that proposed by Kozlov (1986). In this theory, two terms are added to Equation 58, which are functions of dynamic viscosity and of the penetrator diameter. Equation 58 becomes the following:

$$Y + \mu_p \frac{(V - U)}{2 D_0} + k_p \rho_p (V - U)^2 = H + \mu_t \frac{U}{2 D_0} + k_t \rho_t U^2 .$$

The Kozlov paper uses L in the first term rather than D, but in testing the theory, it seems more correct to use D. The difficulty in using this theory is that of determining the values to be used for the viscosity coefficient.

Both Alekseevskii and Tate in their original papers assumed that Y and H should be treated as constants. If Y is the material flow stress, it is reasonable to assume that Y should be constant. As pointed out in the previous case where Y was made to vary exponentially, the treatment of Y as a variable is entirely artificial. A reasonable argument can be made that H is not constant. The value for H developed from cavitation analysis is that deep in the target. When the penetrator-target interface is close to a surface (either front, rear, or side),

the target resistance should be less than the resistance in a highly confined deep cavity. Just how H varies is not clear. At the front surface, a good estimate of the target resistance can be made using the Brinell hardness number of the surface (to convert the BHN to pressure in pascals, multiply by 9.8×10^6 or by 9.8×10^7 for dynes per cm^2). Figure 51 shows how H might vary as a function of depth into the target. The function plotted here is as follows:

$$H = H_{BHN} + (H_{max} - H_{BHN})\left(1 - EXP\left[-cP\right]\right),$$

with H_{max} = 5.5 GPa, and the BHN is [illegible] so that H_{BHN} = 2.352 GPa. Curves are shown for c = 50, 100, and 200. P is the depth into the target in meters.

9.3.4 Computer Codes for Numerical Simulation of Impact. The availability of high-speed, large memory computers has made possible numerical simulation of impact events in either two dimensions or in three dimensions. Three-dimensional codes are needed to model oblique impact cases or yawed penetrator cases. The requirements in terms of memory and execution time for two-dimensional codes are less severe than three-dimensional and are therefore less costly.

Two approaches have been taken with respect to setting up and running a problem. A Eulerian grid system remains spatial fixed, and material is transported through the grid. The Eulerian code is good for problems which involve compressive distortion of material. The other approach is the Lagrangian grid system in which the mass in each grid cell is constant and the grid distorts with time. The Lagrangian code is better suited for problems involving expansive distortion. Some Eulerian codes use a Lagrangian feature of massless tracer particles to define material package boundaries. In any case, the basic differential equations which are solved are those of conservation of mass, conservation of momentum, and conservation of energy. Two methods of solution of the equations have been developed—finite difference and finite element.

The equations which are solved are relatively simple and straightforward. However, they must be solved in discrete time steps. One of the problems in running a hydrocode is in selecting a suitable time step. In Eulerian codes, there is a problem of how to handle cells which contain more than one material (e.g., how to compute densities for the two materials so

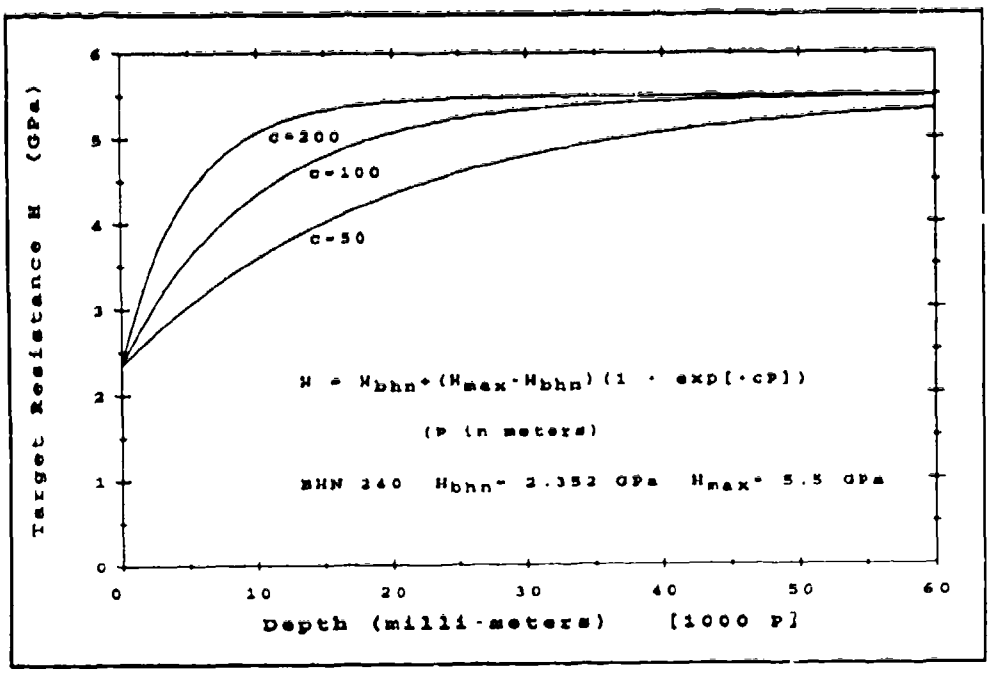

Figure 51. Target Resistance H as a Function of Depth Into the Target.

that the material volumes add up to the cell volume if that cell is completely filled or what should be done it there is void [or gaseous] space in the cell). In Lagrangian codes, the greatest problem is in when and how to rezone when the cells become greatly distorted. For both types of codes, it is usually necessary to include one or more slide lines (material interfaces) where one material is allowed to slide past the other. A number of equations of state have been developed to compute pressures developed by material under compression or tension. Failure criteria and how to implement it adds more complexity to solving problems using hydrocodes.

Some of the hydrocodes which have been used to solve terminal ballistics problems are as follows:

CSQ - Sandia National Laboratories, Albuquerque, NM.
CTH - Sandia National Laboratories, Albuquerque, NM.
DYNA2D - Lawrence Livermore National Laboratory, Livermore, CA.
DYNA3D

EPIC-2 - Honeywell, Inc., Brooklyn Park, MN.

EPIC-3

HELP - Systems, Science and Software, La Jolla, CA.

HEMP - Lawrence Livermore National Laboratory, Livermore, CA.

HEMP3D

HULL - Orlando Technology, Inc., Shalimar, FL.

MESA - Los Alamos National Laboratory, Los Alamos, NM.

TOODY - Sandia National Laboratories, Albuquerque, NM.

Some of the equations of state which have been used are as follows.

JWL (Jones, Wilkins, and Lee)

Los Alamos

Mie-Gruneisen

Tillotson

Wilkins

For more information about the previous codes, refer to Zukas (1991).

INTENTIONALLY LEFT BLANK.

10. REFERENCES

Alekseevskii, V. P. "Penetration of a Rod Into a Target at High Velocity." Fizika Goreniya i Vzryva, vol. 2, no. 2, pp. 99–186 (Combustion, Explosion and Shock Waves, pp. 63–66), 1966.

Arbuckle, A. L., E. L. Herr, and A. J. Ricchiazzi. "A Computerized Method of Obtaining Behind-the-Target Data From Orthogonal Flash Radiographs." BRL-MR-2264, U.S. Army Ballistic Research Laboratory, Aberdeen Proving Ground, MD, January 1973. (AD 908362L)

Backman, M. E., and W. Goldsmith. "The Mechanics of Penetration of Projectiles Into Targets." International Journal of Engineering Science, vol. 16, no. 1-A, U.S. Naval Weapons Center, China Lake, CA, 1978.

Baker, W. E., P. S. Westine, and F. T. Dodge. Similarity Methods in Engineering Dynamics. Rochelle Park, NJ: Hayden Book Company, 1973.

Baumeister, T., and L. S. Marks, eds. Standard Handbook For Mechanical Engineers, 7th ed., McGraw Hill Book Company, pp. 5–16 and 5–17, 1967.

Bjerke, T. W., G. F. Silsby, D. M. Scheffler, and R. M. Mudd. "Yawed Long Rod Armor Penetration at Ordnance and Higher Velocities." BRL-TR-3221, U.S. Army Ballistic Research Laboratory, Aberdeen Proving Ground, MD, March 1991.

Bjerke, T. W., J. Zukas, and K. Kimsey. "Penetration Performance of Tungsten Alloy Penetrators with L/D Ratios of 1 to 1/32." BRL-TR-3246, U.S. Army Ballistic Research Laboratory, Aberdeen Proving Ground, MD, June 1991.

Ference, M., Jr., H. B. Lemon, and R. J. Stephenson. Analytical Experimental Physics. The University of Chicago Press, 1956.

Frank, K., and J. Zook. "Energy-Efficient Penetration and Perforation of Targets in the Hypervelocity Regime." Proceedings of the 1986 Hypervelocity Impact Symposium. International Journal of Impact Engineering, vol. 5, pp. 277–284, 1987.

Frank, K., and J. A. Zook. "Energy-Efficient Penetration of Targets." BRL-MR-3885, U.S. Army Ballistic Research Laboratory, Aberdeen Proving Ground, MD, February 1991.

Golub, A., and F. E. Grubbs. "On Estimating Ballistic Limit and Its Precision." BRL-TN-151, U.S. Army Ballistic Research Laboratory, Aberdeen Proving Ground, MD, March 1950. (AD 51120)

Golub, A., and F. E. Grubbs. "Analysis of Sensitivity Experiment's When the Levels of Stimulus Cannot Be Controlled." American Statistical Association Journal, pp. 257–265, June 1956.

Goodier, J. N. "On the Mechanics of Indentation and Cratering in Solid Targets of Strain-Hardening Metal by Impact of Hard and Soft Spheres." Proceedings of the Seventh Hyper-Velocity Impact Symposium, Volume III - Theory, pp. 215–259, Orlando, FL, 1965.

Grabarek, C. L. "Penetration of Armor by Steel and High Density Penetrators." BRL-MR-2134, U.S. Army Ballistic Research Laboratory, Aberdeen Proving Ground, MD, October 1971. (AD 518394L)

Grabarek, C. L. "An Armor Penetration Predictive Scheme for Small Arms AP Ammunition." BRL-MR-2620, U.S. Army Ballistic Research Laboratory, Aberdeen Proving Ground, MD, April 1976. (AD C006096L)

Grabarek, C. L., and E. L. Herr. "X-ray Multi-Flash System for Measurement of Projectile Performance at the Target." BRL-TN-1634, U.S. Army Ballistic Research Laboratory, Aberdeen Proving Ground, MD, September 1966. (AD807619)

Gray, D. E., ed. American Institute of Physics Handbook. 3rd ed., New York, NY: McGraw-Hill Book Company. pp. 2–39, 1972.

Hagan, J. S., and V. Visnaw. "Analysis of Sensitivity Data following A Normal Distribution." Analytical Section Report 70-A5-K3, Materiel Test Directorate, October 1970.

Hanagud, S., and B. Ross. "Large Deformation, Deep Penetration Theory for a Compressible Strain-Hardening Target Material." AIAA Journal, vol. 9, no. 5, 1971, p. 905ff.

Herr, L., and C. L. Grabarek. "Ballistic Performance and Beyond Armor Data For Rods Impacting Steel Armor Plates." BRL-MR-2575, Aberdeen Proving Ground, MD, Aberdeen Proving Ground, MD, January 1976. (AD B009979L)

Herr, E. L., and C. L. Grabarek. "Standardizing the Evaluation of Candidate Materials for High L/D Penetrators." BRL-MR-2860, U.S. Army Ballistic Research Laboratory, Aberdeen Proving Ground, MD, September 1978. (AD A062101)

Hill, R. The Mathematical Theory of Plasticity. Oxford: Clarendon Press, 1950.

Hopkins, H. G. "Dynamic Expansion of Spherical Cavities in Metals." Progress in Solid Mechanics, vol. 1, chap. 3, edited by I. N. Sneddon and R. Hill, Amsterdam, NY: North-Holland Publishing Company, 1960.

Johnson, W. Impact Strength of Materials. London: Edward Arnold, New York: Crane, Russak, 1972.

Johnson, J. R., and R. E. Mioduski. "Estimation of the Loss of Velocity and Mass of Fragments During Target Perforation." BRL-MR-1777, U.S. Army Ballistic Research Laboratory, Aberdeen Proving Ground, MD, September 1966. (AD 376474)

Kozlov, V. S. "Penetration Model That Accounts for the Ductile Properties of the Materials of Colliding Bodies." Translated from Problemy Prochnosti, no. 3, pp. 47–52, March 1986. Translation by Plenum Publishing Company, UDC 532.5.032, pp. 334–341, 1986.

Lambert, J. P. "The Terminal Ballistics of Certain 65 Gram Long Rod Penetrators Impacting Steel Armor Plate." BRL-TR-2072, U.S. Army Ballistic Research Laboratory, Aberdeen Proving Ground, MD, May 1978.

Lambert, J. P., and G. H. Jonas. "Towards Standardization in Terminal Ballistics Testing: Velocity Representation." BRL-R-1852, U.S. Army Ballistic Research Laboratory, Aberdeen Proving Ground, MD, January 1976. (AD A021389)

MIL-A-12560G(MR). "Armor Plate, Steel, Wrought, Homogeneous (for Use in Combat-Vehicles and for Ammunition Testing)." 5 August 1984.

MIL-A-46100C. "Armor Plate, Steel, Wrought, High Hardness." 13 June 1983.

MIL-S-13812B(MR). "Steel Plate, Wrought, Homogeneous for Ammunition Testing (1/4 TO 12 Inches, Incl.)." 8 February 1971.

Misey, J. "Analysis of Ballistic Limit." BRL-MR-2815, U.S. Army Ballistic Research Laboratory, Aberdeen Proving Ground, MD, March 1978.

Oberg, E., F. D. Jones, and H. L. Holbrook. Machinery's Handbook, p. 308, 21st ed., New York, NY: Industrial Press, Inc., 1979.

Project THOR. "The Resistance of Various Metallic Materials to Perforation by Steel Fragments; Empirical Relationships for Fragment Residual Velocity and Residual Weight." TR-47, U.S. Army Ballistic Analysis Laboratory, Institute for Cooperative Research, The Johns Hopkins University, April 1961.

Project THOR. "The Resistance of Various Non-Metallic Materials to Perforation by Steel Fragments; Empirical Relationships for Fragment Residual Velocity and Residual Weight." TR-51, Ballistic Analysis Laboratory, Institute for Cooperative Research, The Johns Hopkins University, April 1963.

U.S. Army Materiel Command. Engineering Design Handbook, Elements of Armament Engineering, Part 2: Ballistics. AMCP 706-107, September 1963.

Roecker, E., and C. L. Grabarek. "The Effect of Yaw and Pitch on Long Rod Penetration Into Rolled Homogeneous Armor at Various Obliquities." Proceedings of the Ninth International Symposium on Ballistics, Royal Military College of Science, Shrivenham, England, 29 Apr–1 May 1986.

Silsby, G. F. "Penetration of Semi-Infinite Steel Targets by Tungsten Long Rods at 1.3 to 4.5 km/s." Proceedings of the Eighth International Symposium on Ballistics, Orlando FL, 1984.

Silsby, G. F., R. J. Roszak, and L. Giglio-Tos. "BRL's 50-mm High Pressure Powder Gun for Terminal Ballistic Testing - The First Year's Experience." BRL-MR-03236, U.S. Army Ballistic Research Laboratory, Aberdeen Proving Ground, MD, January 1983.

Tate, A. "A Theory for the Deceleration of Long Rods After Impact." Journal of the Mechanics and Physics of Solids, vol. 15, pp. 387–399, 1967.

Tate, A. "Further Results in the Theory of Long Rod Penetration." Journal of the Mechanics and Physics of Solids, vol. 17, pp. 141–150, 1969.

Tate, A. "Long Rod Penetration Models - Part I. A Flow Field Model For High Speed Long Rod Penetration." International Journal of Mechanical Sciences, vol. 28, no. 8, pp. 535–548, 1986a.

Tate, A. "Long Rod Penetration Models - Part II. Extensions to the Hydrodynamic Theory of Penetration." International Journal of Mechanical Sciences, vol. 28, no. 9, pp. 599–612, 1986b.

Taylor, G. I. "The Use of Flat-Ended Projectiles for Determining Dynamic Yield Stress, I: Theoretical Consideration." Proceedings of the Royal Society of London, A194, 289, 1948.

Walters, W. P., and J. A. Zukas. Fundamentals of Shaped Charges. John Wiley and Sons, Inc., 1989.

Wilkins, M. L., and M. W. Guinan. "Impact of Cylinders on a Rigid Boundary." Journal of Applied Physics, vol. 44, no. 3, pp. 1200--1206, March 1973.

Zook, J. "An Analytical Model of Kinetic Energy Projectile/Fragment Penetration." BRL-MR-2797, U.S. Army Ballistic Research Laboratory, Aberdeen Proving Ground, MD, October 1977.

Zook, J. A., and D. F. Merritt. "Advanced Techniques for Analyzing Dynamic Fragments." BRL-MR-3313, U.S. Army Ballistic Research Laboratory, Aberdeen Proving Ground, MD, October 1983. (AD ADA 134348)

Zook, J., W. Slack, and B. Izdebski. "Ricochet and Penetration of Steel Spheres Impacting Aluminum Targets." BRL-MR-3243, U.S. Army Ballistic Research Laboratory, Aberdeen Proving Ground, MD, February 1983. (AD A125330)

Zukas, J. A., ed. High Velocity Impact Dynamics, John Wiley and Sons, Inc., 1991.

Zukas, J. A., T. Nicholas, H. F. Swift, L. B. Greszczuk, and D. R. Curran. Impact Dynamics. John Wiley and Sons, Inc., 1982.

BIBLIOGRAPHY

Backman, M. E. "Terminal Ballistics." NWC TP 5780, Naval Weapons Center, China Lake, CA, February 1976.

Brown, C. J. "Estimates of Residual Mass and Velocity for Tungsten and Steel Fragments." BRL-MR-2794, U.S. Army Ballistic Research Laboratory, Aberdeen Proving Ground, MD, October 1977.

Dehn, J. T. "The Particle Dynamics of Target Penetration." BRL-TR-02188, U.S. Army Ballistic Research Laboratory, Aberdeen Proving Ground, MD, September 1979.

Dehn, J. T. "A Unified Theory of Penetration." BRL-TR-2770, U.S. Army Ballistic Research Laboratory, Aberdeen Proving Ground, MD, December 1986.

Farrand, T. G. "A Database Storage System and the Sonic Digitizer Method for Radiographic Data Reduction Used by the Penetration Mechanics Branch." BRL-MR-3847, U.S. Army Ballistic Research Laboratory, Aberdeen Proving Ground, MD, June 1990.

Hauver, G. E., and A. Melani. "Behavior of Segmented Rods During Penetration." BRL-TR-3129, U.S. Army Ballistic Research Laboratory, Aberdeen Proving Ground, MD, July 1990.

Kimsey, K. D., and J. A. Zukas. "Contact Surface Erosion for Hypervelocity Problems." BRL-MR-3495, U.S. Army Ballistic Research Laboratory, Aberdeen Proving Ground, MD, February 1986.

Kineke, J. H., Jr., and C. E. West, Jr. "Perforation Area Produced by Fragment Impact." BRL-TR-02580, U.S. Army Ballistic Research Laboratory, Aberdeen Proving Ground, MD, August 1984.

Lambert, J. P., and B. E. Ringers. "Standardization of Terminal Ballistics Testing, Data Storage and Retrieval." BRL-TR-02066, U.S. Army Ballistic Research Laboratory, Aberdeen Proving Ground, MD, May 1978.

Merritt, D. F., and C. E. Anderson, Jr. "X-ray Trigger Predictor: Automatic Electronic Time Delay Device for Flash X-ray Systems." BRL-TR-02284, U.S. Army Ballistic Research Laboratory, Aberdeen Proving Ground, MD, January 1981.

Rapacki, E. J. "Instrumentation Techniques for Measuring Large, High Rate Strains With Foil Resistance Strain Gages." BRL-TR-02573, U.S. Army Ballistic Research Laboratory, Aberdeen Proving Ground, MD, August 1984.

Scheffler, D. R., and T. M. Sherrick. "Large-Scale Simulations of Monolithic and Segmented Projectiles Impacting Spaced Armor." BRL-TR-3080, U.S. Army Ballistic Research Laboratory, Aberdeen Proving Ground, MD, February 1990.

Silsby, G. F. "Rectification of Multiflash Radiographs." BRL-MR-03363, U.S. Army Ballistic Research Laboratory, Aberdeen Proving Ground, MD, July 1984.

Walters, W. P., and S. B. Segletes. "Solution of the Long Rod Penetration Equations." BRL-TR-3180, U.S. Army Ballistic Research Laboratory, Aberdeen Proving Ground, MD, December 1990.

Wilbeck, J. S., C. E. Anderson, Jr., J. P. Riegel, III, J. Lankford, S. A. Mullin, and S. R. Bodner. "A Short Course on Penetration Mechanics." Course Notes, Southwest Research Institute, San Antonio, TX.

Wright, T. W., and K. Frank. "Approaches to Penetration Problems." BRL-TR-2957, U.S. Army Ballistic Research Laboratory, Aberdeen Proving Ground, MD, December 1988.

Zook, J. A., and K. Frank. "Comparative Penetration Performance of Tungsten Alloy L/D = 10 Long Rods With Different Nose Shapes Fired at Rolled Homogeneous Armor." BRL-MR-3480, U.S. Army Ballistic Research Laboratory, Aberdeen Proving Ground, MD, November 1985.

Zook, J. A., C. J. Brown, and C. L. Grabarek. "The Penetration Performance of Tungsten Alloy L/D = 10 Long Rods With Different Nose Shapes Fired at Rolled Homogeneous Armor." BRL-MR-03350, U.S. Army Ballistic Research Laboratory, Aberdeen Proving Ground, MD, April 1984.

Zukas, J A. "Impact Dynamics: Theory and Experiment." BRL-TR-02271, U.S. Army Ballistic Research Laboratory, Aberdeen Proving Ground, MD, October 1980.

Zukas, J. A. "Numerical Simulation of Semi-Infinite Target Penetration by Continuous and Segmented Rods." BRL-TR-3081, U.S. Army Ballistic Research Laboratory, Aberdeen Proving Ground, MD, February 1990.

GLOSSARY

ballistic limit - The striking velocity required to just perforate the target configuration (residual velocity of 0). (Army, Navy, and protection criteria define different methods of determining whether a result is a perforation or a penetration.) Can also refer to the angle of obliquity at a particular striking velocity which will result in zero residual velocity (the Θ_{50}).

bore - The hollow cylindrical shaped center portion of a gun barrel.

Brinell hardness number (BHN) - A measure of hardness of the surface of the test specimen based on the diameter of indentation of a sphere (usually 10 mm in diameter) under static pressure (hydraulic press), usually 3,000 kg/mm^2.

caliber - The diameter of the bore of the barrel of a gun.

carrier - The sabot assembly—consists of the obturator, pusher plate, and sabot (the latter envelops the penetrator).

center of mass - The point in a rigid body which moves as if all of the mass of the body and all of the forces acting on the body were concentrated at that point.

Charpy impact test - A measure of a test specimen's resistance to fracture.

ductile - Capable of being drawn out or hammered thin.

empirical - Based on experimental data only without regard to theory or scientific principles.

erosion - The disintegration of the penetrator at the penetrator-target interface due to forces acting at the interface.

exit angle - The angle which the path of the residual penetrator makes with the original shot line after perforating a target.

fiducial - A reference marker.

high hardness armor (HHA) - Steel armor made to meet Army specifications as described in MIL-A-46100C (1983).

K factor - The magnification factor.

magnification factor - The ratio of the size of the object which creates an image on photographic film (due to radiation from a point source) to the size of the image appearing on the film.

maximum likelihood - A procedure to determine the most likely value of the average of values which constitute a zone of mixed results (perforations occurring at velocities below that of nonperforating velocities for a particular penetrator/target configuration).

munition - An abbreviation of ammunition.

normal - Perpendicular (90° angle) to the surface.

obliquity - The angle which the shot line makes with a line perpendicular (normal) to the surface of the target at the point of intersection of both lines.

obturator - The rear portion of the sabot assembly which provides a gas seal to prevent the gasses produced by the burning propellant from escaping in the forward direction while the projectile is travelling down the gun barrel.

orthogonal - At a 90° angle.

partial penetration - A penetrator/target interaction in which the penetrator does not exit the target (a penetration as opposed to a perforation).

penetration - A penetrator/target interaction in which the penetrator does not exit the target.

penetrator - The part of a projectile which impacts the target and is responsible for penetrating or perforating the target.

perforation - A penetrator/target interaction in which the penetrator defeats the target (light can be seen through the hole made by the penetrator).

pitch - The angle that a projectile makes with the flight path when measured in the vertical plane—projectile is tilted either up or down with respect to the flight path.

projectile - A body which is undergoing free flight.

propellant - The chemical explosive which, when initiated, causes the projectile to accelerate down the gun barrel.

pusher plate - Metal disc which is part of the sabot assembly and absorbs the setback forces upon launching the projectile.

radiography - Photography which uses invisible high-frequency radiation such as x-rays or gamma rays to expose the film.

residual velocity - The speed (velocity if the exit angle is included) of the residual penetrator after perforating a target plate.

residual mass - The mass of the portion of the penetrator which exits the target after perforating the target.

Rockwell hardness (R_c) - A measure of the hardness of the surface of a test specimen using a conic-shaped indentor rather than the spherical indentor of the Brinell hardness test. The subscript c refers to the size of the indentor.

rolled homogeneous armor (RHA) - Steel armor plate made to meet Army military specifications as described in MIL-A-12560F(MR) (1984).

sabot - The part of the sabot assembly which envelops the subcaliber penetrator making up the difference between the diameter of the penetrator and the diameter of the bore of the gun barrel.

semi-infinite - A term used to describe a target which is sufficiently thick so that the rear surface does not influence the result of the impact (requires the penetrator to come to rest within the target).

stabilization - The condition in which a projectile in free flight reaches an equilibrium state with respect to forces which cause it to precess (wobble) about its main axis.

striking velocity - The speed (velocity when the obliquity is included) at which the penetrator impacts the target plate.

subcaliber - A diameter which is less than the diameter of the bore of the associated gun barrel.

target - Material which the projectile is intended to impact.

theta 50 - The angle of obliquity which defines the boundary between penetration and perforation for a penetrator impacting at a specific impact velocity (symbollically, Θ_{50}).

V_{50} - The ballistic limit determined by taking the average of an equal number of perforations and penetrations (usually three of each, which makes a six-round V_{50}) within a specified impact velocity range (125 ft/s).

Vicker's test - A measure of the strength of a material.

witness pack - A series of metal plates of varying thickness separated by styrofoam sheets which is used to record the debris (including the residual penetrator) which emanates from a target which has been perforated.

witness panel - A single sheet of material placed behind the target which exhibits the distribution pattern of impacting debris emanating from a target upon being perforated.

yaw - The angle that the axis of a projectile makes with the flight path when measured in the horizontal plane - projectile is tilted sideways with respect to the flight path. Note: Sometimes yaw refers to the maximum deviation angle of the axis of the projectile with respect to the flight path measured in the plane of maximum deviation.

INTENTIONALLY LEFT BLANK.

No. of Copies	Organization
2	Administrator Defense Technical Info Center ATTN: DTIC-DDA Cameron Station Alexandria, VA 22304-6145
1	Commander U.S. Army Materiel Command ATTN: AMCAM 5001 Eisenhower Avenue Alexandria, VA 22333-0001
1	Commander U.S. Army Laboratory Command ATTN: AMSLC-DL 2800 Powder Mill Road Adelphi, MD 20783-1145
2	Commander U.S. Army Armament Research, Development, and Engineering Center ATTN: SMCAR-IMI-I Picatinny Arsenal, NJ 07806-5000
2	Commander U.S. Army Armament Research, Development, and Engineering Center ATTN: SMCAR-TDC Picatinny Arsenal, NJ 07806-5000
1	Director Benet Weapons Laboratory U.S. Army Armament Research, Development, and Engineering Center ATTN: SMCAR-CCB-TL Watervliet, NY 12189-4050
(Unclass. only)1	Commander U.S. Army Armament, Munitions and Chemical Command ATTN: AMSMC-IMF-L Rock Island, IL 61299-5000
1	Director U.S. Army Aviation Research and Technology Activity ATTN: SAVRT-R (Library) M/S 219-3 Ames Research Center Moffett Field, CA 94035-1000

No. of Copies	Organization
1	Commander U.S. Army Missile Command ATTN: AMSMI-RD-CS-R (DOC) Redstone Arsenal, AL 35898-5010
1	Commander U.S. Army Tank-Automotive Command ATTN: ASQNC-TAC-DIT (Technical Information Center) Warren, MI 48397-5000
1	Director U.S. Army TRADOC Analysis Command ATTN: ATRC-WSR White Sands Missile Range, NM 88002-5502
1	Commandant U.S. Army Field Artillery School ATTN: ATSF-CSI Ft. Sill, OK 73503-5000
(Class. only)1	Commandant U.S. Army Infantry School ATTN: ATSH-CD (Security Mgr.) Fort Benning, GA 31905-5660
(Unclass. only)1	Commandant U.S. Army Infantry School ATTN: ATSH-CD-CSO-OR Fort Benning, GA 31905-5660
1	Air Force Armament Laboratory ATTN: WL/MNOI Eglin AFB, FL 32542-5000
	Aberdeen Proving Ground
2	Dir, USAMSAA ATTN: AMXSY-D AMXSY-MP, H. Cohen
1	Cdr, USATECOM ATTN: AMSTE-TC
3	Cdr, CRDEC, AMCCOM ATTN: SMCCR-RSP-A SMCCR-MU SMCCR-MSI
1	Dir, VLAMO ATTN: AMSLC-VL-D
10	Dir, BRL ATTN: SLCBR-DD-T

No. of Copies	Organization
1	SouthWest Research Institute 6220 Culebra Road ATTN: Dr. Charles Anderson, Jr. Postal Drawer 28510 San Antonio, TX 78284

USER EVALUATION SHEET/CHANGE OF ADDRESS

This laboratory undertakes a continuing effort to improve the quality of the reports it publishes. Your comments/answers below will aid us in our efforts.

1. Does this report satisfy a need? (Comment on purpose, related project, or other area of interest for which the report will be used.) _____

2. How, specifically, is the report being used? (Information source, design data, procedure, source of ideas, etc.) _____

3. Has the information in this report led to any quantitative savings as far as man-hours or dollars saved, operating costs avoided, or efficiencies achieved, etc? If so, please elaborate. _____

4. General Comments. What do you think should be changed to improve future reports? (Indicate changes to organization, technical content, format, etc.) _____

BRL Report Number BRL-MR-3960 Division Symbol _____

Check here if desire to be removed from distribution list. ____

Check here for address change. ____

Current address: Organization _____
Address _____

DEPARTMENT OF THE ARMY
Director
U.S. Army Ballistic Research Laboratory
ATTN: SLCBR-DD-T
Aberdeen Proving Ground, MD 21005-5066

OFFICIAL BUSINESS

BUSINESS REPLY MAIL
FIRST CLASS PERMIT No 0001, APG, MD

Postage will be paid by addressee

Director
U.S. Army Ballistic Research Laboratory
ATTN: SLCBR-DD-T
Aberdeen Proving Ground, MD 21005-5066

NO POSTAGE NECESSARY IF MAILED IN THE UNITED STATES